Multichannel grating cavity laser for optically multiplexed communication systems

Zhu, Benyuan

Award date:
1996

Awarding institution:
University of Bath

MULTICHANNEL GRATING CAVITY LASER FOR OPTICALLY MULTIPLEXED COMMUNICATION SYSTEMS

Submitted by Benyuan ZHU
for the degree of PhD
of the University of Bath
January, 1996

Benyuan Zhu
朱本源

ProQuest LLC
789 East Eisenhower Parkway
P.O. Box 1346
Ann Arbor, MI 48106-1346

ABSTRACT

Operating characteristics of a Multichannel Grating Cavity (MGC) laser are experimentally and theoretically investigated with the objective of demonstrating its potential applications in wavelength division multiplexing (WDM) and optical time division multiplexing (TDM) communication networks.

The basic properties such as wavelength switching and simultaneous multiwavelength emission have been demonstrated in both bulk optic and monolithically integrated MGC lasers. Direct modulation rates of the bulk optic MGC laser are found to be limited by the long external cavity at 500 Mbit/s. In contrast, modulation speeds in excess of 1 Gbit/s have been achieved in the integrated device.

The bulk optic MGC laser has been found to be suitable for multiwavelength ultrashort optical pulse generation using active mode-locking techniques. For the first time, simultaneous generation of dual-wavelength picosecond optical pulses with narrow spectral linewidth is successfully demonstrated. Two optical pulse trains are also generated at different wavelengths with a programmable delay between them making them suitable for pump-probe applications. The minimum achievable pulsewidths produced from the actively mode-locked MGC laser are shown to be limited by the resolution bandwidth of the grating used. The effects of the RF drive frequency detuning on the mode-locked pulse width are examined, and the interchannel cross-talk in dual channel short pulse operation is also discussed.

A theoretical dynamic model involving a set of coupled-cavity rate equations has been developed for the MGC laser. The model includes the effects of non-linear gain saturation and optical bandwidth of the grating used. Theoretical modelling of the dynamic modulation properties and multiwavelength mode-locking process have been carried out. The numerical results are compared with the experimental measurements and a good agreement between theory and experiment has been achieved. Finally, high power short pulse generation has been demonstrated by using a broad area tapered laser and amplifier.

SCOPE OF THESIS

Chapter one provides a general introduction to the architectural concepts that are most commonly used in optical multiplexing communication systems, which are basically classified as wavelength division multiplexing (WDM) and optical time division multiplexing (TDM) systems. This helps in establishing general requirements for the laser transmitters that are used in such systems and also gives examples of the kinds of applications for which WDM and optical TDM are currently being considered. The overall objectives of the thesis are also defined.

Chapter two surveys the various approaches for the potential WDM semiconductor laser sources. The ultrashort optical pulse lasers for optical TDM applications are reviewed in chapter four. The issues that are discussed are the device structure, operating principles, characteristics, and drawbacks. Some of these devices are already commercially available, while others are still at the development stage.

Chapter three describes the basic characteristics of the bulk optic MGC laser, including the device structure, operating principles, steady-state and dynamic performance. The experimental implementation of a two channel MGC laser is presented and the properties such as simultaneous dual channel emission and wavelength switching are experimentally demonstrated. A theoretical dynamic model involving a set of coupled cavity rate equations is developed for the MGC laser. The dynamic characteristics, including transient response, modulation speed, and carrier depletion in dual channels, are discussed.

Chapter four discusses the characteristics of mode-locked short pulse operation of the MGC laser in single channel. After a brief introduction of the short pulse generation techniques, generation of narrow linewidth picosecond optical pulses is demonstrated using actively mode-locking of the MGC laser. The dependence of the pulsewidth and spectral linewidth on the device structure are examined. Theoretical modelling of the

mode-locking process of the MGC laser is presented using the coupled cavity rate equation model, and the frequency detuning properties are discussed.

Chapter five studies issues that relate to multiwavelength short optical pulse generation in the actively mode-locked MGC laser. Dual wavelength picosecond optical pulses are generated for the first time either simultaneously or incorporating a relative time delay. Numerical simulation results of two wavelength short pulse generation are compared with the experimental results, and crosstalk between two channels under picosecond pulse operation are discussed.

Chapter six introduces the basic concepts and operating principles of the monolithic integrated MGC laser, which is essentially a two-dimensional implementation of the bulk optic MGC laser. The device structure and lasing characteristics of the first prototype device are discussed, and the dynamic modulation properties are also experimentally and theoretically studied.

Chapter seven discusses issues that relate to the high power ultrashort optical pulse generation using broad area tapered laser and amplifiers. The aim of this chapter is to give a demonstration that the output power of the MGC laser can be increased by using broad area tapered waveguides. High peak power generation and amplification of short optical pulses by using a tapered bow-tie laser and a tapered travelling wave amplifier are experimentally demonstrated.

Chapter eight summarises the findings of this work, draws conclusions based on these findings and discusses some ideas for future work.

LIST OF PUBLICATIONS

During the course of the research, the following papers have already been published in journals and conference proceedings.

Journal Articles

1. **B. Zhu,** K. O. Nyairo, and I. H. White, "Dual-wavelength picosecond optical pulse generation using an actively mode-locked multichannel grating cavity laser", *IEEE Photon. Technol. Lett.*, Vol.6, pp.348-351, 1994.

2. **B. Zhu** and I. H. White, "Variable delay dual wavelength picosecond optical pulse generation using an actively mode-locked multichannel grating cavity laser", *Appl. Phys. Lett.*, Vol.63, pp.2928-2930, 1994.

3. M. Asghari, **B. Zhu**, I. H. White, C. P. Seltzer, C. Nice, I. D. Henning, G. H. B. Thompson, "Demonstration of an integrated multichannel grating cavity laser for WDM applications", *Electron. Lett., Vol.* 30, pp.1674-1675, 1994.

4. **B. Zhu** and I. H. White, "Multiwavelength picosecond optical pulse generation using an actively mode-locked multichannel grating cavity laser", *IEEE J. Lightwave Technol.*, vol. 13, pp.2327-2335, 1995

5. **B. Zhu**, I. H. White, K. A. Williams, F. R. Laughton and R. V. Penty, "High peak power picosecond optical pulse generation from Q-switched bow-tie laser with a tapered travelling wave amplifier", *IEEE Photon.Technol.Lett.*, Vol. 8, pp.503-505,1996.

Conference Presentations

6. **B. Zhu** and I. H. White, "Dual wavelength pulse generation incorporating relative timing control using an actively mode-locked multichannel grating cavity laser", in Conference on Lasers and Electro-Optics, 1994, Vol.12,OSA Technical Digest Series (Optical Society of America, Washington, D.C. 1994) pp.254-255.

7. M. Asghari, **B. Zhu**, I. H. White, C. P. Seltzer, C. Nice, I. D. Henning, G. H. B. Thompson, "A high speed integrated multichannel grating cavity laser source for wavelength division multiplexed optical fibre communication systems", in Optical Fibre Communications Conference, Vol. 8, 1995 OSA Technical Digest Series (Optical Society of America, Washington, D.C. 1995) pp.307-308.

8. M Asghri, I. H. White, **B. Zhu**, C. P. Seltzer, C. Nice, I. D. Henning, G. H. B. Thompson, "Integration of multi-wavelength sources on two dimensional semiconductor waveguides", IOP's 95, Institute of physics Annual Congress, Teford, U.K., March, 1995.

ACKNOWLEDGEMENTS

First and foremost, I wish to thank my supervisor Professor Ian. H. White for introducing me to this exciting field and for his encouragement, guidance and full support over the period in which this research was carried out.

The support from both the UK Engineering ans Physical Sciences Research Council (EPSRC) and Royal Society is gratefully acknowledged. Particular thanks go to Dr C.J. Armistead of BNR Europe Ltd for the supply of the laser arrays used in this work, I also wish to thank BT laboratories for fabrication of the integrated device.

My sincere thanks go to all my fellow researchers at Bath for much technical and linguistic assistance and useful discussions. People deserving special mention include Huw Summers, Kevin Williams, Phil Mason, Adrian Wonfor, Mehdi Asghari, Roger Griffiths, Phil Dowd, Frances Laughton, Richard Penty, Paul Snow, Kennedy Nyairo and Ziping Jiang. In particular, I would like to extend my kindest appreciation to Mr. R. C. J. Draper for his help.

I am very grateful to the Pao Yu-Kong and Pao Zhao-Long Scholarship Board (Zhejiang, China) for personal financial support, which made it possible for me to study in the University of Bath, UK. I would also like to thank the Overseas Research Student Awards and the Christine King Memorial Trust for personal financial support.

Finally I would like to thank my wife for her love, understanding and patience, and my brother Jian-Ming for his constant motivation and encouragement.

CONTENTS

Chapter 1

INTRODUCTION--OPTICALLY MULTIPLEXED COMMUNICATION SYSTEMS

1.1 Optical Fibre Communication Technologies

Remarkable progress has been made in optical fibre communication technologies during the past two decades, in increasing both the information capacity and repeater-spans of transmission systems. In particular, long-distance optical transmission systems now provide reliable digital telecommunication networks and low cost service systems. The bit rate of early optical transmission systems in the late 1970's was 45 Mbit/s. By the mid-1980's, the transmission speed had been increased to rates ranging from 400 Mbit/s to 560 Mbit/s [1]. Recently, high-speed trunk transmission systems up to 10 Gbit/s have been achieved almost to the point of commercial introduction, and time-division-multiplexed optical transmission over 500 km at 100 Gbit/s has been demonstrated in the laboratory [2]. This rapid development is attributed to increasing improvements in the performance of various semiconductor lasers, optical amplifiers and optical fibres.

The performance of the semiconductor laser has been greatly improved since the first demonstration [3]. The distributed feedback (DFB) laser [4] has allowed narrow linewidth single mode operation and the development of the strained-layer multiquantum well laser has led to the extension of the modulation bandwidths to in excess of 20 GHz [5]. The vertical cavity surface emitting laser (VCSEL) now provides low threshold current, small size and high performance [6]. The monolithic semiconductor lasers integrated with an electroabsorption modulator and a distributed Bragg reflector has the potential for the

realising low chirp, reliable and high performance multigigabit/s systems [7]. The semiconductor laser is now being installed in many optical transmission links, such as in intercity and interoffice systems, distribution networks and optical interconnection between computers, and the use of semiconductor lasers has become more and more popular.

A very promising new technology in the optical communication systems is optical amplification. Semiconductor laser optical amplifiers [8-9] have been developed and can be used as repeaters in multi-channel optical transmission systems, or in other high capacity links. A milestone in the development of the optical fibre communication technologies is the development of the erbium-doped fibre amplifiers [10]. These amplifiers, consisting of a short length of optical fibre containing a concentration of erbium ions, pumped by a semiconductor laser, can boost the power of lightwave signals without the need for optoelectronic conversion and subsequent electronic amplification as in conventional lightwave repeaters. This simple and elegent function, which provides high power efficient, low noise, and fibre compatible structural properties, is already affecting system architecture, offering simple and cost-effective means to access the vast transmission capacity of fibre. Thus transoceanic cable systems and terrestrial networks, which employ optical amplifiers, will have significantly increased transmission capacity at low cost in the future.

Great progress has also been achieved on the development of optical fibre. Single mode-optical fibre routes are now found at almost every level of a typical communication network. The information services that are carried on fibre include standard telephone services, media services (such as cable TV) and services for computer to computer and computer-to-database communication. The distances that are spanned consequently range from thousands of miles (as in the case of transoceanic telephone lines) to several tens of metres (as is commonly the case for an inter-office computer network). Both monomode and multimode fibre cables are now being installed at increased rates to meet the increasing demand for transmission capacity both in local area networks and in long distance

communications.

There are many factors that have contributed to fibre's present-day popularity, for example, low cost, freedom from electromagnetic interference, increased system security and noise immunity, but above all, it has been that the fibre is able to give low signal attenuation over an essentially limitless bandwidth. The two low-loss regions of a single-mode fibre (one at a wavelength of ~ 1.3 μm, and the other at a wavelength of ~ 1.55 μm) have a combined bandwidth of roughly 30 THz, sufficient to carry ~ 500 million 64 kBit/s voice-grade telephone lines. However, with even the fastest of present-day transmission systems running at a few tens of GHz, this enormous potential remains a largely untapped resource. On the other hand, there is an increasing need for larger information transmission capability in telecommunications, stemming from a demand for the provision of broadband transmission facilities for services such as high definition video and computer data transmission. This demand cannot be met by present single channel systems because the transmission bit-rates are limited by the speed of the electro-optic converter - a device converting electrical signals to optical signals and vice versa. Such mismatch in bandwidth between the electronic components and the optical fibres is the main obstacle to the realization of terabit lightwave communication systems.

Much research effort has been directed toward accessing the vast bandwidth of optical fibre by employing optical multiplexing technologies [11]. Roughly speaking, there are two approaches to realise optical multiplexing systems, namely, wavelength (frequency) division multiplexing (WDM) [12] and optical time division multiplexing (TDM) [13]. The first approach is, in principle, the revival of frequency multiplexing as used in coaxial cable analogue systems. This technique can alleviate the requirements on the complicated and expensive gigabit-per-second electronic and optoelectronic devices. The second approach is an extension of the current digital technology beyond the limitations of electronics. The WDM and optical TDM systems will be discussed in more detail in section 1.2 and 1.3 respectively.

1.2 Wavelength Division Multiplexing Systems

The basic idea behind WDM [12] is the transmission of several different wavelengths along a single fibre at the same time. If each wavelength carries a separate data stream, the total transmission rate is increased, by the product of the data rate for each individual wavelength and the number of wavelength channels. This technique is made possible by the fact that the different wavelengths do not interfere with one another; each wavelength propagates independently along the fibre.

Recently, both dense and nondense WDM have been considered and have specific systems applications.(There are a few definitions of terms in the literature, and this thesis follows the definition by Brackett [12]). Dense WDM is characterised by wavelength spacing of the order of 1 nm and is expected to find widespread applications for upgrading existing local-area and metropolitan-area networks as well as in future photonic networks. Nondense WDM is mainly directed to point-to-point transmission systems typically using two, four, or eight wavelengths separated by several tens or even hundreds of nanometers. From a practical system viewpoint, the point-to-point WDM link is a special case of interconnection between two nodes in the lightwave networks. In this section we first discuss a typical multiwavelength point-to-point link, then briefly introduce two general types of architecture that are often used in the networking applications.

1.2.1 Point-to-Point WDM Links

A typical N-wavelength point-to-point link is shown schematically in figure 1.1. Each of the wavelengths (λ_1 to λ_n in the figure) is provided by laser sources. A different data stream is encoded onto each wavelength and an external multiplexer device is then used to combine the wavelength onto the transmission fibre. A demultiplexer device separates the wavelengths at the receiver end of the link so that they may be simultaneously detected; this allows the different data streams to be processed in parallel. The principal

advantage of WDM in this particular application is its ability to increase the transmission rate on the fibre without the need to develop faster lasers, photodetectors and electronics. This is an attractive approach for upgrading the capacity of existing fibre links.

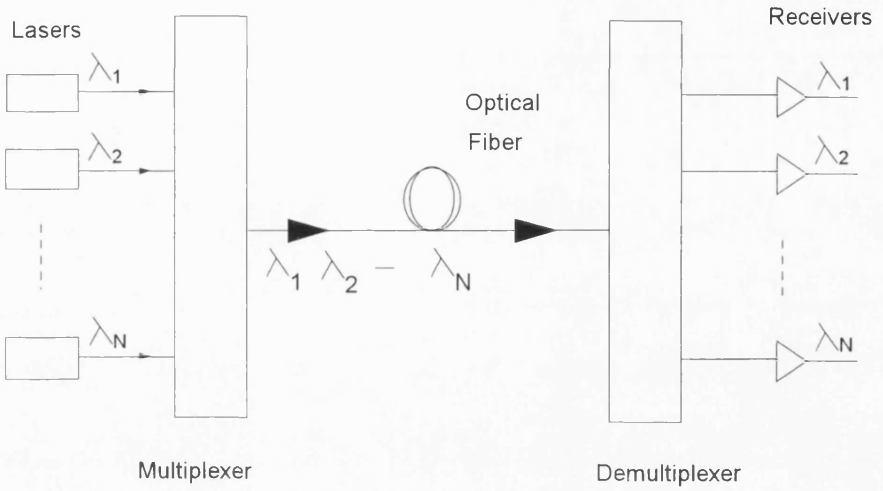

Figure 1.1 Schematic diagram of a N-wavelength point-to-point fibre-optic WDM transmission link.

Early examples of WDM-based point-point links used separate optical carriers in each of the two low-loss fibre bands (i.e. at 1.3 μm and at 1.55 μm) [14]. The wavelength spacing for this type of experiment was therefore about 250 nm. The first dense WDM point to point link was demonstrated in 1985 by a group at AT&T Bell laboratories [15]; they combined ten wavelengths in the range 1.529 μm to 1.561 μm onto a 68.3 km length of fibre. Each wavelength carried a 2 Gbit/s data stream, giving an overall figure of merit of 1.366 Tbit-km/s (defined as the total transmission rate multiplied by the transmission distance).

One of the most critical technologies in the practical deployment of such a dense WDM system is the laser transmitters. The wavelength accuracy and stability, spectral linewidth, tuning speed and range, modulation capacity, and optical power output are important performance parameters which will define the system's bit rate, channel spacing ($\Delta\lambda$) and the number of the channels (N).

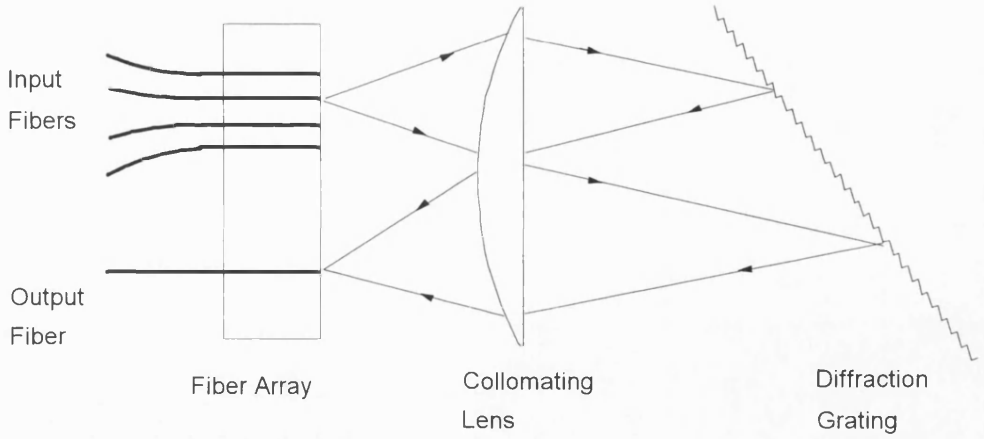

Figure 1.2. Schematic diagram of a bulk-optic grating-based optical multiplexer. The device that is illustrated multiplexes the signals from 4 different input fibres onto a signal output fibre.

The degree of wavelength accuracy that is required depends upon the method that is used to combine and separate the wavelengths (i.e. the multiplexer and demultiplexer). A class of device that is commonly used for combining wavelengths in dense WDM applications is the grating -based multiplexer [16]. A schematic example of a grating-based multiplexer is shown in figure 1.2. In this device, one end of each of a number of optical fibres are brought together in an array. One of these fibres is used as the multiplexer's output port, while the remainder of the fibres are used as input ports. Coupling between the input fibres and the output fibre is achieved using a collimating lens and grating in a near Littrow configuration. The device can be operated as a demultiplexer by reversing the sense of the fibres (i.e. by using the output fibre as an input port and input fibres as output ports). The channel passbands of the grating-based multiplexer, however, tend to be fairly narrow.

The system's transmission wavelengths must coincide with the channel passbands of the multiplexer to within a fraction of the channel width. Mismatch between the wavelengths and passbands results in excess optical loss within both multiplexer and demultiplexer devices. The operating wavelengths of the laser transmitters must be precisely defined, or they must be tunable to within the tolerance that is imposed by the multiplexer. In addition, the wavelength tunability of the laser transmitters is also useful for responding

to drifts in channel passbands that result from environmental fluctuations such as temperature change.

Since the principal aim here is to increase the transmission rate on a single fibre, this particular application tends to be considered for long-distance high capacity links. Therefore, relatively high speed modulation of each wavelength within the device is required in such instance. In addition, for high transmission speeds and long distances, the optical spectrum of the laser is of considerable importance because of fibre chromatic dispersion. Thus narrow spectrum linewidth and low chirp sources are required.

The widespread implementation of WDM in high-capacity point to point links has been delayed partly by the expense of having separate transmitter and receiver components for each wavelength [12]. Technologies that rely upon many separate devices can become prohibitively expensive. This expense is often dominated by the cost of packaging the various components rather than by the cost of the components themselves. This is especially true in single mode optical fibre at 1.55 μm where alignment tolerances between two components can be a fraction of a micrometre (several micrometres being a typical width for the active region of a semiconductor laser). Such tight tolerances can make alignments susceptible to environmental disturbances such as vibrations and temperature fluctuations; great care and skill must therefore be employed so as to package the components in a way that eliminates such susceptibility.

Simplification at the transmitter end of the link calls for a single laser device that can emit several wavelengths simultaneously from a single output port. A multiwavelength laser of this type could replace both the separate laser transmitters and the external multiplexer device of figure 1.1. Each individual wavelength should be precisely defined to match one of the channel passbands of the demultiplexer device used at the receiver end of the link. In addition, it should be possible to independently and simultaneously modulate each of the laser's different wavelengths.

1.2.2 Multiwavelength Network

The increasing diversity of applications for fibre, especially the recent spread of fibre into local-area networks, has brought about the realisation that the benefits of WDM extend well beyond that of simply increasing point-to-point transmission rates. The presence of several wavelengths on the same fibre affords a new degree of flexibility in the networking applications [17-19]. The wavelengths on the fibre may be used to provide service or customer segregation, and even to perform many network-oriented functions such as signal routing and switching. There are two main architectures of WDM optical networks. These are the broadcast-and-select and the wavelength routing networks.

A. Broadcast-and-Select Networks

In the broadcast-and-select network, all inputs from various users are combined in a WDM passive star coupler, and the mixed optical information is broadcast to all outputs. A monolithically integrated star coupler [20] has been reported, in which a slab waveguide functions as a free-space coupling region. Light coupled into any one of the input ports is guided into the coupling region, where the light radiates outwards so that a fraction of it is captured by each of the output ports. The device "broadcasts" the signal from each input to all of the outputs. Such devices are usually designed so that the power from each input is split evenly between the outputs.

Figure 1.3 shows an example of a broadcast-and-select network that relies upon wavelength-tunable lasers for its operation. Situated at each transmitter node is a wavelength-tunable laser. The output from each laser is coupled into one end of an optical fibre; the other ends of these fibres are coupled to the input ports of a star coupler that is situated at the hub of the network. The star coupler broadcasts the optical signal from each transmitter node to all of the receiver nodes. Each receiver node features a wavelength selective photoreceiver that can only detect light of a single fixed wavelength (a different wavelength for each node). For the channel spacing that is used in a dense WDM system, a

wavelength selective photoreceiver can be realised by placing an optical filter in series with a detector. A connection may be established between a transmitter node and a given receiver node by tuning the transmitter's laser to the passband wavelength of the photoreceiver. The connection may be broken, and a new connection established with a different receiver node, by re-tuning the laser's wavelength.

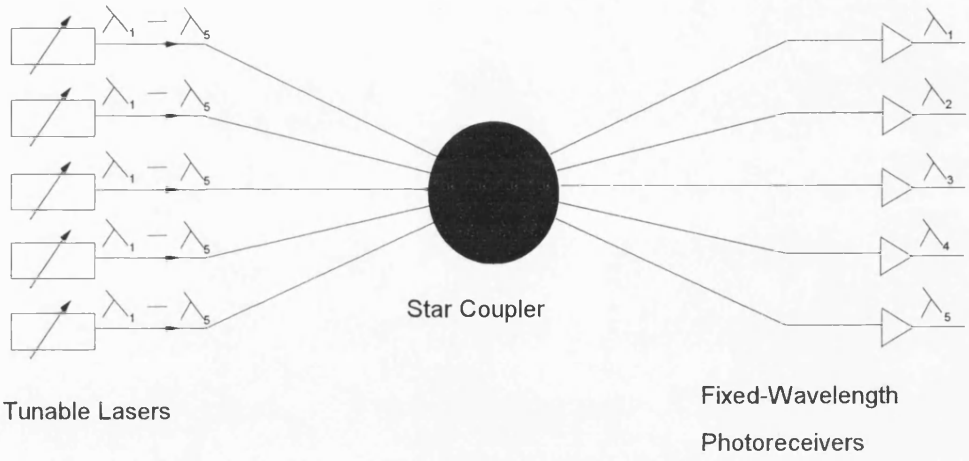

Figure 1.3. An example of one broadcast-and-select network with tunable lasers and fixed-wavelength receivers.

The lasers used in this application are required to have a total tuning range of at least $(N-1)\Delta\lambda$, where N is the total number of receiver nodes and $\Delta\lambda$ is the channel spacing. Thus, with the wavelength spacing of the order of nanometers in a WDM system, the tuning range that is required can be very large (several tens of nanometers). Another important issue is the time that it takes to make a connection between two nodes. The rate at which connections can be established and broken is limited by the tuning speed of the lasers and by the time it takes for the wavelengths to settle down after tuning.

The requirements of the tuning speed and total tuning range (i.e. total number of channels) vary considerably. For example, if achieving the maximum throughput of a star-based network is the goal, then a very large tuning range (or number of channels) will be required. If the transmitters are used for carrying home entertainment video, they may not

require as short tuning time as the transmitter that is operated as an information gateway. If the transmitter is operated in the internal part of a high speed switch, even shorter tuning time may be required.

In addition to the requirement for wavelength tunable lasers, broadcast-and-select networks could also benefit from a multiwavelength laser. Replacing the wavelength tunable laser in figure 1.3 with multiwavelength lasers whose wavelengths correspond to the photoreceiver passbands would allow a transmitter node to be connected to any number of the receiver nodes simultaneously.

B. Wavelength Routing Networks

Wavelength routing networks are composed of one or more wavelength-selective elements (unlike the star coupler used in the broadcast-and-select networks). A good example of a wavelength-selective component is the grating -based multiplexer that was discussed in section 1.2.1. The wavelength routing networks have the property that the network signal path is uniquely determined by the wavelength of signal and the port through which the signal enters the network.

Figure 1.4 is a schematic diagram of 4×4 wavelength routing network, which shows one possible interconnection pattern and arrangement of WDM units and the associated wavelength assignment table. By tuning to a selected wavelength, the signal from a given laser can be routed to a selected output port on the network. A connection is established between a given input port and a given output port by tuning a laser at the input to the appropriate wavelength as determined from the wavelength assignment table. By retuning the laser's wavelength, the connection may be broken and a new connection established with a different output port. It can be seen from the figure that the origin of a signal arriving at an output may be uniquely determined from the signal's wavelength. This is not true in the broadcast-and-select network.

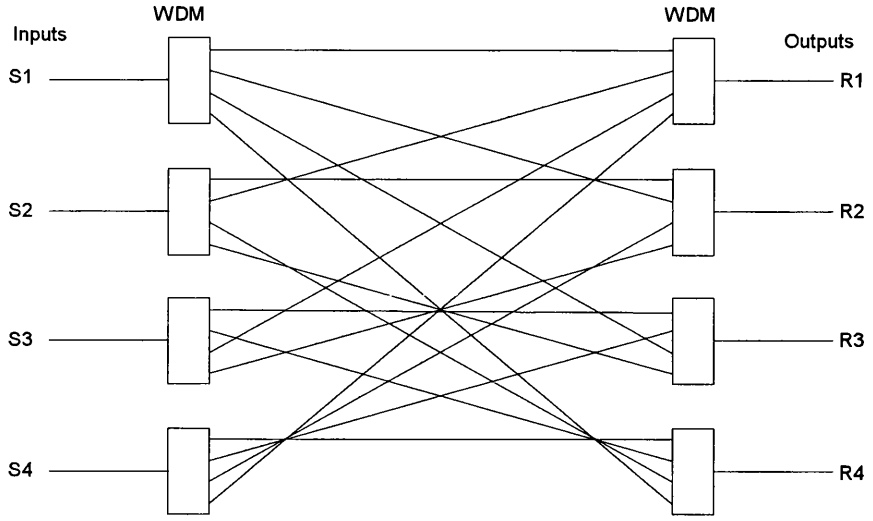

(a)

INPUT	OUTPUT			
	R1	R2	R3	R4
S1	λ0	λ1	λ2	λ3
S2	λ1	λ0	λ3	λ2
S3	λ2	λ3	λ0	λ1
S4	λ3	λ2	λ1	λ0

(b)

Figure 1.4. An example of: (a) a 4×4 WDM interconnection network; and (b) the associated wavelength assignment table. N wavelengths can always be used to complete interconnection an N×N network.

The laser requirements for this wavelength routing network are essentially the same as those for the broadcast-and -select network. In other words, a large tuning range allows more nodes to be included in the network. Fast tuning is required for rapid setting up and breaking down of connections, while an accurate and repeatable tuning mechanism is required to prevent excessive and unpredictable attenuation. In addition, using multiwavelength lasers rather than wavelength-tunable lasers, would make it possible for a single input node to be simultaneously connected to any number of output nodes.

1.3 Optical Time Division Multiplexing Technologies

The basic principle of the optical time-division multiplexing (TDM) is the direct construction of a high bit-rate data stream by time multiplexing several lower bit-rate optical streams [13]. The optical TDM approach is a purely digital technique. Since an optical pulse normally occupies a small portion within the modulation period, it is possible to allocate each of the baseband data streams in a series of time slots on the multiplexed signal. Figure 1.5 shows a schematic diagram of optical time-division multiplexed transmission systems. A train of picosecond duration optical pulses from a suitable laser source is split N ways. Each train is individually modulated by a tributary electrical data signal resulting in N optical data channels. Each of these is optically delayed by a fraction of the clock period and synchronised to allow a passive multiplexer (MUX) to produce a high bit rate multplexed signal. Demultiplexing (DMUX) and clock recovery allows the input optical signal to be split into the discrete channels and terminated.

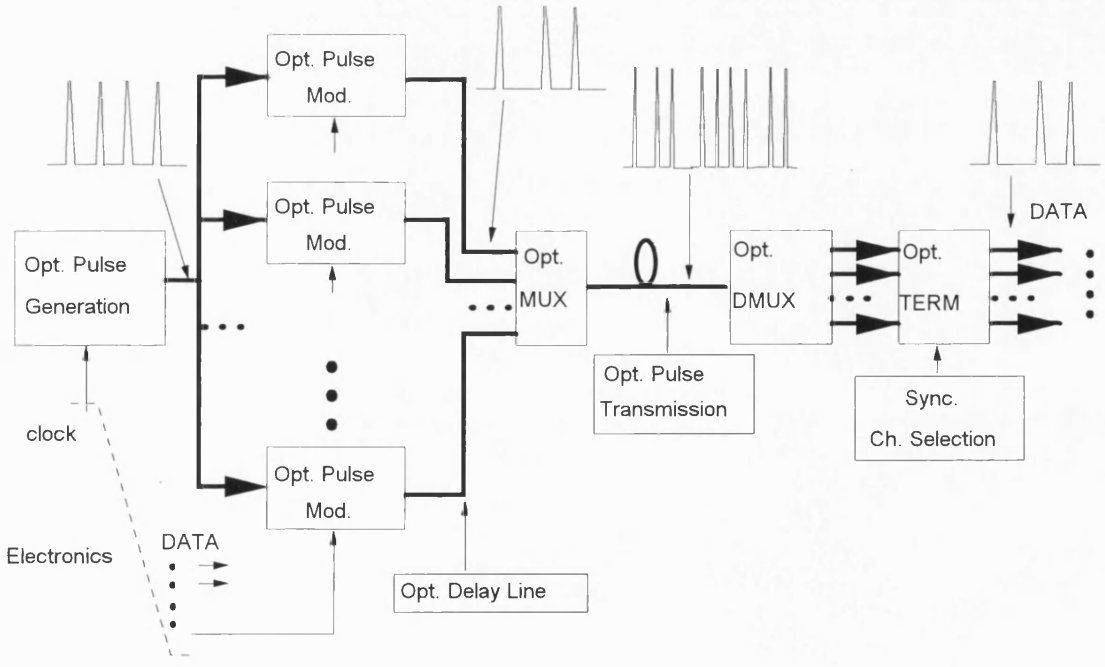

Figure 1.5. Schematic of optical time-division multiplexed lightwave systems.

The operation of time-multiplexing several lower bit rate baseband channels onto a higher bit-rate data can be divided into three subfunctions: sampling, timing, and combining [13]. The sampling function takes samples of the incoming baseband data stream, thereby identifying the value of each incoming bit. The timing function ensures that the samples are available at the correct time slots on the multiplexed channel. The combining function assembles all the sampled baseband data stream to generate the higher bit-rate multiplexed data stream. It is convenient to sample each of the input data streams using short sampling pulses that are timed to correspond to the appropriate time slots on the multiplexed bit system. If the sampling pulsewidths are less than one bit-period of the high bit-rate multiplexed signal, the combiner can be a simple summing circuit. This strategy is a preferred approach to optical time-division multiplexing because it can capitalise on mode-locked and gain-switched semiconductor lasers, which are capable of generating pulses more than ten times shorter than electrical pulses or modulation period. In this approach, the sampling function is carried out in the electro-optic converters (i.e., the system transmitters). Consequently, the MUX in figure 1.5 is required only to do the combining function.

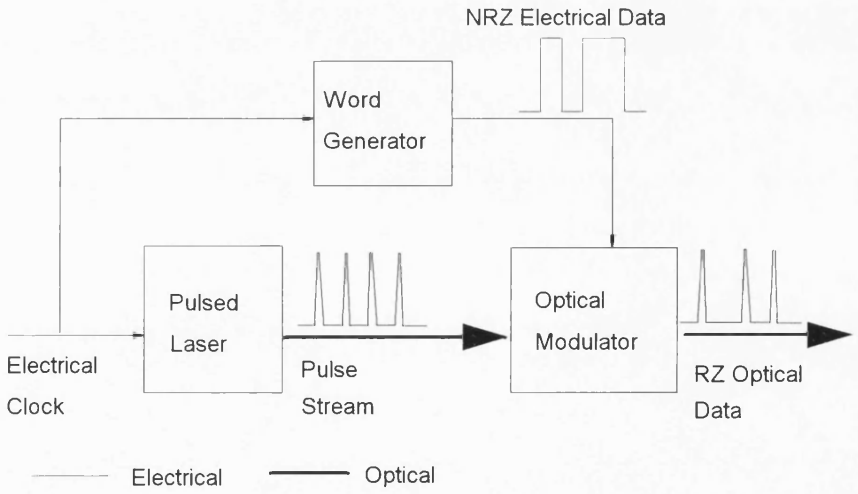

Figure 1.6. Schematic diagram of an electro-optic converter that samples input data using optical short pulse semiconductor laser.

Figure 1.6 shows the schematic of an electro-optic converter (transmitter) that can

be used to sample the input data before optical combining. Short optical pulses from a laser are incident on an optical modulator, which is driven by an input electrical data stream. The electrical data stream could be either in the return-to-zero (RZ) or non-return-zero (NRZ) format, but NRZ is usually preferable because it minimises the bandwidth requirements of the baseband digital electronics, the modulator and its drive laser. The optical pulse train from the laser samples the electrical input data via the modulator, thereby converting it from NRZ in the electrical domain to RZ in the optical domain. In practice, the clock must drive both the laser and word generator, thereby ensuring that the electrical data is synchronised to the optical pulses. Optical modulators such as $LiNbO_3$ waveguide electrooptic device can be used for carrying out data encoding and sampling [21].

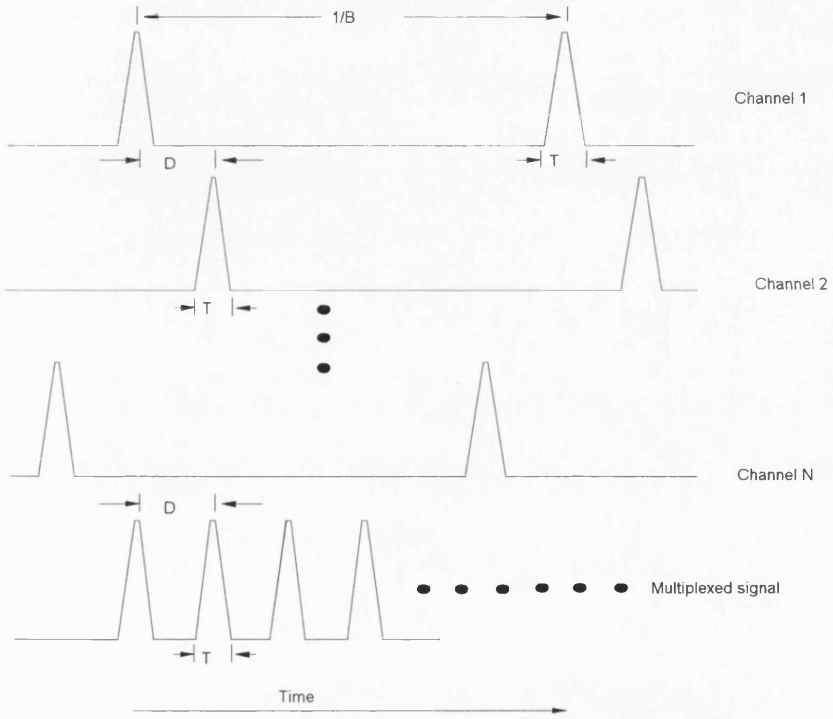

Figure 1.7. Timing scheme for multiplexing in an N channel optical TDM system.

For the timing scheme of a N-channel optical time division multiplexed system, as shown in figure 1.7, the N optical signals incident on the combiner are RZ pulse trains with repetition rates B and with pulsewidth T (measured at the baseline). The incoming bit

streams are temporally offset from one another by the delay D. When the pulse spacing is adjusted for maximum multiplexed bit rate, each pulse in the multiplexed bit stream just comes into contact with its nearest neighbours. Under these circumstances D=T, and the multiplexed bit rate is 1/T. If the pulsewidth of laser is 10 ps at the baseline, the multiplexed bit rate could be as high as 100 Gbit/s. In practice, the pulse streams are delayed with respect to one another using delay elements either in the electrical clock paths [22] (such as microwave delay lines) or in optical signal paths [13].

The combining function can be handled in many ways. One method is to use multiple optical pulse generators [13]. These optical pulse generators could be mode-locked or gain-switched semiconductor lasers, which are all driven by the same master clock. The pulse streams are delayed with respect to one another using delay elements in the electrical clock paths. Data encoding and sampling can be carried out using optical modulators at the outputs of the pulse generators. The data-encoded pulse streams are brought together in the optical combiner. Another way is to use a single optical pulse generator [23] as illustrated in figure 1.5.

Demultiplexing and clock recovery allows the input optical signal to be split into discrete channels and terminated. For good system sensitivity, it is necessary that most photons from each incoming bit are transferred to the appropriate electro-optic converter. The optical demultiplexer should switch the entire bit rather than just sample part of it. In addition, the crosstalk between channels should be small.

To enable demultiplexing with low interchannel crosstalk, optical TDM transmission systems need to operate with optical pulses that are significantly less than the duration of the allowed time slot. The pulses have to be as spectrally pure as possible so that pulse broadening problems due to the interaction of source chirp with fibre chromatic dispersion are minimised. In addition, the power and wavelength of the optical pulse signal should both be adjusted to optimise the transmission characteristics for the fibre system. There are three main types of laser pulse sources that are used in optical TDM system demonstrations; the

semiconductor mode-locked laser [24], gain switched semiconductor laser [25] and colliding pulse mode-locked lasers [26]. The operating principle and practical techniques of these lasers will be discussed in more detail in chapter four.

1.4 Wavelength- and Time- Division Multiplexed Systems

Optical TDM can be used on each wavelength of the WDM systems to further increase the transmission capacity and channel distribution capability. Such a scheme is commonly referred to as wavelength and time division multiplexing (WTDM) [27,28]. A node is assigned time slots during which it may transmit on its allocated wavelength. Each node has the opportunity to transmit to specific receivers in an allocated cycle of time slots. Although time-division multiplexing the WDM channels reduce the bandwidth available to each node, the bandwidth of optical systems usually exceed the ability of the electronics to sustain continuous transmission.

Recently, a network based on WTDM has been demonstrated, which, using 16 wavelengths, provides a total capacity of 39.8 Gbit/s [29]. There are several architectures of WTDM systems, and here a simple example of a WTDM network is given for explanation of its basic principles. Figure 1.8 shows a schematic diagram of a WTDM network using tunable wavelength optical filters. Digital signals are time- division multiplexed into a high speed digital signal at each local centre. Each local centre transmits the TDM signal using an optical transmitter whose wavelength corresponds to the pre-assigned wavelength channel. Optical signals with a different wavelength from the local centres are wavelength-division multiplexed at the centre star-coupler and then sent back to each local centre. The wavelength division and time division multiplexed signals are divided for simultaneous processing and monitoring of a certain number of signals, after which each wavelength tunable filter arbitrarily selects one wavelength channel. After wavelength channel selection, the desired signal is selected using a time division demultiplexer and then converted into the

electronic signals. In this network, all signals can access to all destinations on a single optical-fibre bearer, this minimises cabling whilst ensuring that all sources are available to all destinations. It is also shown that a large number of digital signals can be handled with reasonable wavelength division and time division multiplexers. Moreover, the local centre does not require high speed electrical switching.

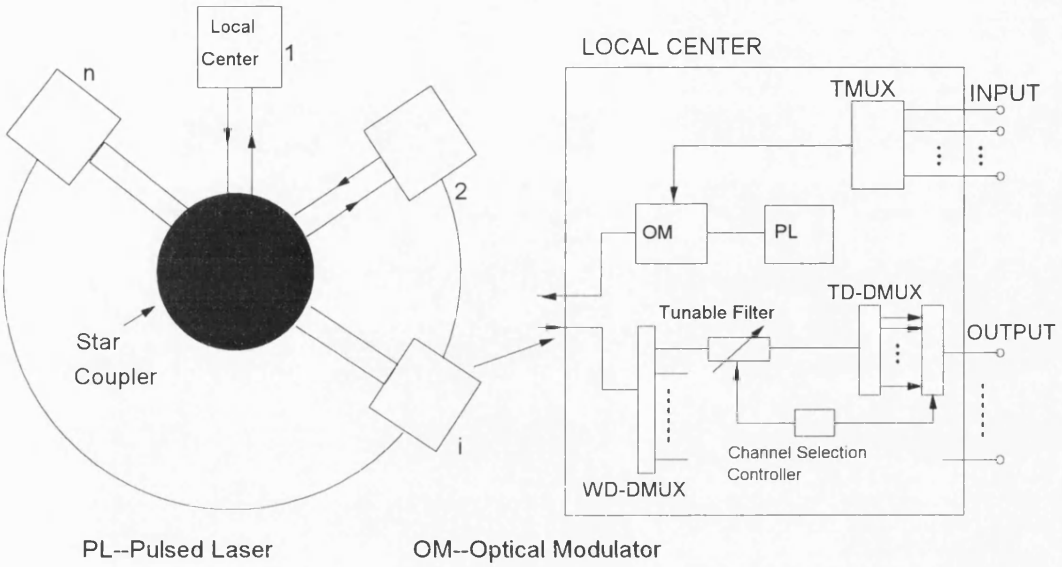

Figure 1.8. A schematic diagram of WTDM network using tunable wavelength optical filters.

The main technologies required for the optical WTDM system are multiwavelength laser technologies, optical pulse generation/modulation and all-optical multi/demultiplexing techniques. The multiwavelength sources capable of generating multiwavelength picosecond optical pulses are essential for the WDM and TDM systems.

The future of WDM and TDM systems is largely determined by the availability of reliable and efficient optical components such as multiwavelength laser sources, tunable filters or optical receivers, broadband optical amplifiers, large transmission star couplers, and ultrashort optical pulse generation in semiconductor lasers. Recently, extensive research efforts in optoelectronics have produced encouraging results in many critical components for the WDM and TDM systems. These results include erbium-doped fibre amplifiers,

tunable optical filters [30], star couplers [20], DFB laser arrays [31-32], and the multiwavelength lasers [33-34]. Some of the above devices have been placed on the market, but some critical components are still in the laboratory, which need to be improved. A brief review of the state of the multiwavelength laser sources is given in the following chapter.

1.5 Objective of Thesis

A key objective of this work is to develop and investigate a type of multi-wavelength semiconductor laser that is intended for use as a transmitter source in optical multiplexing communication systems. We have called this laser multichannel grating cavity (MGC) laser, which is constructed as both bulk optic and integration structures. The research work on the bulk MGC laser is aimed at investigating for more advanced applications such as high speed digital modulation and multi-wavelength picosecond optical pulse generation. For the integrated micro-optic version, the work is basically involved in the design, assessment and demonstration of its proto-type form, and then leads to successful operation of the laser.

The basic properties of the MGC laser can be summarised as follows;

-- The laser gives emission at a number of discrete wavelengths, and each wavelength and spectral channel separation are simply determined by the geometry of the cavity structure. The wavelengths cover a broad spectral range.

-- The laser can be used for both wavelength switching and simultaneous multi-wavelength emission.

-- Each wavelength can be independently digitally modulated by direct current injection into an appropriate stripe of the device. The integrated device is expected to be modulated at rates in excess of 1 Gbit/s.

-- The laser can generate a number of WDM channel picosecond optical pulses which can easily be synchronised, or controlled with a programmable relative delay between the

channels, or switched from one channel to another.

--The laser can produce relatively high power both on the cw and short pulse operation for wide applications in the WDM and TDM systems.

1.6 Summary

This chapter has reviewed the recent advances and trends in the optical fibre communication systems. The immense optical transmission bandwidth of optical fibre has stimulated interest in use of a WDM system combined with TDM technologies in high bit-rate broadband optical communication networks. The WDM promises to add an important new degree of freedom to optical communications. Potential applications include higher-capacity point-to-point transmission, wavelength -based switching systems, and a variety of new networking and routing architectures. The WDM technology requires that different spectral channels are well allocated to different services, where multiwavelength laser sources and tunable filters or optical receivers are required. The TDM technology requires that different services can be transmitted during different time slots, where optical pulse generation/modulation, optical timing extraction and all-optical multi/demultiplexing are essential photonic techniques.

In order to implement efficiently WDM and TDM technologies in multichannel networks, mutliwavelength transmitter laser sources are required. In particular, multiwavelength sources with well a defined channel spacing, of the order of several nanometres, narrow spectral linewidth and high-speed pulse-code modulation could allow cheaper and simpler, direct-detection, broadband WDM and TDM to be constructed.

This thesis describes the design and characteristics of a type of multi-wavelength semiconductor laser for the WDM and TDM applications. The laser should give emission at a number of discrete wavelengths, each wavelength can be independently digitally modulated by direct current injection into an appropriate stripe of the device. The

wavelengths of the laser cover a broad spectral wavelength range. The functionalities of both wavelength switching and simultaneous multiwavelength operation are expected to be implemented in this laser. The laser can generate a number of WDM channel picosecond optical pulses which can easily be synchronised, or controlled with a programmable relative delay between the channels, or switched from one channel to another. The output powers of the MGC laser are relatively high for wide applications in WDM and TDM systems.

References

[1]. T. P. Lee, "Recent advances in long wavelength semiconductor laser for optical fiber communications," *IEEE Proceedings*, vol. 79, pp.253-276, 1991.

[2]. S. Kawanishi, H. Takara, O. Kamatani and T. Motioka, "100 Gbit/s, 500 km optical transmission experiment," *Electron. Lett.*, Vol. 31, pp.737-738, 1995.

[3]. R.N. Hall, G.E. Fenner, J.D. Kingsley, T.J. Soltys, and R.O. Carlson, " Coherent light emission from GaAs junctions", *Phys. Rew. Lett.* vol. 9, pp.366-368, 1962.

[4]. J.E.A. Whiteaway, G.H.B. Thompson, A.J.Collar and C.J. Armistead, "The design and assessment of $\lambda/4$ phase-shifted DFB laser structures" *IEEE J. Quantum Electron*, vol. 25, pp.1261-1279, 1989.

[5].T. R. Chen, J. Ungar, X. L. Yeh, and N. Bar-Chaim, "Very large bandwidth straned MQW DFB laser at 1.3 μm," *IEEE Photon. Technol. Lett.* vol.7. pp.458-460, 1995.

[6]. C.J. Chang-Hasnain, M.W.Maeda, J.P.Harbison, L.T.Florez, and C.Lin, "Monolithic multiple wavelength surface emitting laser arrays", *IEEE J. Lightwave Technol.*, LT-9,pp.1665-1669, 1991.

[7]. P. B. Hansen, G. Raybon, U. Koren, B. I. Miller, M. G. Young, M. A. Newkirk, M.-D. Chien, B. Tell, and C. A. Burrus, " Monolithic semiconductor soliton trasmitter", *IEEE J. Lightwave Technol.*, LT-13,pp.297-301, 1995.

[8]. E. Dietrich, B. Enining, G.Grosskopt, L.Kuller, R.Ludwing, R.Molt, E. Patzak and H.G. Weber, "Semiconductor laser optical amplifier for multichannel coherent optical transmission", *IEEE J. Lightwave Technol.*, LT-7, pp.1941-1955, 1989.

[9]. L. Goldberg, D. Mehuys, M. R. Surette, and D. C. Hall, "High power, neardiffraction limited large area travelling-wave semiconductor amplifers" *IEEE J. Quantum Electron, QE-29.* pp.2028-2043, 1993.

[10]. R.J. Mears and S.R. Baker. "Erbium fibre amplifiers and lasers", *Optical and Quant. Electron.*, vol. 24, pp.517-538, 1992.

[11]. K. Nosu and M.J. O'Mahony."Optically multiplexed networks", *IEEE Communications Magazine*, Dec, pp.20. 1994.

[12]. C.A.Brackett. "Dense wavelength division multiplexing networks: principles and applications". *IEEE J Selected Areas in Commun.*, SAC-8, pp.948-964, 1990.

[13]. R.S.Tucker, G.Eisenstein and S. K. Korotky, "Optical time-division multiplexing for very high bit-rate transmission", *IEEE J. Lightwave Technol.*, LT-6, pp.1737-1749, 1988.

[14]. N. K. Cheung, C. R. Sandahl, J. Lipson and N. A. Olsson, "A three channel wavelength division multiplexing experiment in single mode fiber at 432 Mb/s," in Proc. Optical Fiber Conf., New Orleans, USA, pp.30, 1984.

[15].N.A. Olsson, J. Hegarty, R. A. Logan, L. F. Johnson, K. L. Walker, L. G. Cohen, B. L. Kasper

ans J. C. Campbell, "68.3 km transmission with 1.37 Tbit km/s capacity using wavelength division multiplexing of ten single-frequency lasers at 1.5 μm, " *Electron. Lett.*, Vol. 21, pp.105,1985

[16]. P. A. Kirkby, "Multichannel wavelength switched transmitters and recievers--New component concepts for broad-band networks and distributed switching systems," *IEEE J. Lightwave Technol., LT*-8. pp.202-211, 1990.

[17]. M. S. Goodman, H. Kobrinski M.P. Vecchi, R. M. Bulley and J. L. Gimlett, "The LAMBDANET multiwavelength network: architecture, applications, and demomonstrations," *IEEE J Selected Areas in Commun.*, SAC-8, pp.995-1003, 1990.

[18]. S. S. Wagner and H. L. Lemberg, " Technology and system issues for a WDM-based fiber loop architecture," *IEEE J. Lightwave Technol., LT*-7, pp.479-488, 1989.

[19]. N. R. Dono, P. E. Green, Jr., K. Liu. R. Ramaswami and F. Fuk-Kay Tong, " A wavelength division multiple access network for computer communication," *IEEE J Selected Areas in Commun.*, SAC-8, pp. 983-994, 1990.

[20]. C. Dragone, C.H. Henry, I.P. Kaminow, and R.C. Kistler, "Efficient multichannel integrated optics star coupled on silicon," *IEEE Photon. Technol. Lett.*, vol. 1, pp.241-243, 1989.

[21]. S. K. Korotky, G. Eisenstein, R. C. Alferness, J. J. Veselka, L. L. Buhl, G. T. Harvey, and P. H. Read, "Fully connectorized high-speed Ti: LiNbO3 switch/ modulator for time -division multiplexing and data encoding," *IEEE J. Lightwave Technol.*, LT-3, pp. 1-6, 1985.

[22]. R. S. Tucker, G. Eisenstein, S. K. Korotky, U. Koren, G. Raybon, J. J. Veselka, L. L. Buhl, B. L. Kasper and R. C. Alferness, "Optical time division multiplexing and demultiplexing in a multigigabit /second fiber transmission systems," *Electron. Lett.*, vol. 23, pp.208-209, 1987.

[23]. D. M. Spirit, A. D. Ellis, and P. E. Barnsley."Optical time division multiplexing: Systems and networks", *IEEE Communications Magazine*, pp.56-62, 1994.

[24]. A.Takada, T. Sugie and M. Saruwatari, "High-speed picosecond optical pulse compression from gain-switched 1.3 μm distributed feedback (DFB) laser diode through highly dispersive single-mode fibre", *IEEE J. Lightwave Technol.*, LT-5, pp.1525-1533, 1987.

[25]. D.J. Derickson, R. J. Helkey, A. Mar. J. R. Karin, J. G. Wasserbaner, and J.E. Bowers, " Short pulse generation using multisegenent mode-locked semiconductor laser", *IEEE J. Quantum Electron*, vol. 28, pp.2186-2201, 1992.

[26]. Y.K. Chen and M.C. Wu, "Monolithic colliding-pulse mode-locked quantum-well lasers", *IEEE J. Quantum Electron*, vol. 28, pp.2176-2185, 1992.

[27]. I. Chlamtac and A. Ganz, "Toward alternative high speed network concepts: The swift architecture." *IEEE Trans. Commun.*, Vol. 38, pp.431-439. 1990.

[28]. K.A.Williams, T.Q. Dam and D.H.-C. Du " A media - access protocol for time- and wavelength division multiplexed passive star networks", *IEEE J Selected Areas in Commun.*, SAC-11, pp.560-569, 1993.

[29]. L. J. ST. Ville, C. L. Nuttall, P.W. Walland, J. C. Newell, A. Oliphant, G. J. Cannel, C. Bunney, J. P. Laude, P. Leroux, M. J. Anson,"Developments in WTDM technology for high - capacity optical studio networks", *Optical and Quantum Electron.*, vol. 26, pp. S483-496. 1994.

[30]. M. W. Meada, J.S. Patel, C. Lin, J. Horrobin, and R.S. Spice, " Electrically tunable liquid-crystal-etalon filter for HD-WDM systems", *IEEE Photon. Technol. Lett.*, vol. 2, pp.820-822, 1990.

[31]. M.Nakao, K.Sato, T.Nishida, and T.Tamamura," Distributed feedback laser arrays fabricated by synchrotron orbital radiation lithography", *IEEE J Selected Areas in Commun.*, SAC-8, pp.1178-1182, 1990.

[32]. Y.H.Lo, L.A. Wang, A.S. Gozdz, P.S.D.Lin, M.Z.Iqbal, R.Bhat and T.P. Lee, " Four channel integrated DFB laser array with tunable wavelength spacing and 40-Gb/s signal transmission capacity", *IEEE J. Lightwave Technol.*, vol. LT-11, pp. 619-623, 1993.

[33]. I. H. White, "A multichannel grating cavity laser for wavelength division multiplexing applications", *IEEE J. Lightwave Technol.*, vol. LT-9, pp.893-899, 1991.

[34]. J.B.D. Soole, K. Poguntke, A. Scherer, H. P. Leblance, C. Chang-Hasnain, J.R. Hayes, C.Caneau, R. Bhat and M.A. Koza, "Multistripe array grating integrated cavity (MAGIC) laser; A new semiconductor laser for WDM applications", *Electron. Lett.*, vol. 28, pp.1805-1807, 1992.

Chapter 2

LASER SOURCES FOR WAVELENGTH DIVISION MULTIPLEXING APPLICATIONS

2.1 Introduction

Chapter one has identified the WDM and optical TDM techniques as methods for enhancing the performance of optical communication systems. WDM systems promise not only to increase transmission capacity but also to provide new flexible network-oriented functions such as exchange-free signal routing. However, the practical deployment of WDM and optical TDM communication systems presents major challenges to optical source technology. Depending on the applications, optical terminals may be required to provide rapid wavelength tuning or selection, or to independently provide extraordinary wavelength precision and stability, or simultaneously provide multi-wavelength high speed modulation or ultrashort pulse operation.

This chapter surveys various approaches for achieving WDM sources, whereas short optical pulse sources for the optical TDM will be described in chapter four. The WDM laser sources that are described in this chapter are grouped into three categories based on the device structure and operating properties, i.e., wavelength tunable semiconductor lasers, multiwavelength laser arrays, and monolithic integrated multiwavelength lasers. The issues that are discussed here are the device structure, the principles of operation and the performance criteria such as wavelength stability and reliability, wavelength switching range and speed, modulation capacity, and optical output power. Some of these devices are already available, while others are still at the development stage.

A basic property of the semiconductor laser is that its spectral gain profile of the active material is many times larger than the longitudinal mode spacing of its resonant optical cavity (provided that the cavity length is greater than a few microns). The laser predominantly operates in the mode that has the largest gain margin (defined as the gain minus the loss incurred in one round trip of the cavity). In the case of the basic cleaved-facet Fabry-Perot (FP) laser, the round-trip loss is essentially the same for all of the modes, so the mode selectivity mechanism in this kind of laser is poor and an appreciable fraction of the output power occurs in modes to either side of the dominant mode [1]. As mentioned in the previous chapter, the applications for WDM systems require that the power occur predominantly in a single longitudinal mode (commonly referred to as single-frequency operation) and that the wavelength for each system channel be precisely controlled. Therefore, an alternative mechanism for wavelength definition and tuning is needed. The degree to which emission occurs on a single mode is measured by the ratio of the intensity in the dominant mode to that in the most intense side-mode; this ratio is known as the side-mode suppression ratio (SMSR).

Section 2.2 discusses the wavelength tunable lasers, including grating-tuned external cavity semiconductor lasers [2-5], tunable distributed feedback (DFB) lasers [6-8], and tunable multiple electrode DBR lasers [9-11]. These devices integrate some frequency selective grating elements inside the laser cavity to achieve single-frequency oscillation. The wavelength tuning is obtained either by changing the refractive index in the waveguide region (e.g., DFB/DBR laser), or by mechanically controlling the peak wavelength of the frequency filter passband. Section 2.3 describes two kinds of multiwavelength laser arrays, which are DFB/DBR laser arrays [12-16] and vertical cavity surface emitting laser (VCSEL) arrays [17-18]. These devices comprise a number of wavelength-tunable or single frequency devices (operating at different wavelengths), whose outputs are coupled together. The differences in these lasers are mainly in the structure and method of integration that is employed in an attempt to reduce the component count and packaging

costs. Monolithic integrated multi-wavelength lasers, including the multistripe array grating integrated cavity laser [19-21] and waveguide grating router laser [22-24], are discussed in section 2.4. In these lasers, semiconductor amplifiers are monolithically integrated together with an optical multiplexer, and they are capable of producing a comb of exactly spaced frequency from a single output port. Therefore they do not need an extra optical multiplexer to combine the different wavelength. The differences in these lasers are mainly in the element of optical multiplexer which acts as a wavelength selective filter and the method in which the multiwavelength emission is realised. A brief summary is finally given in section 2.5.

2.2 Wavelength Tunable Semiconductor Laser

This section reviews a range of wavelength tunable semiconductor lasers. These laser devices use some form of spectral filtering to rearrange the gain margins of the various modes. A filter incorporated into the laser cavity increases the optical loss (and therefore decreases the gain margin) of those modes that lie outside of its passband. With sufficient attenuation from the filter, the dominant mode in the laser's spectral output is that which lies closest to the centre of the passband. Single-frequency operation is achieved if the filter passband is narrow enough to select only one cavity mode at a time. Discrete tuning is exhibited by those devices in which the position of the filter passband can be adjusted so as to scan across the cavity modes. This causes the different modes to be selected one after another. Continuous tuning, on the other hand, can be achieved if the wavelength of the filter passband and of the cavity modes can be adjusted in such a way that they scan in unison. Differences between the various wavelength-tunable lasers lie in the type of filter that is used and in the physical mechanism upon which tuning is based.

A. Grating Tuned External-Cavity Lasers

The most common method of constructing a tunable laser is to use a semiconductor chip as the gain medium in an external cavity with a diffraction grating serving both as a mirror and as a narrow band filter [2]. An typical arrangement is shown in figure 2.1. One facet of the Fabry-Perot laser chip is anti-reflection (AR) coated in order to nullify its intrinsic reflectivity. Reflective feedback is provided instead by the collimating lens and diffraction grating. The spectral width of the reflectivity peak (i.e. the filter passband) is determined by the grating resolution, the grating dispersion and the width of the laser diode's active region. With both a good AR coating and efficient feedback from the grating, the external resonant cavity can be formed by the cleaved uncoated facet and the diffraction grating. The laser then operates on the external cavity mode that lies closest in wavelength to the reflectivity peak.

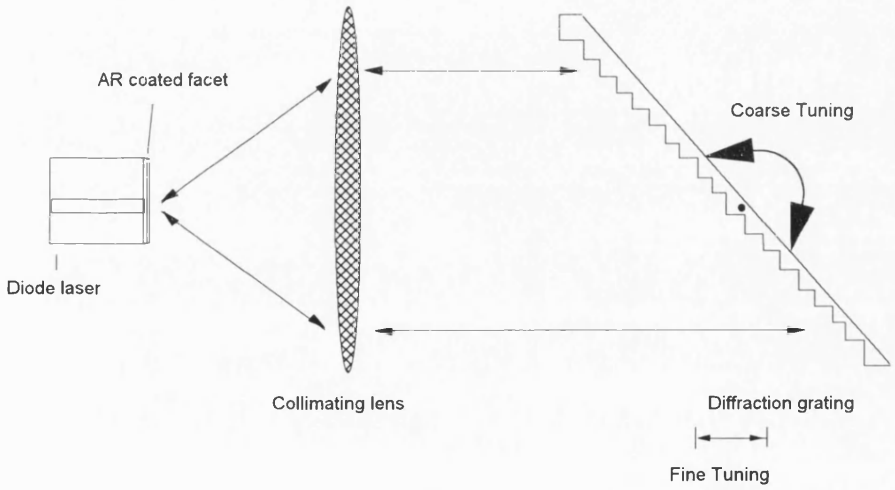

Figure 2.1 Schematic diagram of diffraction grating loaded external cavity laser.

The lasing frequency may be tuned by rotating the diffraction grating. This alters the angle at which the collimated beam of light is incident upon the grating and therefore changes the central wavelength for the filtered external feedback. Fine tuning can be achieved by axial displacement of the grating, or by adding an adjustable phase plate [3]. In principle, a tuning range over the entire width of the gain spectrum is possible. A tuning range in excess of 55 nm was obtained [2] using laser diodes with bulk active regions, while second subband recombination in quantum well active regions was used to

demonstrate a tuning range of 240 nm [4].

In addition to the large tuning range, the grating external cavity laser has advantage of a very narrow linewidth. Replacing the cleaved-facet mirror by an external mirror modifies the laser linewidth by a factor of $(L/L_{ext})^2$ [5], where L_{ext} is the total optical length of the external cavity and L is the optical length of the laser diode's active region. The laser of reference [2], for instance, exhibited a linewidth of just 10kHz.

The principal disadvantage of the grating external cavity laser is its relatively slow tuning speed. Even if piezoelectric transducers are used to rotate and translate the grating, the maximum tuning rates that can be achieved are in the microsecond regime. Other disadvantages of the grating external cavity laser are mainly related to the fact that it is a hybrid device. The bulk-optic components require careful alignment and stabilisation. Residual reflection from the coated facet of the laser diode can also cause excitation of its internal Fabry-Perot modes, and interferometric coupling between these internal modes and modes of the external cavity can result in poor and unpredictable tuning control.

B. Tunable DFB Lasers

The distributed feedback (DFB) laser [6] is one of various monolithic integrated tunable lasers, in which the feedback is distributed throughout the cavity length. Light propagating along the laser waveguide structure experiences a periodic variation in its effective refractive index. This index variation is caused by variation in the thickness of a semiconductor layer lying either above or below the laser's active region. As a result of this structure, a Bragg grating filter provides a frequency-dependent feedback by means of backward Bragg scattering [1].

The basic idea behind the tunability of DFB lasers is simple. The operating wavelength of such lasers is determined by the etched grating through the Bragg wavelength given by $\lambda_o=2\mu\Lambda/m$, where μ is the effective-mode index, Λ is the grating period, and m is the diffraction order of the grating. Even if the grating period Λ is fixed

during grating fabrication, the laser wavelength can be changed by changing the effective-mode index μ. A simple way to change the effective-mode index is to change the refractive index by injecting current into the grating region, since the refractive index depends on the injected carrier density. In general, the refractive index decreases with an increase in the carrier density, resulting in a shift of the Bragg wavelength (and hence the laser wavelength) toward shorter wavelengths with an increase in the injected current.

However, because the Bragg grating region in the single-electrode DFB laser is fabricated in a layer that lies directly above or below the active region, the current that is used to inject free-carriers into the grating region is the same current that is used to control the gain. So that the range over which this current can be varied is somewhat limited. If the current is reduced below its threshold value, then the device will cease to lase; if, on the other hand, the current becomes too high, then the associated increase in optical power could lead to optical induced device degradation. Furthermore, with the laser operating in the above-threshold regime, most injected carriers recombine to produce photons, resulting in a very small increase in carrier density, which in turn leads to a small change in lasing wavelength.

An alternative method for tuning the lasing wavelength of the DFB laser is by changing its operating temperature. This modifies the optical periodicity of the Bragg grating and changes the refractive index, resulting in a change of lasing wavelength. For a typical DFB laser, the tuning rate is about 0.1 nm/ ^{o}C [10]. However, the threshold current and efficiency of the laser are very temperature sensitive, and increasing the temperature causes the output power to decrease, so the practical tuning range is limited to around $\pm$ 1nm.

The range of wavelength tuning can be improved by using a two- or three- electrode DFB laser with a large current applied to one electrode and a small current to the other [7]. A schematic diagram is shown in figure 2.2. In the two electrode DFB laser, the optical field is higher in the region near the output port where the facet is not reflecting

(AR coated for example), and the wavelength is primarily determined by the effective index of refraction in this region. With this section pumped at current densities at or slightly below the normalised threshold current density, which is just enough to overcome the absorption loss, it serves as a Bragg reflector. In addition, because of the low pumping level, the injected carriers do not contribute significantly to photon generation, resulting in large change of the refractive index, thereby a substantial wavelength tuning. The gain is provided by the other section pumped substantially above threshold. In the three electrode DFB laser, the two outer electrodes are electrically connected with a common current supply, while the central electrode is supplied with a different current. A continuous tuning range of 1.9 nm was obtained by varying the ratio of these two currents [8].

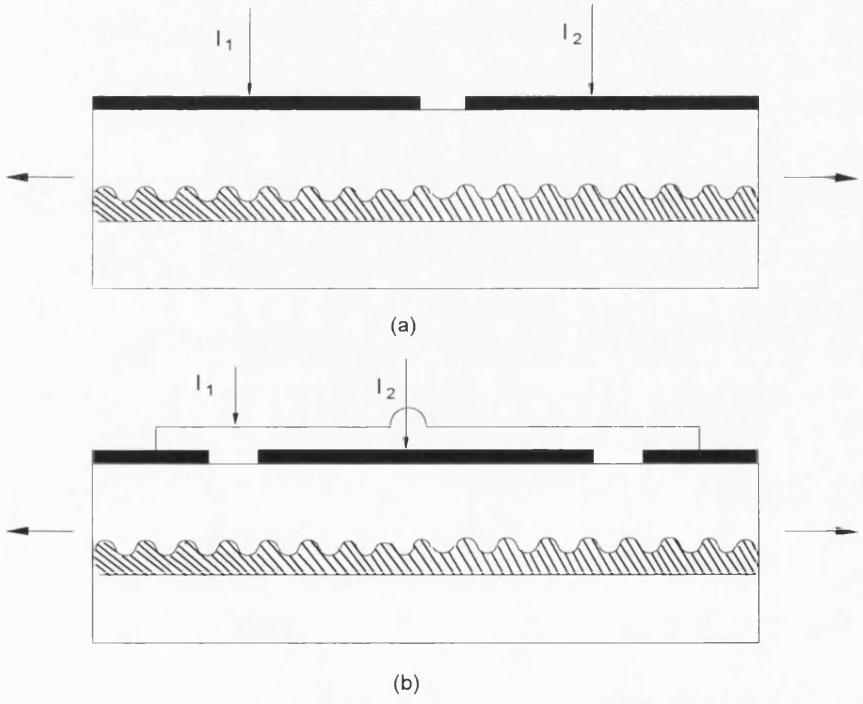

Figure 2.2 Schematic diagram of wavelength tunable DFB laser, (a) two-electrode DFB laser, (b) three-electrode DFB laser.

The advantages of the tunable DFB laser are its high tuning speed (nanosecond regime readily achievable), high SMSR and its ease of fabrication stabilisation [8]. The disadvantage is the limited tuning range (only several nm tuning range can be achieved)

because the tuning section must be biased below the threshold. When the tuning section is biased above threshold, both sections can oscillate independently, resulting in a two-mode operation or mode hopping.

C. Tunable Multiple-Electrode DBR Laser

Improvements of the wavelength tuning range have been made by separating the Bragg grating region in the passive waveguide from the active waveguide inside the laser cavity. This can be achieved by distributed Bragg reflector (DBR) laser [9-11]. A two-electrode DBR laser is schematically shown in figure 2.3 (a). Cavity reflectivities in this device are provided by a cleaved facet at one end of the active region and by the Bragg grating region at the other end. The reflectivity profile of the grating region has a peak at the Bragg wavelength. Current injection into the gain region controls the output power of the laser. The wavelength is electrically tuned by the current injected into the Bragg region. The injected carrier density in the passive Bragg region can be high to increase the refractive index changes, because carriers in the passive region do not contribute to the gain.

The two-electrode DBR laser gives a mixture of discrete and continuous tuning. An index change in the Bragg region affects the effective cavity length as well as the grating periodicity. An increase in the Bragg current therefore causes both the longitudinal modes and the Bragg wavelength to tune towards shorter wavelengths. The tuning rate of the Bragg wavelength is, however, faster than that of the cavity modes. (The ratio of the two tuning rates is roughly equal to the total device length divided by the length of the Bragg region). As a result, the laser tunes continuously on one mode until a point is reached at which a neighbouring mode is closer to the grating's reflectivity peak. The laser then tunes discretely by jumping to the next mode; each mode hop leaves a gap in the wavelength coverage that is equal to the mode spacing. The continuous tuning ranges that occur between hops are relatively small (typically 0.1nm-0.2 nm [10]). By introducing a phase

region in the waveguide, also independently controlled by an injected current, the gaps in the tuning range may be avoided [10]. This is called as three-electrode DBR laser. A schematic of this device is illustrated in figure 2.3 (b). A detailed discussion of the wavelength-tuning in three-electrode DBR may be founded in reference [10]. With proper design and correct adjustment of the three currents in the active, Bragg and phase regions, quasicontinuous tuning ranges from 8 to 10 nm have been achieved [10].

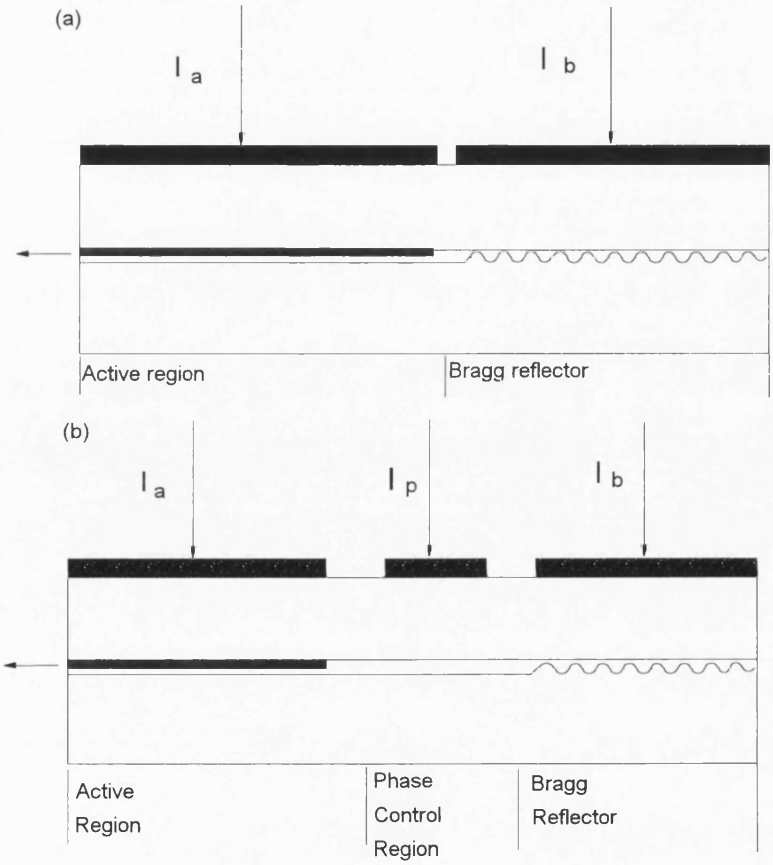

Figure 2.3 . Schematic diagram of wavelength tunable DBR lasers, (a) a two electrode DBR laser and (b) a three-electrode DBR laser.

In a similar way to the tunable DFB laser, high tuning speed, high SMSR and ease of fabrication stabilisation are the advantages of the tunable multiple electrode DBR laser. However, the tuning range of the tunable multisection DBR lasers is still limited in a range of 10 nm and exact tuning versus current characteristics are difficult to predict and are

subject to aging [11].

2.3 Multi-wavelength Laser Arrays

A mutli-wavelength laser source can be formed by taking a number of single-frequency (or wavelength tunable) lasers, such as DFB/DBR lasers, that are operating at different wavelengths and by then combining their outputs using some form of multiplexing or coupling device. These are commonly refered to as laser arrays. The technology for developments of multiwavelength laser arrays that have been reported to date may be put into two categories based on their structures. First, the laser arrays can be formed by a number of DFB or DBR lasers, in which multiwavelength emission can be achieved by varying roughly the optical grating period. Secondly, VCSELs can be used to develop the multiple wavelength laser arrays in two dimensions, by varying their effective cavity length. In this section, we discuss these two kinds of laser arrays.

A. DFB/DBR Laser Arrays

Conventional multi-wavelength DFB/DBR laser arrays comprise a number of single-frequency lasers, whose lasing wavelengths are normally controlled by adjusting the pitch of the built-in corrugation transcribed in the identical active waveguides. In this case, high precision control of the grating period in each laser is required. Twenty wavelength DFB laser arrays with a nominal channel spacing of 1 nm were reported in which each laser operated in a single-longitudinal mode, and had a slightly different grating period [12]. It is well known that the wavelength of a DFB laser is determined not only by the grating period but also by the effective index, which is sensitive to many parameters such as the temperature and the carrier concentration. As a result the wavelength accuracy in such laser arrays is poor. In the best case, the wavelengths of the lasers give a channel spacing accuracy of ± 0.3 nm [12]. With the DFB lasers as discrete components, wavelength

errors of this magnitude can be compensated for by adjusting the operating temperatures (a total range of just 6 ^{O}C in the operating temperature would compensate for a $\pm$0.3 nm wavelength error). However, with the lasers integrated into a single array, any temperature control is applied to all of the devices simultaneously. The poor wavelength accuracy means that, for many applications, either the DFB lasers will have to be electrically tuned, or some other kind of tuning mechanism will have to be used.

Various methods have been investigated to overcome the problem of wavelength inaccuracy and to achieve high performance of DFB or DBR laser arrays. For instance, the laser arrays made of multiple section DBR lasers have been reported to have tunable wavelength spacing and to be modulated at a rate of 2 Gbit/s [14]. A four channel integrated DFB laser array with tunable wavelength spacing has also been reported, in which four metal strip heating resistors were fabricated near the active region of each laser [15]. By changing the power in the heater, the wavelength of each laser can be continuously tuned by as much as 5 nm. Therefore, a tunable wavelength spacing from 1 nm to 2 nm could be achieved, thus increasing the wavelength accuracy. Because of the short laser cavity length used, each DFB laser in the array is capable of 10 Gbit/s operation. Recently, a ten-channel tunable multisection $\lambda/4$ shifted DFB laser array using strained InGaAsP multiple quantum well was fabricated. In this device, the lasing frequencies of the ten channels were set in a single 10 GHz space, particularly for applications in the optical frequency-division multiplexing system. Each channel showed precision wavelength control, narrow spectral linewidth, and flat FM response due to strain employed in the MQW [16].

In addition to wavelength inaccuracy, another important problem for the DFB/DBR laser arrays is the crosstalk due to electrical and/or thermal interaction. This also makes it difficult to increase the number of channels in an array. Electrical crosstalk is mainly due to the inductive coupling of the bonding wires. The principal advantage of the DFB and DBR laser arrays are the high SMSR of each wavelength, large modulation speed and

their ease of fabrication stabilization.

B. VCSEL Arrays

In contrast to the conventional injection lasers, which consist of two cleaved end mirrors perpendicular to the active layer, the resonator of a vertical cavity surface emitting laser (VCSEL) is formed by two wafer surfaces and the light output is taken vertically from the surface. There exists only one longitudinal mode within the mirror bandwidth owing to the ultrashort cavity length, and a SMSR in excess of 30 dB is readily achievable in such lasers. The mode, which is the VCSEL lasing wavelength, depends critically on the total cavity length. For example, a 1% variation of layer thickness over a wafer produces a fairly large wavelength change of 10 nm at a nominal wavelength of 1 μm [18]. Thus the lasing wavelength of VCSELs can be tailored to either longer or shorter wavelengths with a small variation in cavity thickness.

Owing to the vertical surface emitting structure in VCSEL, two-dimensional multi-wavelength laser arrays may be realized, in which the lasing wavelength of each VCSEL can be varied by a small variation in cavity thickness. Chang-Hasnain et. al first reported both one and two-dimensional multiwavelength laser arrays, by using the inherent beam flux gradient in MBE growth [17]. A 7×20 two-dimensional multiwavelength laser array at wavelength of 980 nm regime, which consisted of 20 μm square lasers on 354 μm centers, was fabricated, and provided 140 unique single mode wavelengths with wavelength separation of 0.3 nm in the rows and 2.1 nm in the columns. Four lasers in this device were also simultaneously operated at a modulation rate of 155 Mbit/s with a bit-error-ratio of 10^{-9} [17].

One of the advantages of the multiwavelength VCSEL array is mainly related to its 2-D array configuration, which will dramatically increase the connection density in optical interconnects and enhance the system capabilities. Very high data rate throughput is expected using the additional dimension of freedom--wavelength. Other advantages are

low threshold current and small size. The principal disadvantage of the multiwavelength VCSEL array is poor accuracy of both the centre lasing wavelength and the channel separation of the device, owing to the difficulties of local control of layer thickness. The stability of wavelength is also a problem because of heating [17]. The processing for these laser arrays is complicated and it is difficult to make laser arrays repeatable with the same centre wavelength from the same wafer, so it could become prohibitively expensive.

In addition to the two kinds of multiwavelength laser arrays described above, strained-layer quantum well laser arrays can be fabricated by using a selective area epitaxy technique [25]. The controlled selection of the quantum well thickness results in lasers with different wavelengths. Further information about this device can be found in references [25-26].

2.4 Monolithic Integrated Multiwavelength Lasers

Recently another approach for the development of WDM sources is to monolithically integrate optical amplifiers with an optical mulitplexer. The optical cavity, that includes a multiplexer and gain section, is defined by two cleaved facets. When one of the amplifiers is turned on, it will receive optical feedback that has been filtered by the multiplexer. Above threshold, lasing will occur at the wavelength of peak filter transmission. This wavelength will shift by exactly one multiplexer channel spacing if the neighboring amplifier is pumped instead. The device can be digitally tuned to the desired wavelength channel by driving the appropriate gain section. Tuning is no longer limited by the obtainable change in refractive index, but only by the gain bandwidth of the amplifier. The device is also capable of simultaneously generating a comb of optical wavelengths that are spectrally well aligned. As all channels can be emitted from a single output port, they do not need an extra optical multiplexer to combine the different wavelengths. We discuss

two types of this monolithic integrated multi-wavelength laser in this section.

A. MAGIC Laser

The basic idea of the multistripe array grating integrated cavity (MAGIC) laser [19-21] is derived from the MGC laser [27], and it is essentially a two-dimensional implementation of the external grating cavity laser. It is formed by the monolithic integration of an active stripe array with a curved diffraction grating, which acts as wavelength selective intracavity filter. A schematic diagram of this device is shown in figure 2.4 (a). The external facet of the active stripes together with the grating form the reflective boundaries of the resonant cavity. The active stripes comprise a conventional multiquantum well (MQW) active region that lies directly on top of the waveguiding core. The grating is formed by a reflective wall vertically etched down through the planar-waveguide core (as shown in figure 2.4 (b)). A standard Rowland circle configuration is used for the curved diffraction grating-- the etched grating retrodiffracts the light emerging from the end of a pumped stripe, dispersing and focusing it onto the line-segment formed by the same stripe ends, as these lie on the Rowland circle of the grating. Thus the curved diffraction grating provides focusing as well as diffraction.

The operation of the MAGIC laser resembles that of a bulk optic external cavity laser. If a single active stripe of this device is electrically pumped, laser emission occurs from its cleaved end facet at a wavelength determined by the optical feedback from the grating. The lasing wavelength is different for each stripe, being defined by the stripe's position relative to the grating [20]. Laser emission at different wavelengths from a single output port can also be achieved in this device. In order to do this, an "output" stripe toward one end of the array is selected and pumped, and a "second" stripe towards the opposite of the array is also pumped. If the two stripes are chosen such that the direct grating feedback wavelengths for each occur at opposite extremes of the active material gain spectrum, then the wavelength at which the grating "connects" the two lies towards

the middle of this spectrum, and so lasing occurs preferentially at the connecting wavelength [20], By then, pumping different second stripes, the emission from the output stripe may be switched from one wavelength to another. If a number of different second stripes together with the single output stripe are simultaneously pumped, simultaneous multiple wavelength operation of the device can be achieved [21]. Each emission wavelength is determined by the resonance between the output stripe and one second stripe.

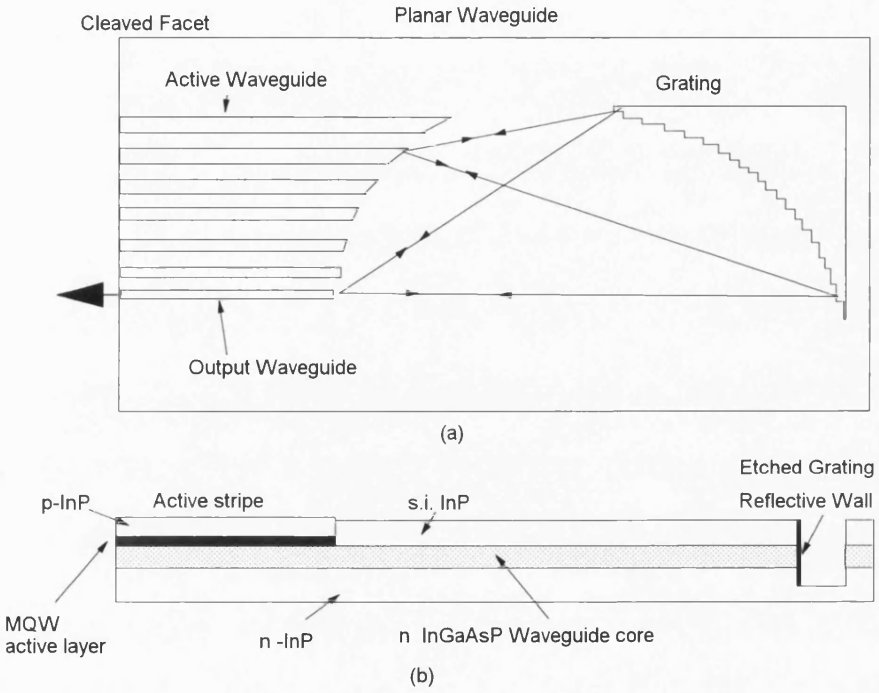

Figure 2.4. Schematic diagram of a MGGIC laser formed in the InP-based material systems.

An MAGIC laser with a size of 14×3 mm^2 was fabricated by Bellcore [20]. The channel spacing was designed to be 2 nm in the wavelength range of 1507 to 1553 nm. The lasing intensities were typically 20-25 dB above the background spontaneous emission. All basic properties such as wide tuning range and simultaneous multiwavelength emission from a single output were demonstrated in this device. One of the advantages of this device is that the lasing wavelength can be accurately set at the

design stage. For example, the device reported in [19] had an individual wavelength variation of 0.09 nm. This device, however, did only operate under pulsed current injection and had a relatively small background spontaneous suppression of about 20 dB, which might be due to the high loss of the curved reflective grating. Moreover, owing to high losses in the reflection grating, the device was only capable of generating output powers in the order of 1 mW. In terms of modulation performance, no experimental results have yet been reported for this device. However, the maximum speed of the operation is expected to be of the order of several hundred MHz due to large size of the cavity.

B. Waveguide Grating Router Laser

The waveguide grating router (WGR) laser [22-24] is based on a waveguide grating router integrated with semiconductor optical amplifiers. The waveguide grating multiplexer works by conducting light from an input port into a free-space region where it expands and couples into grating arms. A constant path length difference between adjacent grating arms causes a wavelength dependent phase shift. This linear phase progression affects the propagation direction of the converging wave radiated in the second free space region toward the output ports.

A schematic diagram of the waveguide grating router laser is depicted in figure 2.5. Optical amplifiers are integrated on both sides of WGR. Two cleaved facets define an optical cavity that comprises amplifiers and a router which acts as an wavelength selective intracavity filter. The wavelength of maximum transmission between port i on the left side and port j on the right side is defined as λ_{ij} (i,j=1,...,N). The channel spacing is primarily determined by the multiplexer filter characteristics. By turning on two amplifiers, one on each side of the router as shown in the figure 2.5, say 2 and 11, lasing occurs at wavelength $\lambda_{2,11}$ provided that the amplifiers deliver sufficient gain to compensate for cavity losses. Pumping amplifier 1 instead of 2 shifts the lasing frequency to $\lambda_{1,11}$ and so

on. Thus a comb of exactly spaced frequencies $\lambda_{1,11}$, ..., $\lambda_{12,11}$ into a single output port will be produced. A multifrequency signal could also be generated by simultaneously pumping several amplifiers.

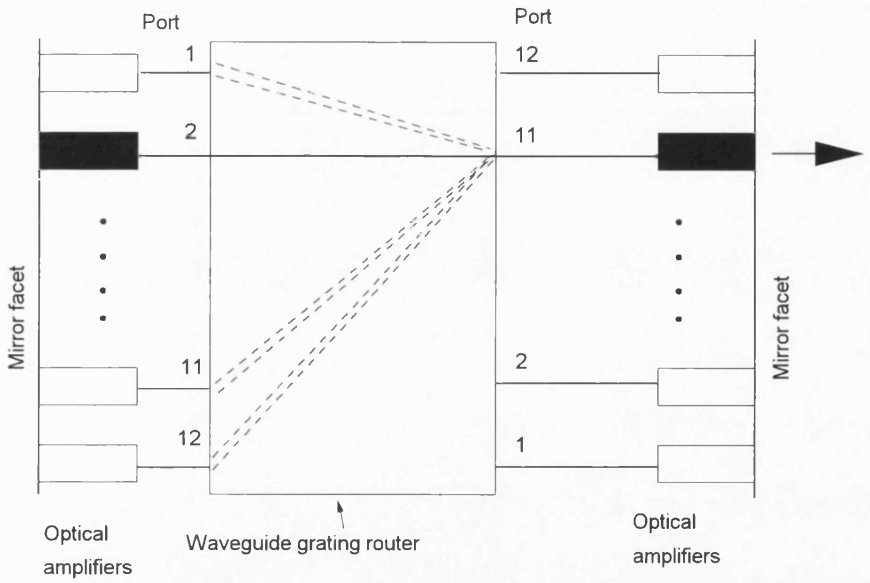

Figure 2.5. Schematic diagram of waveguide grating router laser

A WGR laser was fabricated with optical amplifiers integrated on both sides of a 12×12 WGR [22-23]. The multiplexer had 12 input/output ports and 36 grating arms, and the channel spacing was designed to be 3.2 nm in a wavelength range of 1499 nm-1533 nm. The amplifiers on both sides of the WGR were 1.1 mm long and the whole device had a size of 14.4×3.6 mm^2. Digital wavelength tuning and simultaneous multiwavelength operation have been demonstrated in this device and each channel showed operated at a single longitudinal mode with a 5 MHz line width. One of the advantages of this device is that the channel spacing could be obtained precisely and stably because all the individual laser wavelengths are locked to the same intracavity filter element. Another advantage is that the waveguide grating router can be fabricated reproducibly with very low loss on InP in one step, thus cutting the cost of the laser source. In addition, this laser can be used to fulfill many different WDM functions owing

to the versatility of the WGR [28]. However, owing to high losses in the large size waveguide grating router, the device could only produce an output power of the order 1 mW. In addition, the long laser cavity limited the direct modulation rate to a few hundred Mbit/s per wavelength channel [23].

2.5 Summary

This chapter has described the semiconductor lasers that appear to be the most promising candidates for use in the WDM systems that were described in previous chapter. These lasers may be broadly categorized as wavelength-tunable lasers, multiwavelength laser arrays and monolithic integrated multiwavelength lasers.

In respect of wavelength-tunable lasers, the challenge has been to develop a device whose operating wavelength can be rapidly tuned over a broad spectral range. Moreover, the laser must be capable of being accurately and repeatably tuned to the wavelength of each and every channel of a system. A very narrow linewidth (kHz regime), wide tuning range(up to 240 nm already demonstrated) on both discrete and continuous tuning are readily achievable in the grating loaded external cavity laser. However the device requires careful alignment and stabilization of the bulk-optic components. In addition, the device shows low tuning speed (ms regime). The tunable multi-electrode DFB and DBR lasers have the advantages of high SMSR (typically >30 dB) and high tuning speed (nanosecond regime), although the tuning ranges are relatively narrow.

Two kinds of conventional multiwavelength laser arrays have been discussed in this chapter, which are DFB/DBR laser arrays and VCSEL arrays. The DFB/DBR laser arrays are formed by a number of DFB or DBR lasers, in which multiwavelength emission can be achieved by varying the optical grating period. One of the main problems of the DFB/DBR laser arrays is that of wavelength accuracy. Therefore various efforts have been made to develop devices with precisely defined wavelengths and tunable wavelength spacing. Two-

dimensional multiwavelength VCSEL arrays can be realized, in which lasing wavelength of each VCSEL can be varied by a small variation in cavity thickness. Owning to its 2-D array configuration, very high data rate throughput is expected using the additional dimension of freedom--wavelength.

Monolithic integrated multiwavelength lasers, including the MAGIC laser and WGR laser exhibit many advantages in terms of performance, cost and versatility. In these lasers, semiconductor amplifiers are monolithically integrated together with an optical multiplexer, and they are capable of producing a comb of exactly spaced frequencies from a single output port, and hence they do not need an extra optical multiplexer to combine the different wavelengths. Therefore, monolithic integrated multiwavelength lasers are very attractive for applications in future WDM networks.

References

[1]. G. P. Agrawal and N. K. Dutta, "Long-wavelength semiconductor lasers," Van Nostrand Reinhold, New York, 1986.

[2]. R. Wyatt and W. J. Devlin, "10 KHz linewidth of 1.5 μm InGaAS external cavity laser with 55 nm tuning range," *Electron. Lett.*, vol. 19, pp.110, 1983.

[3]. F. Favre, D. Leguen, J. C. Simon and B. Landousies, "External cavity semiconductor laser with 15 nm continuous tuning range," *Electron. Lett.*, vol. 22, pp, 795, 1986.

[4]. H. Tabuchi and H. Ishikawa,"External grating tunable MQW laser with wide tuning range of 240 nm," *Electron. Lett.*, vol. 26, pp. 742, 1990.

[5]. C. H. Henry, "Phase noise in semiconductor lasers," *J. Lightwave Technol.*, vol. 4, pp.298, 1986.

[6]. H. Kogelnik and C. V. Shark, "Stimulated emission in a periodic structure," *Appl. Phys. Lett.*, vol. 18, pp.152, 1971.

[7]. M. Kuznetsov, "Theory of wavelength tuning in two-segment distributed feedback lasers," *IEEE J. Quantum Electron.*, vol 24, pp.1837-1844, 1988.

[8]. M. Horita, M. Tsurusawa, K. Utaka, and Y. Matsushima, "Wavelength-tunable InGaAsP-InP multople λ/4 shifted distributed feedback laser," *IEEE J. Quantum Electron.*, vol 29, pp.1810-1815, 1993.

[9]. M. Teshima, "Dynamic wavelength tuning characteristics of the 1.5 μm three section DBR lasers: Analysis and experiment," *IEEE J. Quantum Electron.*, vol 31, pp.1389-1400, 1995.

[10]. T. L. Koch and U. Koren, "Semiconductor lasers for conherent optical fibre communications," *J. Lightwave Technol.*, vol. 8, pp.274, 1990.

[11]. S. L. Woodward, P. Parayanthal, and U. Koren, "Effects of aging on the Bragg section of DBR laser," *IEEE Photon. Technol. Lett.*, vol.5, pp.750-752, 1993.

[12]. M. Nakao, K. Sato, T. Nishida and T. Tamamura,"Distributed feedback laser arrays fabricated by synchrotron orbital radiation lithography," IEEE J. Select. Areas Commun., vol. 8, pp. 1178, 1990.

[13]. M. Aoki, T. Taniwatari, M. Suzuki, and T. Tsutsui, "Detuning adjustable multiwavelength MQW-DFB laser array grown by effective Index/quantum energy control selective area MOVPE," *IEEE Photon. Technol. Lett.*, vol.6, pp.965-968, 1994.

[14]. L. A. Wang et al " Low-threshold four-wavelength DFB laser array for multigigabit/s high density WDM system applications," *IEEE Photon. Technol. Lett.*, vol. 3, pp.965-968, 1991.

[15]. Y.H.Lo, L.A. Wang, A.S. Gozdz, P.S.D.Lin, M.Z.Iqbal, R.Bhat and T.P. Lee, " Four

channel integrated DFB laser array with tunable wavelength spacing and 40-Gb/s signal transmission capacity", *J. Lightwave Technol.*, LT-11, pp.619-623, 1993.

[16]. K. Sato, S. Sekine, Y. Kondo, and M. Yamamoto, "Simultaneous operation of ten channel tunable DFB laser arrays using strained-InGaAsP multiple quantum wells," *IEEE J. Quantum Electron.*, vol. 29, pp.1805-1809, 1993.

[17]. C. J. Chang-Hasnain, M. W. Maeda, J. P. Harbison, L. T. Florez, and C. Lin, "Monolithic multiple wavelength surface emitting laser arrays", *J. Lightwave Technol.*, vol. 9, pp. 1665-1672, 1991.

[18]. F. Koyama, T. Muksihara, Y. Hayashi, N. Ohnoki, N. Hatori, and K. Iga, "Wavelength control of vertical cavity surface-emitting lasers by using nonplanar MOCVD," *IEEE Photon. Technol. Lett.*, vol.7, pp.10-12, 1995.

[19]. J.B.D. Sool, K. Poguntke, A. Scherer, H. P. Leblance, C. Chang-Hasnain, J.R. Hayes, C.Caneau, R. Bhat and M.A. Koza, "Multistripe array grating integrated cavity (MAGIC) laser; A new semiconductor laser for WDM applications", *Electron. Lett.*, vol. 28, pp.1805-1807, 1992.

[20]. J. B. D. Sool, K. R. Poguntke, A. Scherer, H. P. LeBlanc, C. Chang-Hasnain, J. R. Hayes, C. Caneau, R. Bhat, and M. A. Koza, "Wavelength-selectable laser emission from a multistripe array integrated cavity laser," *Appl. Phys. Lett.*, vol. 61, pp.2750-2752,1992.

[21]. K. R. Poguntke, J. B. Soole,A. Scherer, H. P. LeBlanc, M. A. Koza, "Simultaneous multiple wavelength operation of a multistripe array integrated cavity laser," *Appl. Phys. Lett.*, vol. 62, pp.2034-2036,1993.

[22]. M. Zirngibl and C. H. Joyner,"12 frequency WDM laser based on a transmissive waveguide grating router," *Electron. Lett.*, vol.30, pp.701-702, 1994.

[23]. M. Zirngibl, B. Glance, L. W. Stulz, C. H. Joyner, G. Raybon, and I. P. Kaminow,"Characterization of a multiwavelength waveguide grating router laser," *IEEE Photon. Technol. Lett.*, vol.6, pp.1082-1084, 1994.

[24]. M. Zirngibl, C. H. Joyner, and L. W. Stulz, "Demontration of 9X200 Mbit/s wavelength division multiplexed transmitter," *Electron. Lett.*, vol.30, pp.1484-1485, 1994.

[25]. T. M. Cockerill, R. M. Lammert, D. V. Forbes, M. L. Osowski and J. J. Coleman, " Twelve-channel strained-layer InGaAs-GaAs-AlGaAs buried heterpostructure quantum well laser array for WDM applications by selective-area MOCVD," *IEEE Photon. Technol. Lett.*, vol.6, pp.786-788, 1994.

[26]. R. M. Lammert, T. M. Cockerill, D. V. Forbes, and J. J. Coleman, " Dual-channel strained-layer InGaAs-GaAs-AlGaAs WDM source with integrated coupler by selective-area MOCVD," *IEEE Photon. Technol. Lett.*, vol.6, pp.1167-1169, 1994

[27].I. H. White, "A multichannel grating cavity laser for wavelength division multiplexing applications", *J. Lightwave Technol.*, vol. 9, pp. 893-899, 1991.

[28]. B. Glance, I. P. Kaminow and R.W. Wilson, "Application of the integrated waveguide grating router", *J. Lightwave Technol.*, LT-12, pp.957-961,1994.

Chapter 3

BULK OPTIC MULTICHANNEL GRATING CAVITY LASER

3.1 Introduction

In Chapter 1 and 2 we have addressed the issues related to multiwavelength communication systems and muliwavelength laser sources. The development of multiwavelength semiconductor laser sources is a prerequisite for the successful implementation of WDM systems in broadband communication systems. The WDM system with channel separations in the range of 1 nm-10 nm has potential advantages over high density systems particularly in terms of easing the restrictions on receiver design. However, the transmitter design becomes difficult as optical sources are specially required which can switch over a wide range of wavelength without significant change in optical power or spectral bandwidth.

This chapter describes a type of multiwavelength laser, called the multichannel grating cavity (MGC) laser, which is based on an external grating-loaded cavity system [1]. The laser is able to generate a series of different wavelengths simultaneously, hence it is suitable for application in WDM communication systems. The wavelength switching across a wide wavelength range has been demonstrated [2-3]. Multiwavelength picosecond optical pulses are also generated with this laser using actively mode-locking techniques [4-5]. In a similar manner to that of the multiwavelength laser [6], the MGC laser has an advantage in using a compact folded external cavity system, which can readily be extended to allow simultaneous generation of over 8 channels at the channel spacing of about 2 nm.

The main consideration of this chapter is on the basic characteristics of this

laser, such as fast wavelength switching, simultaneous multi-channel generation and digital modulation. The following two chapters detail the demonstration of picosecond pulse generation using this laser. The organisation of this chapter is as follows: The MGC laser structure is described in section 3.2, and consideration is given to the basic operating principles, chief requirements in designing its structure and advanced functions. Section 3.3 presents the experimental CW performance of the MGC laser. The experimental implementation of a two channel MGC laser is described in detail. The performance of both fast wavelength switching and simultaneous dual-channel generation is demonstrated along with their operational characteristics. Section 3.4 introduces a theoretical dynamic model for the MGC laser. Using the simple rate equation model for a semiconductor laser, we have developed a set of coupled-cavity rate equations, which incorporate the effects of the external passive resonator as well as the delay in optical feedback, thus making it possible to have a correct picture of the dynamics and interaction between channels in the MGC laser system. Section 3.5 discusses the dynamic and digital modulation characteristics of the MGC laser, particularly considering the relaxation oscillation frequency, and modulation responses. The theoretical simulation results are given in detail using the coupled-cavity rate equations, and compared with the experimental results. Section 3.6 is concerned with the carrier depletion effects and crosstalk between channels under dual channel CW operation. Finally, section 3.7 gives the conclusions of this chapter.

3.2 MGC laser structure

The MGC laser has been proposed with a geometrical structure as shown in figure 3.1. It consists of individually addressable ridge laser stripes on a single laser bar, an antireflection coated collimating lens and a diffraction grating reflection filter, all set to form an external optical cavity system. A high quality anti-reflection (AR) coating is applied to one facet of the laser bar, so that lasing within each individual stripe is inhibited. The laser bar is etched to allow independent current injection into

each ridge laser. One stripe, which acts as a 'master ' laser output amplifier (stripe 3 in figure 1) is set at one end of the bar. The other stripes act as reflector stripes. The optical output can be monitored from any of the uncoated facets of the laser stripes, but is normally taken from the 'master' laser stripe.

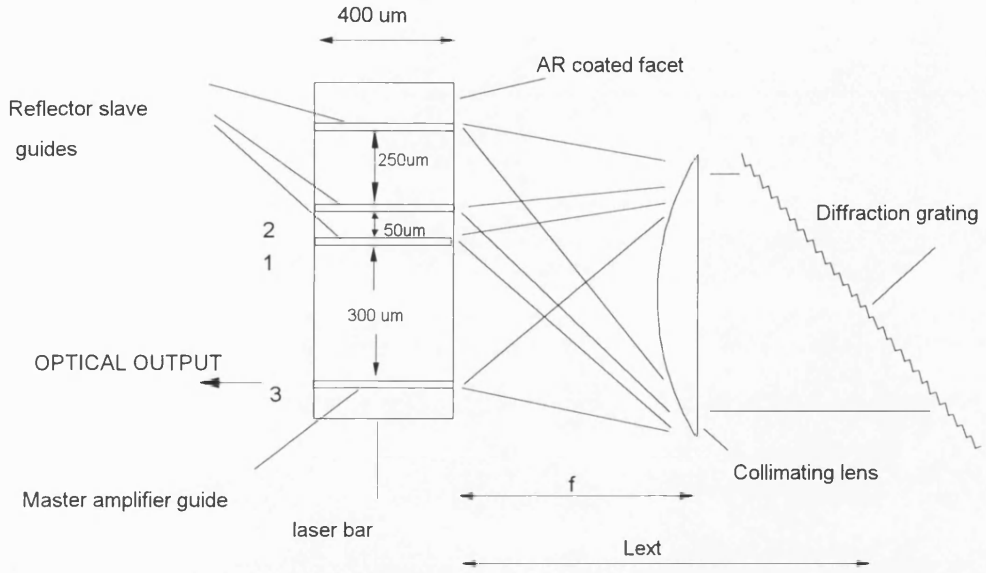

Figure 3.1 Schematic diagram of MGC laser

In operation, the grating is set and remains fixed at such an angle that lasing can only be achieved when two ridge stripes (say 1 and 3 in figure 1) are pumped simultaneously. Injection pumping one of the reflector stripes (say stripe 1 in figure 1) causes it to emit light over a broad spectral range. Light emitted from the AR coated facet is collimated by the lens, and the resulting parallel beam falls upon the diffraction grating. The grating disperses the different wavelengths within the output spectrum, diffracting each to a slightly different angle. Only one wavelength can be focused onto the end of the master output amplifier stripe 3, and so only a single wavelength of light can resonate between the two driven laser stripes via the lens and diffraction grating. Therefore, the lasing output from stripe 3 is limited to that wavelength. The absolute wavelength of the lasing channels is simply set by the geometry of the cavity. The wavelength can be switched by continuously driving ridge 3 and redirecting the drive current from one reflector guide to another. More channels can be added by fabricating more reflector stripes and the maximum potential number of channels which can be

generated is given by the laser gain bandwidth of semiconductor material divided by the channel spacing required per channel to avoid cross-talk. The speed at which the wavelengths can be switched depends on the carrier-recombination properties of the semiconductor laser material and the cavity round trip time and is of the order of a few nanoseconds. Using a multi-quantum well (MQW) laser higher switching speed can be envisioned in addition providing a wider tuning range.

The device can also operate as a simultaneous multiple wavelength generator. For example, by continuously driving the output amplifier stripe 3 and the two reflector stripes 1 and 2 simultaneously, two parallel WDM channels (or more if more reflector stripes are driven) can be generated simultaneously, This feature is particularly attractive as it enables each bit of a word to be transmitted on a different wavelength.

As the device is an extension of the external grating cavity laser, it can readily be used as multi-WDM channel ultrashort pulse generator using active mode-locking techniques [4-5]. For instance, if the output amplifier laser stripe 3 is continuously driven, and two RF signals at the cavity resonance frequency are superimposed on the dc drive currents applied to the two reflector stripes 1 and 2, dual wavelength picosecond pulses with repetition rates corresponding to the cavity round-trip time can be generated. Since the bias and RF current in each stripe of the device can be individually adjusted, this proposed actively mode-locked MGC laser can provide a number of WDM channel ultrashort optical pulses which can easily be synchronised, or controlled with a programmable relative delay between the channels or switched from one channel to another. This allows both WDM and TDM techniques to be combined for application in broad communication systems.

Although the device has been primarily designed for application in WDM systems with large channel spacing, the MGC source can also be configured with almost identical operating wavelengths. Therefore, the controlled beating of such wavelengths for microwave signal generation may be possible.

In designing the MGC laser, a variety of requirements must be satisfied,

typically requiring compromise in some structural aspects. A major practical requirement for this device is that of efficient optical coupling between stripes via the diffraction grating and collimating lens. This requirement is partially eased as the stripes have the same structure and hence output beam profiles, so that optical overlap should be high. However, the grating should be normally angled to provide the maximum resolution or narrowest reflection bandwidth, so that the potential optical crosstalk can be minimised. As shown in appendix 1, the MGC laser is typically formed with the grating set nearly in the Littrow configuration. Furthermore, the grating should be aligned so that individual stripes do not lase on their own with external cavity feedback. The lens must have a large enough diameter to cover as many lines of the grating as possible and hence improve the overall resolution. However, the lens focal length must not be so large that the resulting increased spotsize causes low coupling efficiencies.

Other requirements on the cavity design include the realisation of a high-quality reflection coating on the laser bar over the range of required wavelengths. The effect of an imperfect coating causes an internal Fabry-Perot cavity which can cause multimode operation and ultimately high independence of the grating cavity. This latter effect may limit the maximum output power of the device.

3.3 CW Performance

In the previous section, we have discussed the MGC laser structure and its operational principle. The purpose of this section is to describe the practical implementation and performance of a bulk two channel MGC laser prototype system by considering the CW operation. The features to be considered are initial characteristics of the laser stripe, the L-I curves, fast wavelength switching and simultaneous dual-wavelength operation.

3.3.1. MGC Laser Construction

For experimental investigation of the MGC laser, a 1×2 MGC device (with one output master and two reflector slave stripes) was fabricated by BNR Europe Ltd. The laser array consisted of InGaAsP/InP ridge diode laser stripes set parallel with each other operating in the 1.52 μm wavelength range. Each laser stripe was 400 μm long, with an active emitting region width of 3.8 μm and thickness of 0.18 μm. The laser stripes were arranged in a pair with 50 μm between them. The pairs were repeated at intervals of 250 μm. The laser bar was etched into metallization on the p-side so that current could be injected independently into each laser ridge. A high quality antireflection (AR) coating was applied to one facet of the laser bar.

To construct the MGC laser, the laser bar was bonded p-side up on a copper blade using indium solder, which provided good electrical contact with the n-side of the device. The copper blade with the bonded laser bar was then fixed to a mount with a circuit board terminated by 47 Ω at one end and SMA connectors at the other. Gold wires were bonded to each laser stripe and to the ends of the electrical circuit board using bonding machine (Dynapert TCB 21H). The laser mount was finally fixed on a rotating and tilting mount fitted with a Peltier temperature controller, which provided a stable temperature for the MGC laser system.

The diffraction grating and lens were mounted on a Photon control translation stage, which was capable of precise and stable motion in the x, y and z directions. In the experiments reported here, the diffraction grating had 1200 lines/mm and was set at a diffraction angle of 69^{o} at 1.52 μm. The collimating lens had a focal length of 6.5 mm, a numerical aperture of 0.62 and spot size of 0.8 μm. The external cavity length L_{ext} was varied between 3 and 5 cm.

3.3.2. Experimental Arrangement

Figure 3.2 is the experiment set-up for demonstration of the MGC laser. The light output was monitored mainly from master amplifier stripe 3 and split so that it could be analysed using a grating monochromater or a scanning Fabry-Perot

interferometer. An oscilloscope was used to display the output spectrum.

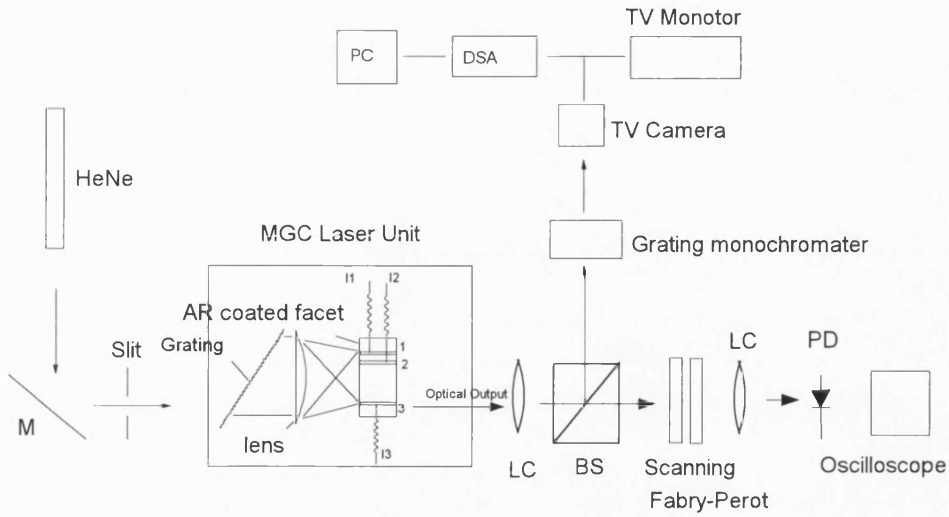

(PD-Photodiode, LC- collimating lens, BS- Beam Splitter and M-Mirror)

Figure 3.2; Experiment set-up for demonstration of MGC laser

The optical system was aligned using a HeNe laser beam after passing through a circular slit as shown in figure 3.2. Before the MGC laser unit was placed in position, the beam set a common working axis for all optical components at the same height of the slit above the optical table. The MGC laser unit was then inserted in the system, with the lens and grating removed. The reflection from the laser ridge facet of a perpendicular HeNe beam provided a method by which the laser orientation on the bar could be checked. Thus by guiding the reflection on axis with the slit the laser could well aligned. The collimating lens was then inserted and its focal point easily checked by noting when the reflection of the HeNe beam from the laser facet back to the slit formed the smallest possible image. At this point the light which was emitted from the laser was collimated. The grating was also aligned by ensuring that light diffracted from the grating remained at same height for all diffraction orders.

For pumping the laser stripes, two Lyons pulse generators each with double output channels with risetime of about 5 ns were used to provide electrical currents. The amplitudes of the currents were measured using 50 Ω, 5 mV/mA current probes. Electrical pulse width of about 1 μs and separation of about 10 μs were usually used

for checking and adjusting the MGC laser coupling. After a good coupling had been achieved between the stripes of MGC laser, the laser was operated under CW conditions. A fast germanium Avalanche photodiode was used to monitor the output light.

3.3.3. Preliminary Assessment

The initial experimental characterisation included the checking of the residual reflectivity of the AR-coated facet and effective reflectivity from the grating. In order to find out the residual reflectivity of the AR-coated facet, the light current characteristic of each individual laser stripe was measured and found to be nearly the same. Figure 3.3 (a) shows a typical light current characteristic of the power output from the AR-coated and uncoated facets. Using the technique of reference [7], the residual reflectivity R_{AR} of the AR-coated facet can be determined using the following equation

$$\frac{\Delta P_u}{\Delta P_{AR}} = \sqrt{\frac{R_{AR}}{R_u}}\left(\frac{1-R_u}{1-R_{AR}}\right) \qquad (3.1)$$

Where R_u is the power reflectivity of the uncoated laser facet, the ΔP_u and ΔP_{AR} are the slope efficiencies of the uncoated facet and AR-coated facet respectively. As the laser emits mainly TE polarised light, the power reflectivity of the uncoated cleaved facet, R_u may be assumed to be 32%, the residual reflectivity R_{AR} is found to be about 1 % from the equation (3.1) and figure 3.3 (a).

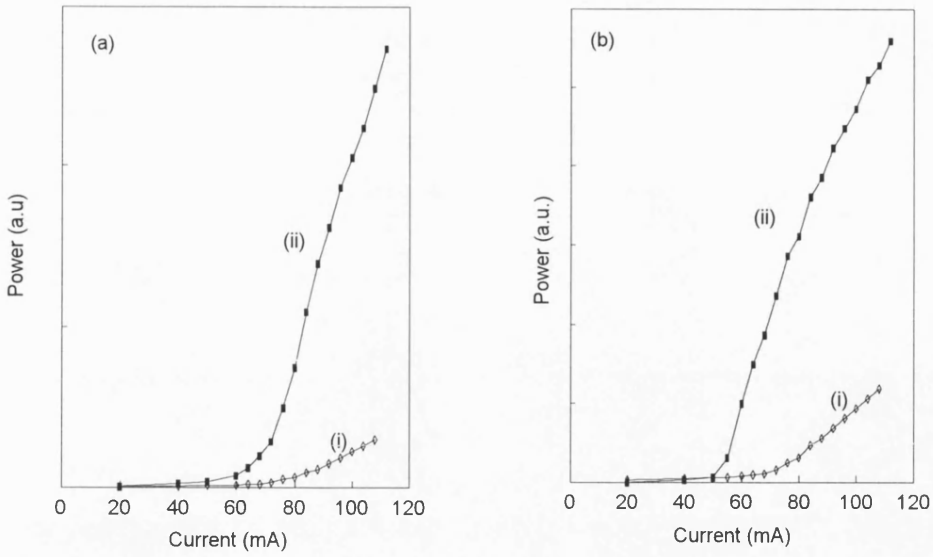

Figure 3.3. (a) Typical light current characteristics of the laser output from (i) uncoated facet, (ii) AR-coated facet. (b)Typical light current characteristics of power output from uncoated facet; (i) without optical feedback, (ii) with optical feedback.

The grating was set in the Littrow configuration so that the emitted light from the laser facet was fed back into the laser after reflection at the grating. With the optical feedback, there was a reduction in the threshold current of the laser. The typical light current characteristics of power output from the uncoated facet with and without optical feedback from the external cavity are shown in figure 3.3 (b), with a threshold current reduction from 80 mA to 55 mA. This enables a determination of the grating filter facet reflectivity including the coupling losses through the lens. The effective facet reflectivity (or feedback fraction x) can be estimated using the following expression [8-9].

$$\frac{\Delta I_{th}}{I_{tho}} = \frac{\ln\left[1+\left(1-R_{AR}\right)\frac{x}{R_{AR}}\right]}{2\alpha_i l + \ln(R_u R_{AR})} \qquad (3.2)$$

where ΔI_{th} is the change in threshold current due to external feedback, I_{tho} is the threshold current of the solitary laser, α_i is the effective absorption coefficient, and l is the laser chip length. For the buried-heterostructure laser, a value of 40 cm^{-1} for α_i is relevant. So the effective reflectivity at chip facet due to external feedback is found to be 20%-30%. It should be pointed out that effective reflectivity is a function of

wavelength, and the above figure is the optimum number for our laser system.

3.3.4. Operating Characteristics

To ensure the successful implementation of MGC operation, the grating was aligned again so that individual stripes did not lase on their own with external cavity feedback and a MGC laser coupling was formed. When current to master stripe 3, I_3, was set to 60 mA and current injection to stripe 1, I_1, was increased to 58 mA, a cross-coupled lasing between stripes 3 and 1 at wavelength λ_1 was achieved. With I_3 maintained at 60 mA, the current was switched from stripe 1 to stripe 2. In this case, cross-coupled lasing between stripes 3 and 2 at wavelength λ_2 was formed at I_2= 59 mA. An output power of about 2.5 mW was obtained for each channel. If the current to the master stripe 3 was increased beyond 100 mA, the internal cavity took control, and this effectively represented the upper limit on the output power of the MGC laser caused by imperfect AR coatings.

Figure 3.4 shows the output spectrum, measured using a grating monochrometer, from stripe 3 when stripes 1 and 2 were independently driven, and indicates that a channel spacing of 2.2 nm was achieved using this configuration. The measured channel separations agree well with the theoretical prediction. Using a scanning Febry-Perot interferometer, a good side mode suppression (SMSR) of more than 20 dB was observed. The observed spectral linewidth of 0.1 nm (FWHM) was obtained, which was the resolution limit of the measurement system. Different channel spacing could be achieved by changing the physical parameters of the MGC laser such as the focal length of the lens, grating constant etc. The speed of operation had been investigated and wavelength switching speeds as fast as 2 ns had been achieved [3].

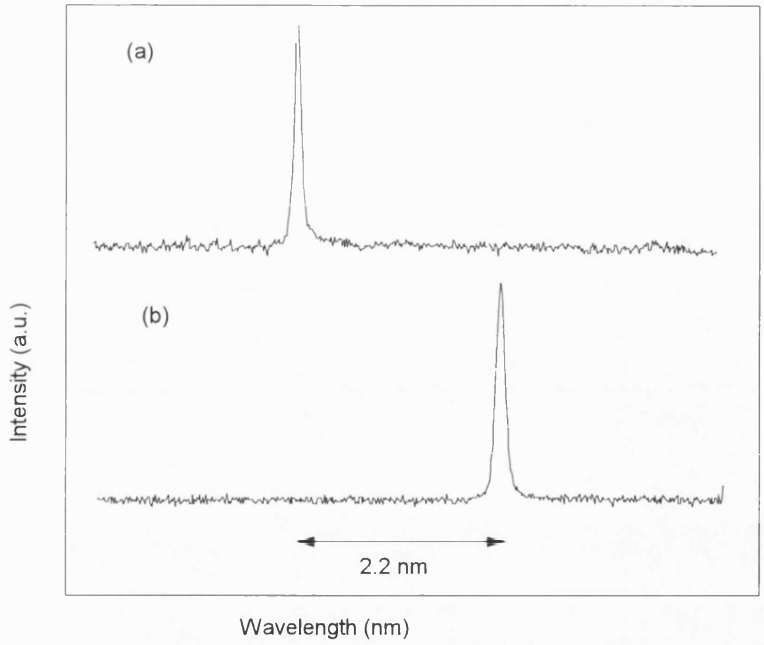

Figure 3.4. Optical spectra generated by the two channel MGC laser (a) I_1=58 mA, I_2=0 mA, I_3=60 mA; (b) I_1=0mA, I_2=59 mA, I_3=60 mA.

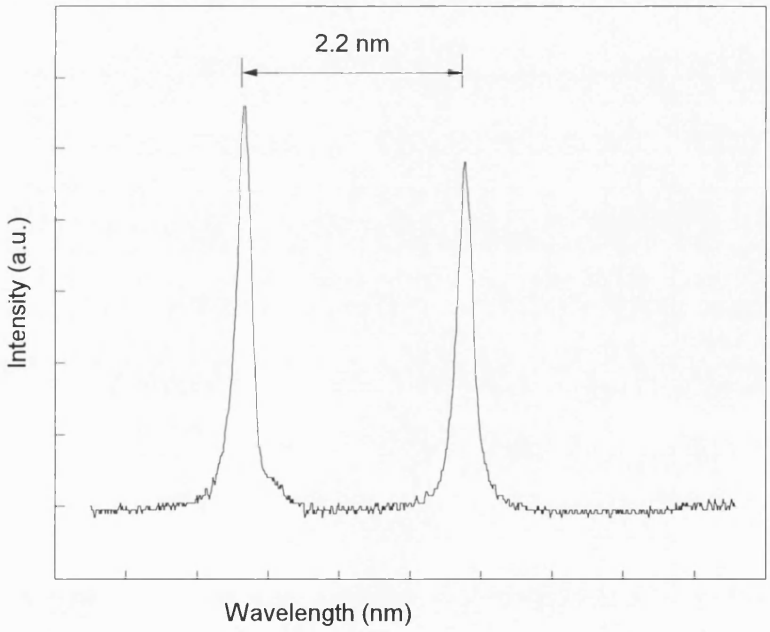

Figure 3.5. Dual wavelength simultaneous generation by the MGC laser; I_1=58 mA, I_2=59 mA, I_3=62 mA.

By driving all three stripes (say, 1, 2 and 3) simultaneously with the currents of I_3= 62 mA, I_1=58 mA, and I_2=59 mA respectively, dual WDM channels were simultaneously generated as shown in figure 3.5. The optical spectra remained well

defined with channel spacing of 2.2 nm. In this case, for similar drive current, the output power for each channel was less than that for single channel operation. This is because both channels share the same gain medium in the output master stripe. The carrier depletion, hence the crosstalk arises as the gain of either signal in the output stripe is dependent on the power of the other.

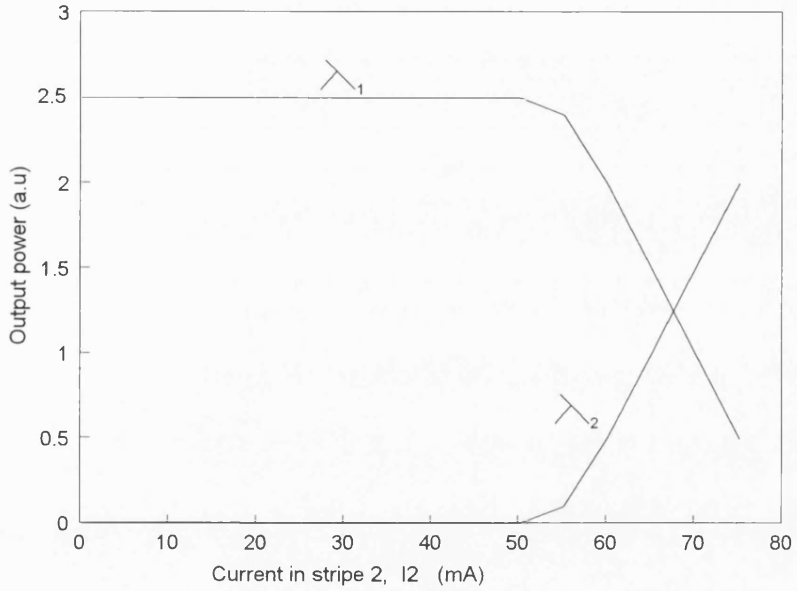

Figure 3.6. Light current characteristics of the MGC laser under dual channel simultaneous generation. I_1=58 mA, I_3=60mA; (a),wavelength λ_1, and (b). wavelength λ_2.

Experimental results of light current characteristics of the MGC laser under simultaneous dual channel operation was depicted in figure 3.6, which shows a plot of output powers at wavelengths λ_1 and λ_2 against current to reflector stripe 2. If the laser was driven such that it was generating light at wavelength λ_1, the power output at this wavelength remained constant until the current to reflector stripe 2 reached the threshold value for light at wavelength λ_2. At this point, substantial optical power at wavelength λ_2 was generated within the output amplifier stripe 3 by stimulated emission along with that at wavelength λ_1 so that increasing carrier depletion occurred. This depletion caused gain reduction which, in turn, caused a reduction in the output power at wavelength λ_1. However, the depletion of gain in the output amplifier stripe

can be compensated for by increasing the current to the output stripe, so that the carrier concentration is restored. Crosstalk suppression of better than 20 dB has experimentally been demonstrated [10].

3.4 Coupled-Cavity Rate Equation for MGC Laser

Before we carry out a discussion of the dynamic and modulation characteristics of the MGC laser, we introduce a theoretical model for the MGC laser in this section. The model uses a set of coupled-cavity rate equations which incorporates the effects of the external passive resonator formed by the collimating lens and diffraction grating, thus making it possible to have a correct picture of the dynamic characteristics of the MGC laser [5].

Several theories on the coupled-cavity laser (like C^3 laser) have been published, i.e., Agrawal's single mode rate equation model [11-12] and Coldren's multimode rate equation model [13]. These models assumed that the cavity coupled instantaneously and neglected time delay along the mutual coupling path. The problem in the MGC laser differs from that of the C^3 laser, in which the gap width between cavities is much smaller than the length of laser chip. A long external cavity will give a delay to the feedback pulse. This will have an important bearing on the modulation response of the device [14]. A possible model for the MGC laser is to use multimode rate equations with average densities [1], which is suitable for the device under CW operating conditions, because the feedback delay will have no consequences when the device is unmodulated. However, if the device is to be modulated, the modulation characteristics will be affected by the delayed optical feedback.

Rate equations have proven to be extremely successful in accounting for the dynamics of semiconductor lasers [11]. Although the MGC laser shows single-mode oscillation at CW operation as shown in the previous section, it becomes multimode under high speed modulation or ultrashort pulse operation, and so a set of multimode rate equations must be used. As the dynamics and high speed modulation

characteristics are affected by the delayed optical feedback, modified sets of equations are used incorporating the delayed feedback owing to long intra-cavity coupling via lens and grating. For each reflector stripe, the modified coupled-cavity rate equations are as follows;

$$\frac{dN_j(t)}{dt} = -\sum_m g_m\left(N_j(t) - N_o\right)\frac{P_{jm}(t)}{1+\varepsilon P_{jall}(t)} - \frac{N_j(t)}{\tau_{sj}} + \frac{J_j}{ed}; \tag{3.3}$$

$$\frac{dP_{jm}(t)}{dt} = \Gamma g_m\left(N_j(t) - N_o\right)\frac{P_{jm}(t)}{1+\varepsilon P_{jall}(t)} - \frac{P_{jm}(t)}{\tau_p} + \frac{\beta N_j(t)}{\tau_{sj}} + K_{jm}P^j_{3m}\left(t-\tau_{ext}\right) \tag{3.4}$$

where N_j and J_j are charge carrier and current densities in each reflector stripe (j=1,2), and P_{jm} is photon density for each mode m in each reflector stripe (j=1,2) respectively. Since both channels share the same gain medium in the output amplifier stripe, the rate equations of the output stripe 3 are;

$$\frac{dN_3(t)}{dt} = -\sum_{j=1}^{2}\sum_m g_m\left(N_3(t) - N_o\right)\frac{P^j_{3m}(t)}{1+\varepsilon P_{3all}(t)} - \frac{N_3(t)}{\tau_{s3}} + \frac{J_3}{ed}; \tag{3.5}$$

$$\frac{dP^j_{3m}(t)}{dt} = \Gamma g_m\left(N_3(t) - N_o\right)\frac{P^j_{3m}(t)}{1+\varepsilon P_{3all}(t)} - \frac{P^j_{3m}(t)}{\tau_p} + \frac{\beta N_3(t)}{\tau_{s3}} + K_{jm}P_{jm}\left(t-\tau_{ext}\right) \tag{3.6}$$

where N_3 and J_3 are charge carrier and current densities in the output amplifier stripe, and P^j_{3m} is photon density for each mode m in the output amplifier stripe for each channel (j=1,2) respectively. No is the transparency carrier density, e is the electronic charge, d is the active layer thickness. Γ is the optical confinement factor, β is the spontaneous coupling coefficient, g_m is the differential gain for each mode m within the optical cavity, and τ_{sj} (j=1,2 and 3) is the recombination time in the stripe j.

Due to the strong effect of gain saturation on the dynamics of InGaAsP semiconductor lasers [11,15], the non-linear gain effect is included in the model. As the degree of gain suppression is uniquely determined by the total photon intensity within the active material rather than by the intensity at any single wavelength [15-16], a gain saturation factor of $\frac{1}{1+\varepsilon P_{jall}(t)}$ is used in the above coupled-cavity rate equations (1)-

$P_{jall}(t) = \sum_m P_{jm}(t)$ (4), where is the total photon density in the laser stripe and ε is the gain saturation coefficient. The model neglects the dependence of peak gain wavelength with carrier concentration. As a result the differential gain coefficient g_m is written in terms of mode number using the standard parabolic approximation [11] so that

$$g_m = g_o\left(1-\left(\frac{m}{M_g}\right)^2\right); \tag{3.7}$$

where g_o and M_g are constants.

The terms $K_{jm}P_{jm}(t-\tau_{ext})$ and $K_{jm}P^j{}_{3m}(t-\tau_{ext})$ account for delayed optical feedback from one stripe to another stripe via the lens and grating. $\tau_{ext}(=2(l_{ext}+m_g l)/c)$ is the feedback delay time, where l_{ext} is the external cavity length and l is the laser chip cavity length. The effect of the spectral selectivity of the diffraction grating in the cavity is included in the above equations through the coupling coefficient, K_{jm} , given by

$$K_{jm} = \frac{(1-L_l)^2(1-R_{AR})R_{gjm}}{\tau\left(1+\sqrt{\frac{R_{AR}}{R_u}}\left(\frac{1-R_u}{1-R_{AR}}\right)\right)}; \tag{3.8}$$

where τ is the laser chip cavity round-trip time, R_u and R_{AR} are the power reflectivity of the uncoated and AR coated laser facet respectively, the L_l is the lens loss and R_{gjm} is given as

$$R_{gjm} = R_{gc}\exp\left(-\frac{2\ln 2(\lambda_{jm}-\lambda_{jo})^2}{\delta\lambda_G^2}\right); \tag{3.9}$$

where the impulse response of the diffraction grating is assumed to be a Gaussian function [17], R_{gc} is the maximum effective grating reflection coefficient (including coupling losses), $\delta\lambda_G$ is the grating resolution bandwidth, and λ_{jo} is the wavelength of the maximum reflection from the grating for channel j (j=1,2).

The effective recombination time is a function of carrier concentration, taking into account Auger and bimolecular recombination so that:

$$\tau_{sj} = \left(A_r + BN_j + CN_j^2\right)^{-1}; \tag{3.10}$$

and the photon lifetime τ_p is given by

$$\tau_p = \frac{\mu_g}{c\left(\alpha + \frac{1}{2l}\ln\left(\frac{1}{R_u R_{AR}}\right)\right)}; \qquad (3.11)$$

where α is the waveguide and scattering loss, and μ_g is the group velocity of the light in the active layer.

As in other rate equation semiconductor laser theories [18-19], the following assumptions have implicitly been made in the above coupled-cavity rate equations ; (1) A single lateral and transverse mode is assumed. This is a good approximation and allows a one dimensional treatment to be used. (2) Homogeneous current injection is assumed for the sake of simplicity, and diffusion is neglected in all directions. This is acceptable for narrow waveguides. (3) Dispersion due to the refractive index dependence of the laser material on the carrier concentration is ignored, and a finite spectral width of the gain medium is neglected. (4) Beating between modes is neglected as the monomode regime is of prime interest and non-linear crosstalk and beating terms are neglected as interchannel spacing of several manometers are envisaged where such effects, for example arising from four-wave mixing, are small. (5) It is assumed that lasing gain is linear with carrier density, and both Γ and β are constant with wavelength.

Having derived the coupled-cavity rate equations for the MGC laser, we will examine the dynamic and modulation characteristics of the MGC laser in the following sections. These rate equations are also able to predict the mode-locking process within the MGC laser, which will be given in the following chapter.

3.5 Dynamic Characteristics

As described in the last three sections, the MGC laser is a very complex system, where two active laser guides are coupled through an external passive resonator, which is formed by a collimating lens and a diffraction grating (as shown in

figure 3.1). The frequency dependent optical power feeds back into the active laser guide from each other via the lens and grating. Like the external cavity laser [20-21] and coupled cavity laser [11,12], this coupled-cavity laser system can improve the laser performance by reducing the linewidth and frequency chirp. The reduced linewidth is useful in coherent communication application and low frequency chirp is necessary for direct detection systems in which information is transmitted along dispersive fibres at high bit rates [22]. In addition, The MGC laser device offers an additional degree of control since the bias and modulation currents in each stripe can be individually adjusted. These can not only greatly reduce the spectral linewidth, but also alter the dynamic response of the MGC laser, especially on the damped relaxation oscillation under certain circumstances.

In this section we discuss the dynamic response and digital modulation characteristics of the MGC laser in single channel operation. Our dynamic modulation analysis is considerably simplified by following the dynamics of a dominant single longitudinal mode. This is justified since the MGC laser maintains the same longitudinal mode with sufficient side-mode suppression (greater than about 20 dB) through out modulation [23]. Such weak side modes do not significantly affect the modulation response of the main mode,

3.5.1. Transient Response

When a semiconductor laser is turned on by changing the current I, a relatively long time (~10 ns) elapses before the steady state is reached. In the transient regime, the power distribution varies periodically as the laser goes through relaxation oscillation, such relaxation oscillations are due to an intrinsic resonance in the non-linear laser system [11]. The relaxation frequency sets a limit on the modulation bandwidth for the laser system. Therefore, in this section we theoretically consider the transient response of the MGC laser under the single channel operation by using the laser model. In order to examine the transient evolution of the MGC laser, the output master stripe 3 was driven continually and the reflector slave stripe 1 was modulated

with a rectangular pulse current.

$$I_1(t) = I_{1b} + I_{1m}\left(H(t-T)\right)\left(1-\exp(-t/t_o)\right); \qquad (3.12)$$

where I_{1b} and I_{1m} are bias and modulation currents in the reflector slave stripe 1. The heaviside step function H(t-T)=1 for t>T, and H(t-T)=0 for t<T. If we define the rise time t_r as the time during which the current changes from 10% to 90 % of the peak value, t_r is related to the exponential decay time to by $t_r=(\ln 9)t_o=2.2t_o$. T is the turning-on time. In the calculation, a pulse current rise time of 200 ps was assumed.

The numerical values for the MGC laser parameters used in the above equations are given in table 3.1. Some of the values are standard values for ridge lasers working at the 1.5 μm wavelength, while other values are based on measured parameters of the MGC laser used in the experiment. These non-linear and coupled equations were solved numerically using a fourth-order Runge-Kutta algorithm, and the initial conditions for the calculations were obtained from Eqs.(3.3)-(3.6) by setting the left-hand side of the equations equal to zero. Standard checks were performed to verify the validity of the solutions, these checks including the insensitivity to initial conditions and time steps, and the stability of the solution after many repeated round-trips. The time step was chosen to be 1 ps. This gave accurate results and the shortest calculation time.

Table 3.1: MGC laser parameters

Parameters	Symbol	Value	Unit
Laser cavity length	l	400	μm
Typical external cavity length	l_{ext}	30	mm
Active-region width	w	3.8	μm
Active-layer thickness	d	0.18	μm
Optical confinement factor	Γ	0.35	
Differential gain constant	g	1.8×10^{-6}	cm^3/s
Spontaneous coupling factor	β	10^{-4}	
Waveguide and scattering loss	α	40	cm^{-1}
Transparency carrier density	n_o	1.1×10^{18}	cm^{-3}
Nonradiative recombination rate	A	1×10^{8}	s^{-1}
Radiative recombination coefficient	B	1×10^{-10}	cm^3/s
Auger recombination coefficient	C	3×10^{-29}	cm^6/s
Gain compression	ε	1×10^{-17}	cm^3
Group refractive index	u_g	3.7	
Power reflectivity of uncoated facet	R_u	0.32	
Power reflectivity of AR coating facet	R_{AR}	0.01	
Grating reflectivity	R_g	0.6	
Lens losses	L_l	0.5	
Vacuum velocity of light	c	3×10^{10}	cm/s

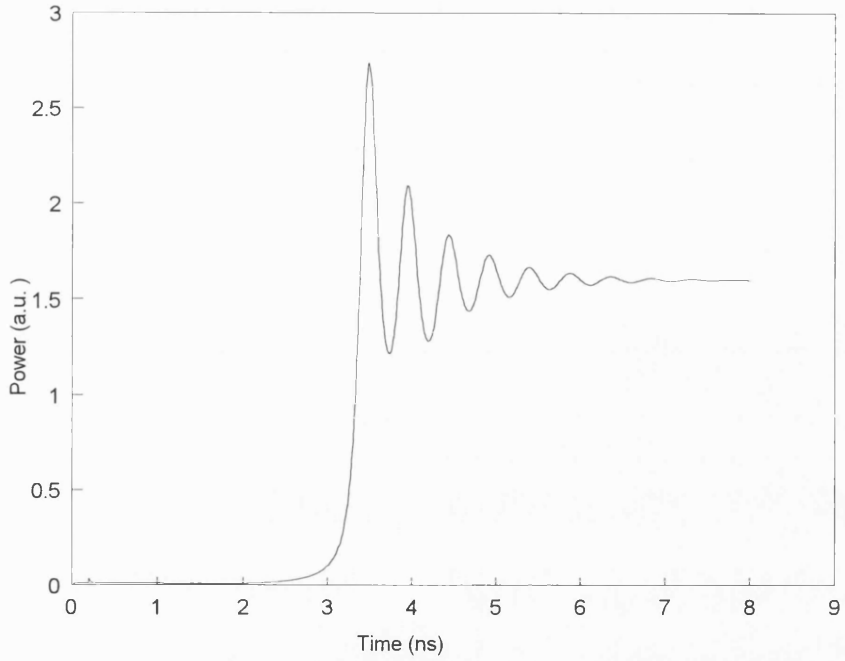

Figure 3.7. Temporal power response of the MGC laser in single channel operation.

Figure 3.7. shows computed results for power transient evolution. Here the bias current in the output master stripe was set just below the threshold current I_{3b}=60 mA, The dc bias current in the reflector slave stripe was 0.7 times its threshold and the step pulse current was 0.5 times threshold. The classic damped relaxation oscillation is shown in the figure 3.7. The oscillation period is approximately 0.5 ns, corresponding to the relaxation oscillation frequency of 2 GHz. When the modulation current was changed from 0.4 to 0.8 times the threshold, the oscillation periods were changed from about 0.5 ns to 0.33 ns, which corresponded to the relaxation oscillation frequency, from about 2 GHz to 3 GHz. It should be noted that the output master stripe should not lase if there is no optical feedback from the diffraction grating because its driven current is below the threshold current. The pulse damped relaxation oscillation means that the dynamic characteristics of the MGC laser are affected by the mutual optical feedback.

The theoretical results are in agreement with the experimental results in terms of relaxation oscillation frequency. Measurement of the relaxation oscillation frequency has been carried out using a fast photodetector (with risetime of 18 ps) and sample

oscilloscope. When the output amplifier stripe was continuously driven with dc bias current of 64 mA, and the reflector stripe 1 was biased with dc current of 40 mA and modulation current of 32 mA, The output signal depicted an effective relaxation oscillation frequency of about 2 GHz is shown in figure 3.8. It may be due to the parasitic capacitance of the device structure, such as bond wire inductance, bonding pad capacitance and resistance of the contact, the first peak of the relaxation oscillation is depressed in the figure 3.8.

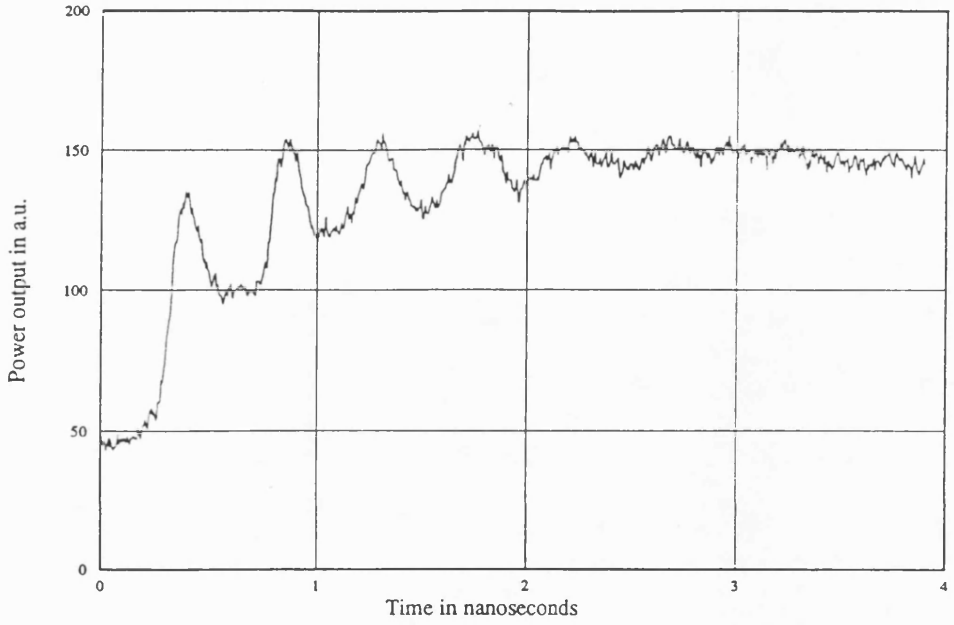

Figure 3.8. Experimental transient response of the MGC laser in single channel operation; with output amplifier stripe dc bias current of 64 mA, and reflector stripe dc bias current of 40 mA and modulation current of 32 mA.

3.5.2. Modulation Characteristics of MGC Laser

For the applications in optical fibre communications, semiconductor lasers are directly modulated to provide pulsed output. Here we consider the modulation response for the MGC laser in order to check on the potential and the limitations of the device for various applications. The performance of the MGC laser under large signal modulation condition can be simulated using coupled cavity rate equations. We assume that the laser current is modulated with a random sequence of on-off pulses of

duration in the nonreturn -to zero (NRZ) format. In our simulations, the output master stripe 3 was injected with dc current and the reflector slave stripe was modulated with NRZ format pulse. A pulse current rise time of 200 ps was assumed. Figure 3.9 shows the pulse shape of the MGC laser after choosing bit rate =500 Mbits/s with current I_{3b}=62 mA, I_{1b}=0.7 I_{th}, I_{1m}=0.4 I_{th}. The pulse shape is slightly distorted because of a decrease in the damping rate of the relaxation oscillation.

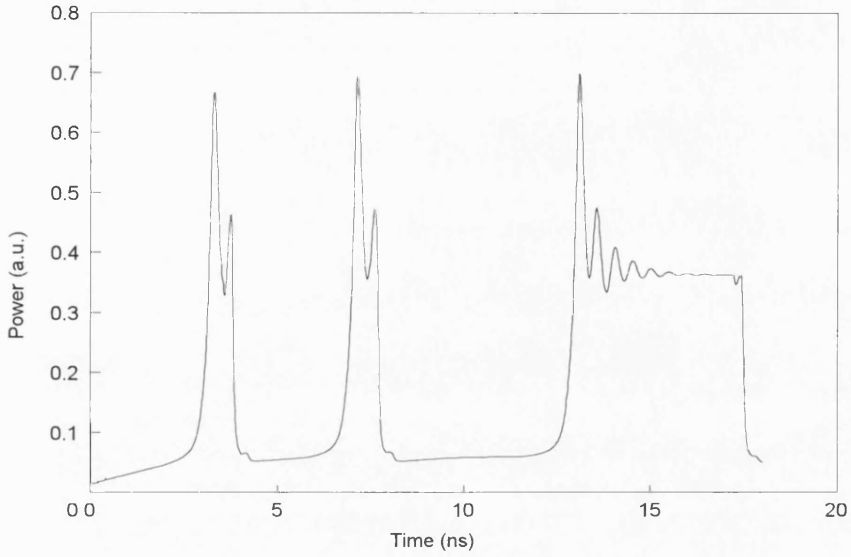

Figure 3.9. Theoretical results of the MGC laser modulated with NRZ bit pattern under a 500 Mbit/s

The experimental investigation on the dynamic modulation of the MGC laser has been made. The modulation response of the MGC laser was achieved by biasing stripes 1 and 3 below threshold and a modulation consisting of pseudo-random NRZ bit sequence was applied to slave stripe 1. Figure 3.10 shows a typical optical output of the single MGC laser channel under a modulation of 400 Mbit/s. Depending on the dc bias to the lasing stripes, the MGC laser exhibited typical rise and fall times of the pulses in the order of 0.5 ns and 2 ns. The modulation bandwidth of the MGC laser is limited by the round trip cavity time. This limitation could readily be overcome by either making the cavity more compact or by integrating the device [24]. The discrepancy between experimental and theoretical results of the modulation response is probably due to the response limitation of the detection system and to the parasitic

capacitance of the device structure, which is not included in the model.

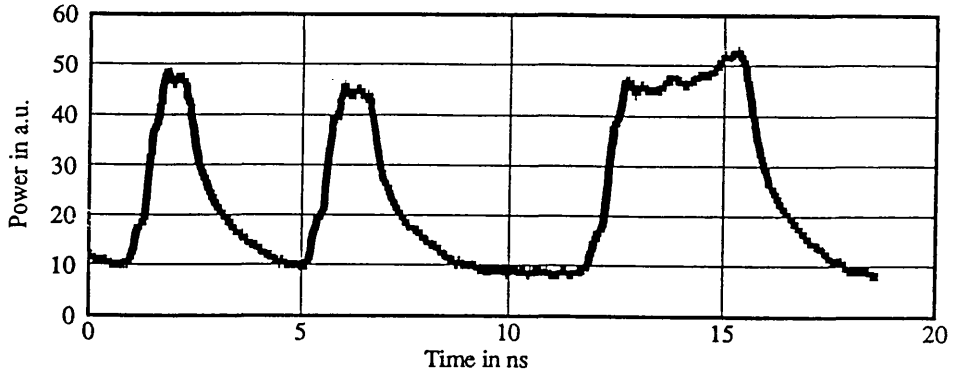

Figure 3.10. Experimental results of the MGC laser modulated with NRZ bit pattern under a 400 Mbit/s.

3.6 Carrier Depletion and Crosstalk in Dual Channels

Simultaneous generation of multi-channels is another advantage of the MGC laser. However, as both channels share the same gain medium in the output master stripe, there is carrier depletion and hence crosstalk between channels occurs. This effect can be modelled using coupled-cavity rate equations. In our simulation, the output master stripe 3 was driven continually and two reflector slave stripes were modulated with rectangular pulse current as described in the last section, but with different turn-on times. Normally, the pulse current in channel 2 was turned on after channel 1 reached the steady-state. Here the bias current in the output master stripe 3 was set just below threshold current I_{3b} =60 mA. The currents of two reflector slave stripes were the same with a bias current of 0.7 times the threshold and step pulse

current of 0.5 times the threshold. The delay time between two step currents was 6 ns, which was enough for channel 1 to reach the steady state.

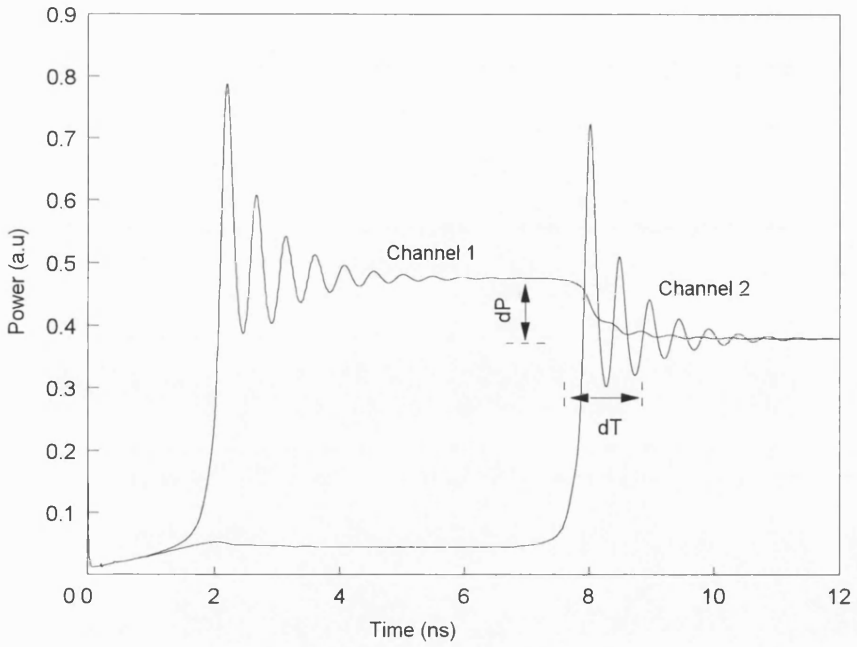

Figure 3.11 Power response of two channel MGC laser, It shows the carrier depletion effects.

Figure 3.11 shows the simulated results for the two channel power transient evolution, from which the influence of one channel on the other due to carrier depletion can be appreciated. While channel 1 (λ_1) was generated by driving both stripe 1 and 3 to reach the steady state through a damped oscillation transient regime, and if the step current in channel 2 was turned on, the light at wavelength λ_2 was generated. At this point, substantial optical power at wavelength λ_2 was generated within the output master guide by stimulated emission along with that at wavelength, λ_1, so that increasing carrier depletion occurred. This in turn caused a reduction in power level at wavelength λ_1 and in the quantum efficiency of emission process at wavelength λ_2. Depending on the injected current to the lasing stripes, a reduction in power of about 0.25 mW for each channel and switch-off delay time of about 1 ns to 1.5 ns were observed.

3.6 Conclusion

In this chapter, an MGC laser with properties suitable for WDM and wavelength switching in broadband communication systems has been described. The source potentially allows wavelength switching across the whole gain bandwidth of the semiconductor material as well as simultaneous multichannel generation.

The MGC laser produces stable and narrow linewidth output and has a major advantage in that wavelength switching is achieved by changing the current input from one stripe into another. As it consists of no moving parts (the grating remains unmoved), the MGC laser is likely to be stable.

The experimental investigation of a two channel bulk MGC laser, used for wavelength switching and simultaneous generation has been presented. The construction and experimental implementation have been outlined and possible practical limitations have been given. Two channels are simultaneously generated with careful control of the input current to the output laser amplifier stripe.

A theoretical dynamic model involving a set of coupled cavity rate equations has been developed for the MGC laser. Non-linear gain saturation effects, the optical bandwidth of the diffraction grating used, and the delay optical feedback are included in the theoretical model. The dynamic and modulation characteristics of the MGC laser have been discussed in this chapter. The transient response and modulation characteristics in single channel operation are investigated by numerical simulation. The carrier density depletion effects in dual channel operation is also considered using the coupled-cavity rate equations. The simulated results agree closely with those of experiments, indicating that the coupled-cavity rate equation model gives a useful understanding of the dynamics of this device.

References

[1] I. H. White, "A multichannel grating cavity laser for wavelength division multiplexing applications", *J. Lightwave Technol.*, LT-9,(7) pp.893-899, 1991.

[2] I.H. White, K. O. Kyairo,P. A. Kirkby and C.J. Armistead, "Demonstration of a 1X2 multichannel grating cavity laser for wavelength multiplexing applications", *Electron Lett.* 26, pp823-833. 1990

[3] K.O. Kyairo I.H. White, P. A. Kirkby and C.J. Armistead, "Multichannel grating cavity (MGC) laser transmitter for wavelength division multiplexing applications", *IEE Proceedings-J.* 138, pp.337-342.1991

[4] B. Zhu, K.O. Kyairo and I.H. White,"Dual-wavelength picosecond optical pulse generation using an actively mode-locked multichannel grating cavity laser", *IEEE Photon. Technol. Lett,* Vol.6, pp.348-351, 1994

[5] B. Zhu and I. H. White, " Multiwavelength short optical pulse generation using an actively mode-locked multichannel grating cavity laser", *J. Lightwave Technol.*, vol. 13, pp.2327-2335, 1995.

[6] C.M. Foster, R. Cush, T. J. Reid, and A. C. Carter, "Four channel multiwavelength source with individually addressable elements," *Electron. Lett.* vol.29, pp. 930-931, 1993.

[7] K. Peterman; " Laser Doide Modulation and Noise", (Kluwer Academic Publishers), pp.35, 1988.

[8] H. Rongqing, Y. Shanping, Y. Wu and H. Peng," An experimental study on stable single frequency semiconductor laser with external cavity", *IEEE. Photon Technol. Lett,* Vol.1, pp.255-257, 1989.

[9] N. K. Dutta and N. A. Olsson, "Effect of external feedback on spectral properties of external cavity semiconductor lasers," *Electron. Lett.*, vol. 2, pp.588-590, 1984.

[10] K. O., Nyairo, I. H., White, C. J., Armistead, P. A., Kirkby,: "Multiple channel signal generation using multichannel grating cavity laser With crosstalk compensation", *Electron. Lett.*, vol. 28, pp.261-268, 1992.

[11] G. P. Agrawal and N. K. Dutta, " Long-wavelength semiconductor lasers", pp333-371, New York: Van Nostrand Reinhold, 1986.

[12] G. P. Agrawal, " Generalized rate equations and modulation characteristics of external-cavity semiconductor lasers", *J. Appl. Phys.*, vol. 56, pp. 3110-3115, 1984.

[13] L. A. Coldren, and T. L. Koch, "Analysis and design of coupled-cavity lasers-- Part 2: Transient analysis", *IEEE J. Quantum Electron,* vol.20, pp. 671-681, 1984.

[14] A. J. Lowery, "New dynamic multimode model for external cavity semiconductor lasers", *IEE Proceedings- J.* 136, pp.229-237.1989

[15] M. Tohyama, R. Takahashi, and T. Kamiya, "A scheme of picosecond pulse shaping

using gain saturation characteristics of semiconductor laser amplifiers" *IEEE J. Quantum Electron.*, vol. QE-27, pp.2201-2210, 1991.

[16] T. Mukai, K. Inoue, and T. Saitoh, "Signal gain saturation in two-channel common amplification using a 1.5 mm InGsAsP travelling wave laser amplifier," *Electron. Lett.*, vol. 23, pp. 396-397, 1987.

[17] J. O. Binder, G. D. Cormack, and A. Somani, "Intermodal tuning characteristics of an InGaAsP laser with optical feedback from an external-grating reflector," *IEEE J. Quantum Electron.*, vol. QE-26, pp.1191-1199, 1990.

[18] M. Ito and T. Kimura, " Oscillation properties of AlGaAs DH lasers with an external grating", IEEE J. *Quantum Electron,* vol. 16, pp. 69-77, 1980.

[19] T.K. Yee and D. Welford, "A multimode rate-equation analysis for semiconductor lasers applied to the direct intensity modulation of individual longitudinal modes," *IEEE J. Quantum Electron*, vol. 22,(11) pp.2116-2122, 1986.

[20] C. H. Henry and R. F. Kazarinov, "Instability of semiconductor lasers due to optical feedback from distant reflectors," *IEEE J. Quantum Electron*, vol. 22,(2) pp. 294-300, 1986.

[21] G. P. Agrawal and C. H. Henry, "Modulation performance of a semiconductor laser coupled to an external high-Q resonator ", *IEEE J. Quantum Electron*, vol. 24,(2) pp. 134-142, 1988.

[22] R. A. Linke, " Modulation induced transient chirping in single frequency laser", *IEEE J. Quantum Electron,* QE-21, pp. 69-77.1985.

[23] K. O Nyairo, N. Badr and I.H.White, "High bit rate narrow line modulation characteristics of multichannel grating cavity Laser", LEOS' 92 Conference Proceedings, pp.341-342. 1992.

[24] M. Asghari, B. Zhu, I. H. White, Cp. P Seltzer, C. Nice, I. D. Henning, A. L. Burness, and G. H. B. Thompson,"Demonstration of an integrated multichannel grating cavity laser for WDM applications", *Electron. Lett.*, vol. 30, pp. 1674-1675, 1994.

Chapter 4

SINGLE CHANNEL NARROW LINEWIDTH PICOSECOND OPTICAL PULSE GENERATION USING AN ACTIVELY MODE-LOCKED MGC LASER

4.1 Introduction

The last chapter has detailed the basic characteristics of the bulk optical MGC laser, such as fast wavelength switching, simultaneous multi-channel generation and digital modulation. In this chapter, we describe narrow linewidth picosecond optical pulse generation by active mode-locking of a MGC laser. The MGC laser has the advantage of using a compact folded external cavity system, which can readily be extended to allow multiwavelength short pulse generation [1]. The spectral linewidth of the optical pulse is efficiently narrowed by the coupled grating-loaded external cavity structure. This feature is very attractive for the soliton based communication systems.

The organisation of this chapter is as follows. Ultrashort optical pulse laser sources for optical TDM applications are briefly reviewed in section 4.2. Techniques discussed here for generation of short optical pulses using diode lasers include active mode-locking, passive mode-locking, hybrid mode-locking and gain switching. Section 4.3 of this chapter describes the mode-locked MGC laser system generating in a single channel, and presents an experimental investigation of the dependence of pulsewidth and spectral width on the external structures. The multiwavelength ultrashort pulse generation will be presented in the following chapter. Section 4.4 gives a single channel coupled cavity rate equation analysis, which shows good agreement with experimental results. A conclusion is finally given in section 4.5.

4.2 Review of Optical Pulse Generation Techniques Using Semiconductor Lasers

The generation of ultrashort optical pulses using semiconductor lasers is of great interest because of its potential applications in electro-optic sampling, solition transmission, optical sensing, and optical TDM communication systems [2-4]. The simplest idea for the generation of optical pulses from a laser is to switch the gain or loss of the laser. The main techniques for the generation of ultrashort optical pulses are mode-locking, gain switching and Q-switching. Theoretically, it is possible to generate very short optical pulses (~50fs) in a semiconductor gain medium because of its broad gain spectrum (~100nm). Producing pulses with the minimum duration attainable for a given spectral width (the so called "bandwidth limited" pulses) are very important for low-chirp or soliton transmission systems.

This section introduces short pulse generation techniques, including gain switching [5-6] and mode-locking [7-9]. The operating principles and the advantages and dis-advantages of each technique are discussed in terms of their performance characteristics for pulsewidth, spectral width, repetition rate, and pulse energy. The main emphasis is on active mode-locking since it is used in this work. Further information about these techniques can be found in references [10-12].

4.2.1 Mode Locking

Mode-locking of a semiconductor laser offers a common way to produce optical short pulses [7-9], and typical output pulse durations are generally of the order of less than one picosecond to several picoseconds. Normally, the optical pulses of a single external cavity laser using mode-locking techniques exhibit excess optical bandwidth beyond the Fourier transform limit because of the self-phase modulation of the optical pulses. Mode-locking is achieved by introducing a mechanism inside the laser cavity to cause the longitudinal modes to interact with one another thereby locking them in phase [12]. There are three categories of mode-locking, i.e., active (forced) mode-

locking [7,13-14], passive mode-locking [8-9,15], and hybrid mode-locking [8,16,21]. An actively mode-locked laser generates accurately timed pulses and provides synchronisation between electrical clocks and optical pulses. By using a stable microwave oscillator to modulate an intracavity gain, loss, or phase element at the intercavity mode spacing frequency, the longitudinal modes of the laser are phase-locked together to produce short optical pulses. Ho et al. reported the first mode-locked semiconductor laser with a pulsewidth of 23 ps [17]. The shortest pulsewidth of 0.58 ps was obtained by modulating the laser at higher harmonics of the fundamental cavity frequency [7]. Lau indicated that narrow-band modulation of semiconductor lasers could be possible above 100 GHz at the intercavity mode frequency [18]. Passive mode-locking is performed by using a saturable absorber in the cavity. The first passively mode-locked semiconductor laser was observed by Ippen et al. [19] in 1980. Very short subpicosecond optical pulses have been demonstrated since then [15], and pulse repetition rates of up to 100 GHz have been reported [20]. In hybrid mode-locking, an intracavity saturable absorber shortens the pulses and brings the laser close to the passive mode-locking condition. Shorter and synchronised pulses at high repetition rates can be obtained. A pulsewidth of 1.4 ps was reported from a monolithic hybrid mode-locked laser at repetition rate of 15 GHz [21]. In addition, a colliding-pulse mode-locking (CPM) scheme [22-23] has been used to generate ultrashort pulse in the monolithic semiconductor laser. Instead of having a single pulse passing through the saturable absorber at one time, CPM lasers utilize the coherent interaction of two counter propagating pulses colliding at the saturable absorber to produce shorter pulses with doubled repetition frequency. Transform-limited optical pulses with duration as short as 0.64 ps were achieved at repetition rates of 350 GHz in the monolithic CPM quantum well lasers. Other devices, such as surface emitting laser diodes, also show potential as sources of ultrafast optical pulses [24].

A. Active Mode Locking:

An example configuration for the active mode-locking is shown in figure 4.1. It

consists of a semiconductor diode laser with an antireflection coated facet coupled to an external cavity. The external cavity contains a collimating lens, a feedback mirror, and possibly a wavelength control filter. The cavity resonance frequency is determined by the cavity round-trip time of the laser

$$f_{cav} = \frac{c}{2(l_{ext} + \mu_g l)} \tag{4.1}$$

where l_{ext} and l are the length of the external cavity and the laser chip respectively, c is the velocity of light in a vacuum, and μ_g is a group refractive index.

In active mode-locking, the gain of the laser is modulated with electrical pulses that have a period nearly equal to the round-trip time in the laser cavity, so that the pulse circulating in the cavity arrives at the active medium at the instant where the modulated gain reaches its maximum value. Therefore, the returning pulse from the external cavity receives maximum gain during its peak, and so is amplified. The duration of output pulses is a tenth or hundredth of the period of the gain modulation, depending on the pulse repetition rate [13,25]. This is because the returning pulse will not be amplified unless the gain exceeds the loss within the cavity. The "window" of amplification is usually narrow under an appropriate operation condition, and so the pulse is shortened every round trip. This process continues until it is limited by the pulse-broadening (dispersive) mechanisms inside the cavity.

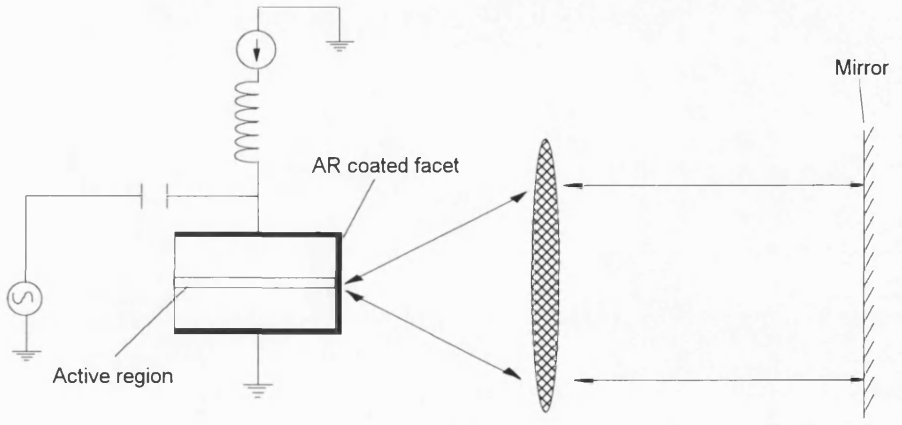

Figure 4.1. Schematic diagram of active mode-locking of semiconductor laser by coupling to an external cavity.

In order to get very short optical pulses from the devices, the coupling to the external cavity must be strong, and the electrical modulation pulse must be stable, narrow and of large amplitude in order to create a very short time window of net gain in the device. Pulses as short as 0.58 ps with 0.024 pJ of energy have been generated using active mode-locking of single semiconductor lasers [7]. The device was actively mode-locked with a 27dBm sinusoid at a 16 GHz repetition rate. The problem with this kind of device is that it is difficult to get short *single* pulse output (i.e., the optical pulses are produced with temporal substructure within the pulse envelope). These substructures are initiated from imperfect anti-reflection (AR) coatings of the laser chip. The spectrum has groups of external cavity modes clustered around the laser chip modes due to the three facet cavity. These laser chip modes cause a serious problem because the phases of the external cavity modes within one group have no fixed relationship with the phases of the modes within the neighbouring group. This is because the refractive index of the active medium is a function of frequency and this gives rise to the undesirable effect of the axial modes being unequally spaced due to material dispersion [26]. Therefore, the modes within different groups can not be locked to each other, resulting in substructure within the pulses [7,27]. The numerical results of Schell et al. [28] have shown that the substructure does not vanish even for rear facet AR reflectivities as low as 10^{-6}.

In order to overcome the detrimental effects of residual facet reflectivity, bandwidth-limiting elements or dispersive elements, such as grating or etalons, can be used to select only one chip mode, and so enable stable and single peaked optical pulses to be generated [29]. The drawback of this technique is that it limits the spectral width of the mode-locked optical pulse and as a result limits the minimum pulse duration obtainable with this method. Recently, by separating the gain and gain modulation functions into two segments, the multiple pulsation problem has been suppressed. Single pulses as short as 1.4 ps and energies as high as 3.5 pJ [8] have been achieved using a two-section active mode-locking technique.

B. Passive Mode Locking

A typical configuration for passive mode-locking is shown in figure 4.2. The laser diode provides gain medium, and is coupled to the external cavity through the facet with an antireflection coating. The external cavity is formed with a plane mirror. The key component necessary for passive mode-locking is a saturable absorber which is either inserted into an external cavity or induced inside the laser [15]. The laser is driven only by a DC current, in contrast with active mode-locking where a periodic drive current is used. With appropriate diode biasing conditions (usually above the threshold current of the laser), the optical pulses are generated at a repetition rate inversely proportional to the round trip time of the external cavity.

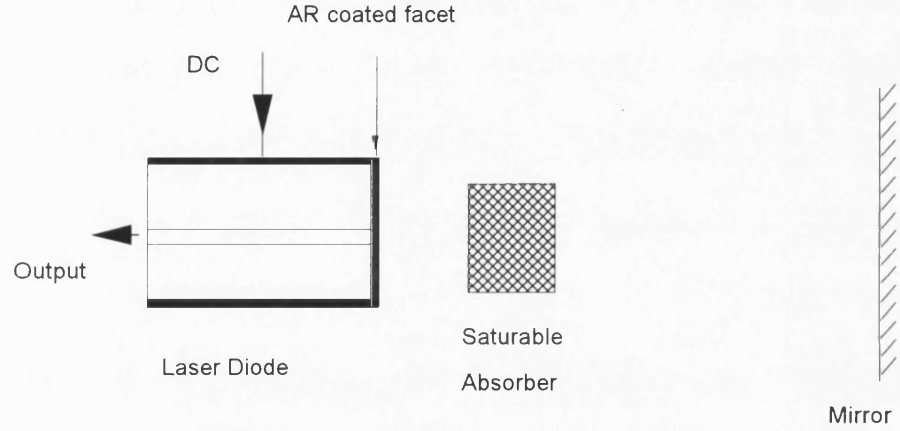

Figure 4.2. Configuration of a passively mode-locked semiconductor laser

The essential requirement for passive mode-locking is that the recovery time of the absorber is faster than the recovery time of the gain [8,10]. Also, the saturable absorbers should be chosen so that they saturate more easily than the gain medium. In this case, the net gain increases rapidly after the loss is saturated, as shown in figure 4.3. The rapid increase in the net gain speeds up the rise time of circulating optical pulse followed by gain saturation. The gain saturation results in an abrupt quenching of the pulse. The presence of the saturable absorber gives rise to a short time of net gain so that shorter pulses can be generated.

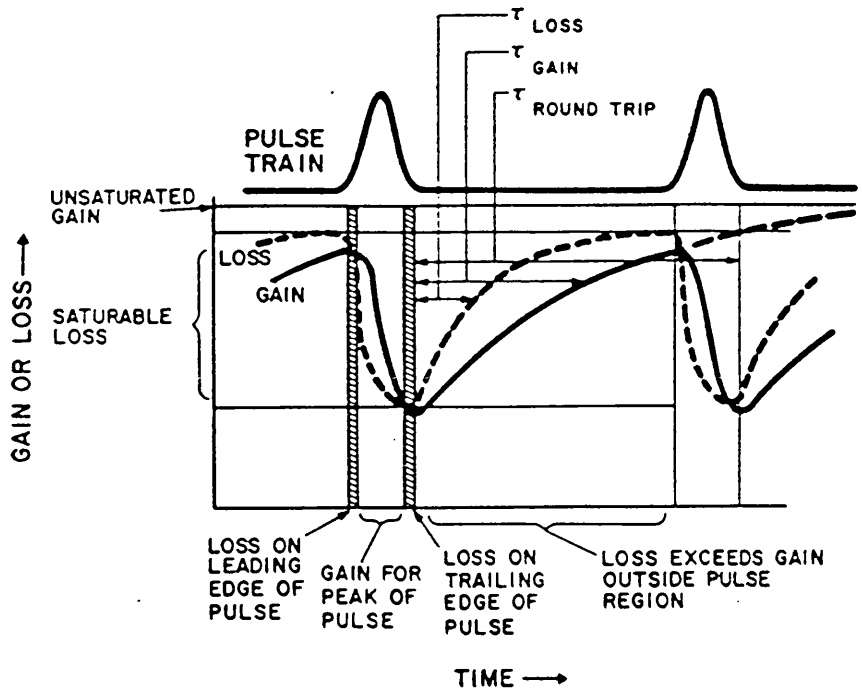

Figure 4.3. Gain and loss dynamics for passive mode-locking by a saturable absorber. (After Ref. [41])

From the pulsewidth point of view, passive mode-locking is superior to active mode-locking and gain switching because of pulse shaping due to the absorber. However, with passive mode-locking, the random fluctuation in spontaneous emission influences the pulse shaping mechanism, and leads to a high timing jitter [8-9]. The other subsidiary phenomena of passive mode-locking is "self-pulsation", which is caused by the presence of a saturable absorber [30]. Self-pulsation can inhibit mode-locking. Therefore, it should be avoided when operating a passively mode-locked laser. Palaski and Lau [30] have shown that with a proper biasing condition and high reflectivity coatings passive mode-locking can be achieved without the effect of self-pulsation.

C. Hybrid Mode-Locking

In practice, it is difficult to couple the modulation signal to the device at high frequency because of parasitics (such as junction capacitance and bond wire inductance). In order to synchronise the pulses at a high repetition rate, the hybrid

mode-locking technique is very useful. In hybrid mode-locking, a segmentation in the p-side contact allows electrical isolation between the gain modulation and saturable absorption section. Saturable absorption is the dominant mechanism for achieving very short pulses, so that it is not as important to have an extremely short electrical modulation waveform. A larger capacitance on the modulation section can be tolerated resulting in simpler device fabrication. Since the saturable absorber can be dc reverse biased, the absorber can recover to an absorbing state only a few tens of picosecond after the passage of the optical pulse leading to an effective multiple pulse suppression mechanism. A pulsewidth of 1.9 ps was reported from a three-section hybrid mode-locked semiconductor laser at 6 GHz [8].

4.2.2 Gain Switching

Gain switching is easily achieved by optimising the first period of the relaxation oscillation by rapidly switching on the diode laser with subnanosecond duration electrical pulses [5-6]. Typical output pulse durations are generally of the order of 20 ps to 30 ps by direct gain switching. Gain-switching does not require special device structures or an external cavity. The laser action takes place between the two facets of the laser chip and the laser chip is driven by either a short electrical pulse train or a strong RF signal with a bias current usually below the threshold level. The repetition rate of the output pulses is not restricted to the cavity resonant frequency, and is limited by relaxation oscillation frequency of the laser and device parastic.

The principle of gain-switching is related to relaxation oscillations in lasers. The relaxation oscillation in the transient response of the laser is due to interaction between photons and carriers [31]. When the laser current is turned on from below to above the threshold current, the output of the laser oscillates periodically for a few cycles before is reaches its steady-state value. The initial carrier density is rather small since the laser is biased below the threshold. The carrier density starts to build up as the leading edge of the electrical pulse arrives. The first spike of relaxation oscillation is emitted after the carrier density rises to the threshold current density. The following spikes of

relaxation oscillation can be quenched by turning-off the electrical pulse in order to generate a single peak output pulse train. If the bias current is too high, the depleted carrier density could recover to reach the threshold again, resulting in a secondary peak of the output pulse being generated.

The advantage of using the gain-switched pulses is the flexibility to change the repetition rate without modifying the cavity length. However, when the laser is suddenly switched from below to above threshold, significant fluctuations in both the carrier density and the time delay between the excitation and optical output are produced. These produce significant frequency chirp and timing jitter [32] associated with the gain-switched optical pulses. Therefore, the optical spectrum of the gain-switched pulses is normally very broad, and the time-bandwidth product of the gain switched pulse is typically several times the Fourier transform limit. In order to obtain near Fourier transform limit pulses, additional optical filtering of the output optical pulses, or pulse compression techniques are required. Recently, grating compressors [33] and fibre compression techniques [6] have been employed to compress the chirped optical pulses generated from gain switched diodes. A gain-switched DFB diode laser has exploited the soliton compression effect to produce optical pulses of 0.63 ps [6].

4.3 Single Channel Narrow Linewidth Picosecond Optical Pulse Generation

A. Device Operation:

Figure 4.4 shows the experimental set-up for ultrashort pulse generation using the MGC laser. The physical construction of the MGC laser used in the experimental work is depicted in the MGC laser unit of figure 4.4. The laser contains a laser bar, a collimating lens and diffraction grating reflection filter, all set to form the same structure as described in last chapter. To achieve active mode-locking in single channel, the output amplifier stripe 3 is biased with continuous current, so that when reflector stripe 1 is also dc biased, a lasing mode propagates between the uncoated

facets of the two stripes via the lens and grating. Applying an RF signal at a frequency corresponding to the cavity resonance frequency to the reflector laser stripe 1 allows picosecond pulses to be generated at the repetition rate corresponding to the cavity round-trip time.

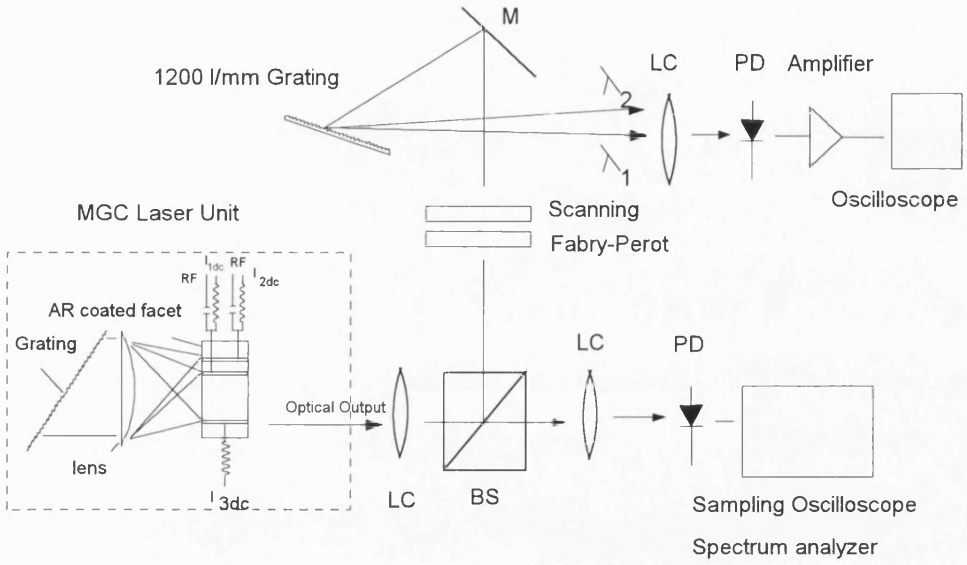

(PD- Photodiode, LC- collimating lens, BS- Beam Splitter and M- Mirror)

Figure 4.4. Experimental set-up for picoseond pulse generation using actively mode-locked MGC laser.

This cavity configuration has an advantage compared with a single external cavity laser, in that the picosecond optical pulses can be easily switched from one wavelength to another. This can be achieved by continuously driving the output amplifier stripe with a dc bias current, and redirecting the dc bias current and RF signal from one reflector stripe to another. Also the two active laser guides are coupled through the frequency filter element of a diffraction grating, thus it is efficient in narrowing the spectral linewidth. In addition, the two current inputs required to generate a single channel can be varied to obtain optimum narrow picosecond pulse generation in a more robust manner than for the case of mode-locking of a single stripe device.

B. Experimental Arrangement:

In the experiment, the laser bar was bonded p-side up on a temperature controlled mount and set in the external cavity to form a compact system. The diffraction grating had 1200 lines/mm and was set for overall lasing operation at 1.52 μm wavelength. The collimating lens was used with a focal length 6.5 mm and numerical aperture 0.62 and spot size of 0.8 μm. The external cavity length was varied between of 3 and 5 cm. The measurement arrangements to characterise the picosecond optical pulse from the actively mode-locked MGC laser are then shown in figure 4.4, which allows simultaneous measurement of pulse width and spectral linewidth under mode-locking conditions.

The output laser amplifier and the reflector laser guide were dc biased and a sinusoidal RF signal at a frequency of around 1.65 GHz, corresponding to the cavity round-trip time, was superimposed on the dc bias via a commercial bias-tee and applied to the output laser guide. The RF signal was generated by a microwave sweep oscillator (HP 8350B) and amplified by ZHL-42 Mini-Circuits amplifier to provide about 30 dBm RF power required for active mode-locking. Three instruments were used to measure the performance of the MGC laser. The pulse shape was monitored using a fast InGaAs photodiode (risetime<18ps) and digital sampling scope. The detected pulses were also coupled to a spectrum analyser (HP 8593A) with 26.5 GHz bandwidth, which provided the electrical spectrum of the generated pulses. An inverse fast Fourier transform (IFFT) was performed on the electrical spectrum analyser data to determine the pulsewidth of the generated optical pulses [34]. The optical spectrum of the output pulses was characterised by using a scanning Fabry-Perot interferometer with a finesse of about 50 combined with a 1200 lines/mm grating. This combination allowed the locked modes to be fully resolved and give an accurate measurement of the spectral linewidth.

C. Experimental Results:

In order to achieve picosecond pulse generation using an actively mode-locking

MGC laser system, a laser array comprising of InGaAsP/InP ridge laser stripes operating at the 1.5 μm wavelength range was used. The individual stripes had the same structure as that described in the last chapter. The light current characteristics of the two individual laser stripes were investigated and were found to be nearly the same as reported in last chapter. Based on the measured light current characteristic of the power output from the AR-coated and uncoated facets, the residual reflectivity of the AR-coated facet was estimated to be less than 1% . By aligning the external cavity, the threshold current was reduced from 80 mA to 55 mA without and with optical feedback from the external cavity. In practice, optimum coupling between the MGC laser bar and the grating was achieved by adjusting the grating angle and collimating lens positions. In addition, before actively mode-locking, the optical spectra of the MGC laser operating at CW condition was measured. Figure 4.5 shows the single mode operation of the MGC laser and the side mode suppression ratio (SMSR) was estimated to be above 20 dB.

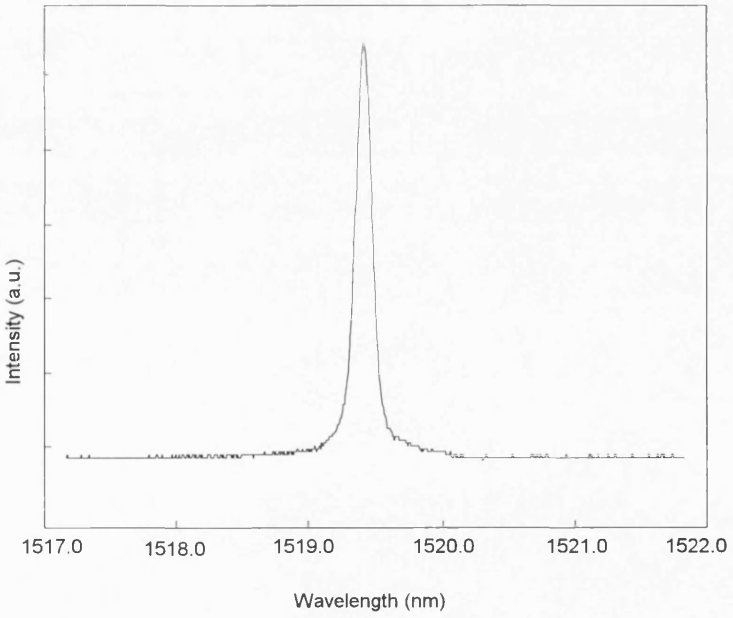

Figure 4.5. Optical spectrum of the MGC laser in single channel CW operation.

Under mode-locking, the MGC laser system was adjusted to produce the shortest pulse possible (estimated using the sampling scope) by adjusting the frequency

detuning, RF drive power and by varying the dc bias levels of the output stripe and reflector stripe. The optical pulse was monitored from the output amplifier stripe, and the temporal pulsewidth was measured with the sampling scope. An inverse fast Fourier transform (IFFT) was performed on the spectrum data, recorded from the spectral analyser, to provide further information on the pulsewidth of the generated optical pulsewidth [34]. A typical temporal pulse shape is shown in figure 4.6 (a). This was the shortest pulse and recorded when the output amplifier and reflector stripes were driven with dc currents of I_3=62 mA and I_1=61 mA respectively, and a sinusoidal RF signal at a frequency of around 1.65 GHz was superimposed on the dc bias to the reflector stripe 1. The measured full width at half maximum (FWHM) of the pulse profile was 45 ps, and the peak power of the pulses was estimated using average power measurement to be about 45 mW. The corresponding optical spectrum was recorded using a Fabry-Perot interferometer combined with the measurement grating as shown in figure 4.6 (b). The well defined spectrum has a mode spacing of 1.65 GHz. This indicates that the modes around the peak wavelength are tightly locked together. The measured FWHM of the optical spectra is 0.088nm (11.5GHz). This gives a time-bandwidth product (TBP) of 0.51, which indicates that the generated optical pulse is near the Fourier transform limit of a Gaussian shaped pulse. The pulsewidths are limited by the spectral dispersion of the grating used. However the optical spectrum is narrower than that of a conventional single stripe external cavity actively mode-locked laser with identical components and cavity length. This feature is very attractive for potential applications in soliton transmission systems.

It has already been shown that the bandwidth-limiting element filter such as a diffraction grating has an important effect on the pulsewidth and optical linewidth of the pulses in mode-locked external cavity semiconductor lasers [7]. The bandwidth-limiting element filters out the excess bandwidth at expense of a wider optical pulsewidth. To assess the effectiveness of the diffraction grating on the pulsewidth and spectral linewidth, the MGC laser mode-locking experiment was repeated using a 600 lines/mm diffraction grating. This also worked in the near Littrow configuration, with a

diffraction angle of 30^0 at 1.52 μm wavelength. Fig.4.6 (c) and (d) show the results of the laser using this configuration. The measured pulsewidth is found to be 38 ps as opposed to 45 ps observed using the 1200 lines/mm grating, however the optical linewidth increases from 0.088nm (11.5GHz) to 0.12 nm (16GHz), causing the time-bandwidth product to increase from 0.51 to 0.61.

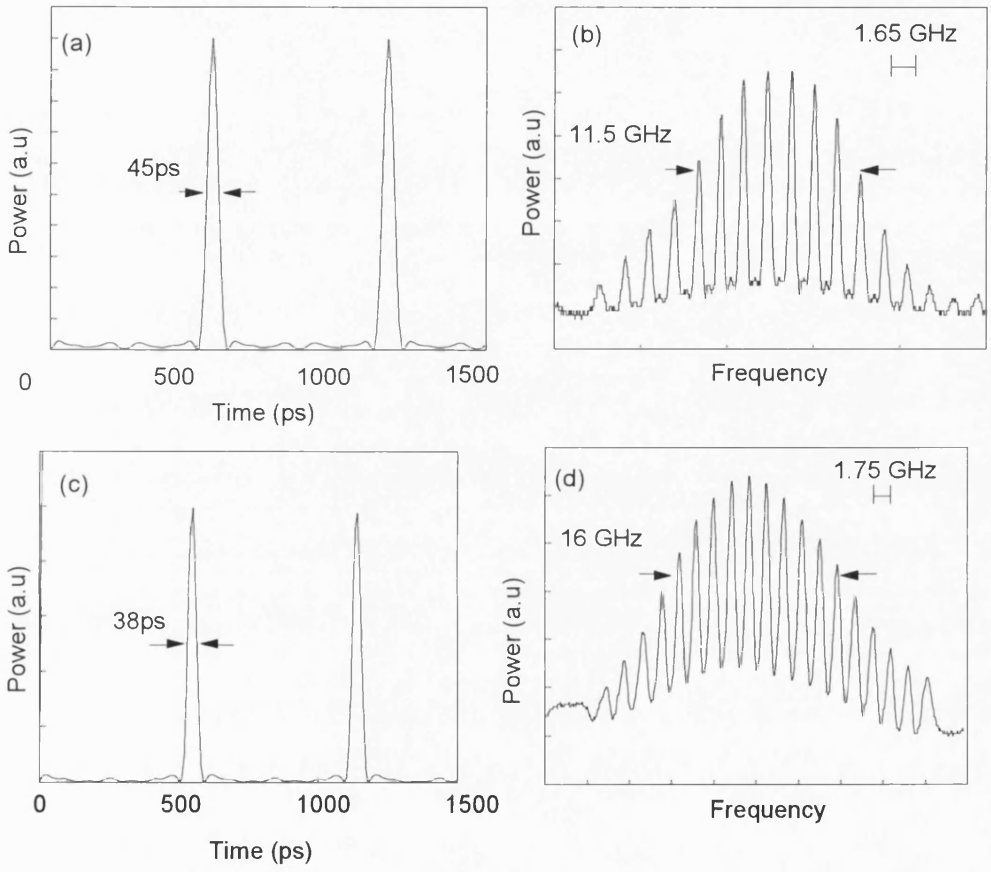

Figure 4.6. Measured pulse shapes and spectra of the active mode-locked MGC laser; (a)&(b), 1200 lines/mm grating, RF=1.65 GHz, (c)&(d), 600 lines/mm grating, RF=1.75 GHz.

D. Comparison with external cavity laser and Discussion:

We have experimentally compared the mode-locking of the MGC laser with that of a single external cavity laser. The external-cavity configuration for mode-locking is formed by driving only one stripe in the laser array and setting the grating for efficient lasing. However, the RF frequency needed to generate mode-locking pulses is now

twice that used with the MGC laser. In the experiment, the 1200 lines/mm and 600 lines/mm diffraction gratings were again used as feedback bandwidth limiting elements, and worked nearly in the Littrow configuration with diffraction angles of 67° and 28° at 1.52 μm wavelength respectively. The results for the mode-locked external cavity laser are shown in figure 4.7 (a) - (d). The measured FWHM of pulses with 1200 lines/mm and 600 lines/mm grating are 40 ps and 35 ps respectively. The corresponding optical spectral linewidths are 0.15 nm (19 GHz) and 0.18 nm (23 GHz) and their time-bandwidth product (TBP) are 0.76 and 0.81 respectively. For comparison, all measured results are shown in table 4.1.

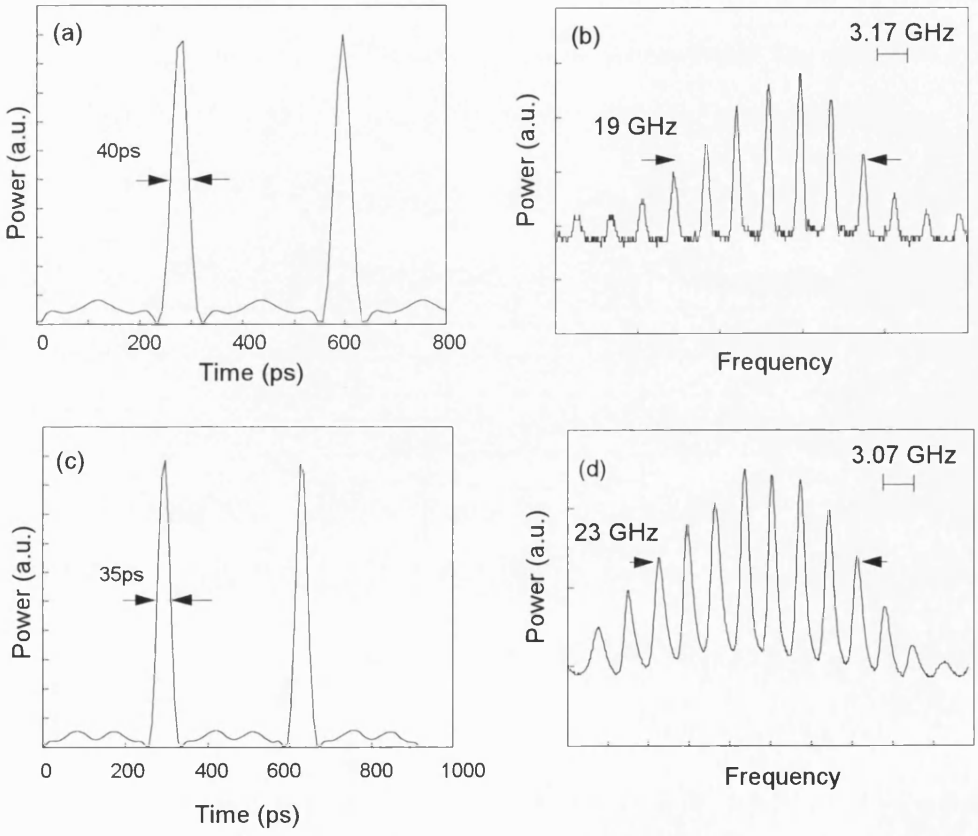

Figure 4.7. Measured pulse shapes and spectra of an actively mode-locked external cavity laser: (a) and (b), 1200 lines/mm grating, RF=3.17 GHz, (c) and (d), 600 lines/mm grating RF=3.07 GHz.

Table 4.1

	MGC Laser		External Cavity Laser	
Grating	1200 l/mm	600 l/mm	1200 l/mm	600 l/mm
Pulsewidth (ps)	45	38	40	35
Spectral width(nm)	0.09	0.12	0.15	0.18
TBP	0.5	0.61	0.76	0.81

From the table 4.1, it can be seen that the MGC laser has a narrower optical linewidth and a lower TBP, although the pulsewidth of MGC is larger than that of a single external cavity laser. The differences can be explained as follows: in the actively mode-locked MGC laser, one stripe is driven continuously, which can reduce the frequency chirp induced by the carrier density change. Also the MGC laser uses the diffraction grating to select the lasing wavelength twice in a round-trip time; this helps to narrow the optical linewidth more efficiently than that of a single external cavity laser.

E. Demonstration of switching for the picosecond pulse:

Switching of ultrashort optical pulses from one wavelength to another has also been experimentally demonstrated in the actively mode-locked MGC laser. This has been achieved by continuously driving output amplifier stripe 3 with a dc bias current, and switching the dc bias current and RF signal from reflector stripe 1 to stripe 2. Experiments have shown that the temporal and spectral performance of the mode-locking pulses are stable while switching from one channel to another.

4.4 Coupled-Cavity Rate Equation Analysis

A. Model:

Several theories of active mode-locking for semiconductor lasers have been

proposed [7, 9, 14, 27-28, 35-39]. Haus [35] has developed an analytical model for mode-locking of laser diodes in the frequency domain. Since frequency-domain models cannot account for transient effects, his model cannot give an insight into the dynamic behaviour of a laser with a cavity. An early time domain model for active mode-locking developed by Aspin and Carroll [36] is the rate equation model, where photon and carrier densities are assumed to be uniform along the diode length. This simple model is able to show the evolution of the pulse after the laser is turned on. Au Yeung [37] and van der Ziel [26] have attempted "self-consistent profile" approach which assumes that the pulse profile is reproduced exactly after one round trip of the cavity. Another time-domain model for actively mode-locked lasers is the transmission-line laser model (TLLM) [38]. The TLLM simulates the propagating optical field rather than the propagating photon density. The use of optical fields allows the pulse spectrum to be correctly modelled. Recent achievements in the theory of active mode-locking are concerned with computer numerical simulations using the travelling-wave rate equation [7,14,27-28,39]. The significant difference between this model and the previous model, is that this model treats the photon and carrier densities as a function of time and position. This is necessary, especially for the case where pulsewidths are an order of magnitude shorter than the laser chip round trip time, and variations of carrier and photon density along the length of the gain region are large.

In order to explain the experimental findings and to understand the methods of optimum generation of picosecond optical pulses, we employ the coupled-cavity rate equations which has been introduced in chapter 3 to simulate the mode-locking process of the MGC laser. Although this theory is based on spatially averaged quantities along the diode length, this is justified since the optical pulses generated from the MGC laser are longer than the laser chip round trip time [1]. However, as the pulse widths are significantly shorter than the cavity round-trip time, modified sets of rate equations are used incorporating the delayed feedback owing to long intracavity coupling via lens and grating. In addition, the bandwidth effects of the diffraction grating are included in the theoretical model. This is important, especially concerning the investigation of the

bandwidth effects on the mode-locking pulsewidth. For single channel operation, only two laser stripes 1 and 3 are pumped and coupled together through the diffraction grating and lens, so that a set of four equations is used to simulate the mode-locking process of the MGC laser in single channel, and these equations are rewritten as follows;

$$\frac{dN_1(t)}{dt} = -\sum_m g_m\left(N_1(t)-N_o\right)\frac{P_{1m}(t)}{1+\varepsilon P_{1all}(t)} - \frac{N_1(t)}{\tau_{s1}} + \frac{J_1}{ed} \tag{4.2}$$

$$\frac{dP_{1m}(t)}{dt} = -\Gamma g_m\left(N_1(t)-N_o\right)\frac{P_{1m}(t)}{1+\varepsilon P_{1all}(t)} - \frac{P_{1m}(t)}{\tau_p} + \frac{\beta N_1(t)}{\tau_{s1}} + K_{1m}P_{3m}(t-\tau_{ext}) \tag{4.3}$$

$$\frac{dN_3(t)}{dt} = -\sum_m g_m\left(N_3(t)-N_o\right)\frac{P_{3m}(t)}{1+\varepsilon P_{3all}(t)} - \frac{N_3(t)}{\tau_{s3}} + \frac{J_3}{ed} \tag{4.4}$$

$$\frac{dP_{3m}(t)}{dt} = -\Gamma g_m\left(N_3(t)-N_o\right)\frac{P_{3m}(t)}{1+\varepsilon P_{3all}(t)} - \frac{P_{3m}(t)}{\tau_p} + \frac{\beta N_3(t)}{\tau_{s3}} + K_{3m}P_{1m}(t-\tau_{ext}) \tag{4.5}$$

Definitions of physical and geometric parameters are the same as those described as in chapter 3. As in other mode-locking semiconductor laser theories [27,37,39], the following assumptions have implicitly been made in the above coupled -cavity rate equations; (1) Homogeneous current injection is assumed for the sake of simplicity, and diffusion is neglected in all directions. This is acceptable for narrow waveguides. (2) Dispersion due to the refractive index dependence of the laser material on the carrier concentration is ignored. This effect is very small for the pulsewidth on the order of 0.5 ps or larger, although for the pulsewidth lower than 100 fs, this effect must be included [26]. (3) It is assumed that the lasing gain is linear with carrier density, and both Γ and β are constant with wavelength.

B. Numerical Methods

In order to simulate active mode-locking process of the MGC laser in single channel operation, the output laser stripe 3 was driven continually and the reflector stripe 1 is modulated sinusoidally at a period equal to the MGC laser round-trip time. In this case, the injection-current was given by

$$I(t) = I_{dc} + I_{rf} \sin(\omega_{\text{mod}} t) \tag{4.6}$$

where $\omega_{\text{mod}} = 2\pi / \tau_m$ and τ_m is the MGC laser cavity round-trip time which is given by

$$\tau_m = \frac{4l_{ext} + 4l\mu_g}{c} \tag{4.7}$$

The numerical values for the MGC laser parameters in above equations are the same as used in previous chapter. The non-linear and coupled equations have been solved numerically using a fourth-order Runge-Kutta algorithm, and the initial conditions for the calculations were obtained from Eq.(4.1)-(4.4) by setting the left-hand side of the equations equal to zero. The total number of the optical modes (i.e., those falling within the grating spectral reflection peak) that can be generated potentially is determined by the grating bandwidth divided by the longitudinal mode spacing of the MGC laser. Standard checks were performed to verify the validity of the solutions, these checks including the insensitivity to initial conditions and time steps, and the stability of the solution after many repeated round-trips. The time step is chosen to be 1 ps. This gave accurate results and the shortest calculation time.

C. Results and discussion

Figure 4.8 shows the typical results of carrier density and waveforms of the pulse in the output amplifier guide using dc current of 2 mA above the threshold applied to both stripe 1 and 3, with an 85 mA peak-peak RF current at 1.66 GHz applied to reflector stripe 1. The pulses in this simulation have almost linear sides and a little broadening at their base, and appear consistent with those recorded by the digital sampling scope in our experiment. The significant depletion in carrier density that occurs with each optical pulse emission is also shown in figure 4.9.

The simulation indicates that the pulsewidth not only depends on the RF power, RF frequency, and the bias levels of the two stripes, but also on the resolution bandwidth of the grating used. The shortest pulsewidth is obtained when the lasers are biased at just above the threshold currents. The pulsewidth is limited by the optical

bandwidth of the diffraction grating used, which determines the system bandwidth of the MGC laser [40]. For the 1200 line/mm diffraction grating used (the resolution bandwidth of the grating is estimated to be about 33 GHz), the shortest pulsewidth is calculated to be 43 ps. The simulation shows that the minimum pulsewidth can be lowered by using a larger reflection bandwidth (i.e., lower resolution) diffraction grating. However, it is difficult to get sufficient optical coupling for both channels if a low resolution grating is used. For cw operation, a low resolution also enables the ratio of the power in the adjacent modes to that in the main lasing mode to be significant, hence the side mode suppression ratio becomes small. A compromise must be made therefore to obtain overall optimum performance.

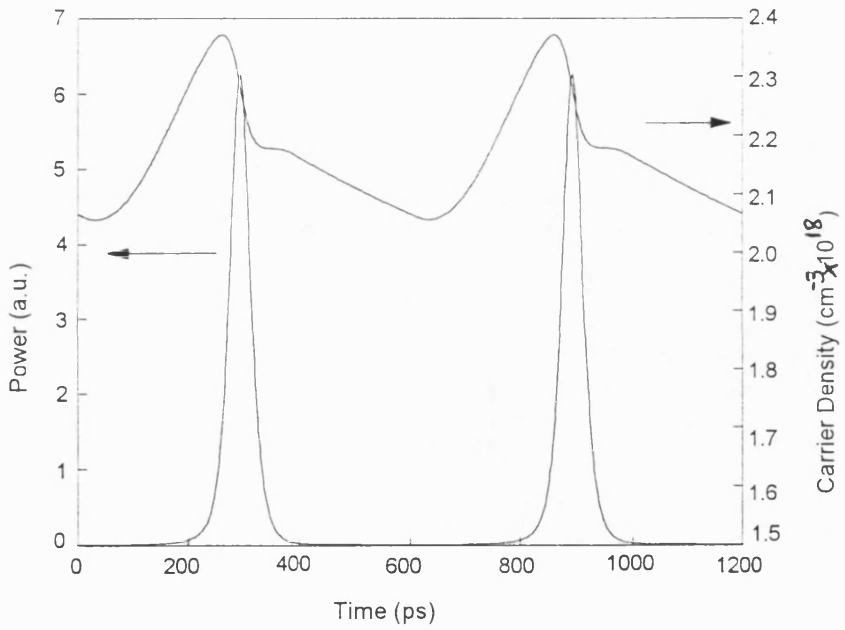

Figure 4.8. Simulated resulted of the ultrashort pulse generation by an actively mode-locked MGC laser under single channel operation. The calculations assume dc currents of 2 mA above threshold applied to stripes 1 and 3. A 90 mA peak-peak RF current at 1.66 GHz is also applied to stripe 1.

Frequency detuning is thought to improve pulse stability and minimise pulse width in an external cavity mode-locked laser and this has been studied experimentally and theoretically [38,40]. The effect of frequency detuning on the mode-locked MGC laser under single channel operation has been investigated. Here, several different RF

drive frequencies, which are set at a value less than or more than the round-trip frequency, are applied and the temporal evolution of the pulses and the pulse FWHM are theoretically and experimentally examined. A plot of the pulsewidth as a function of frequency detuning is shown in figure 4.9. In the experiment, the cavity length, hence the absolute detuning, is difficult to measure. Thus we label zero detuning as the point at which the shortest pulses occurred. The experimental points in figure 4.9 are obtained by keeping the cavity length fixed, changing the modulation frequency and repeating the process of measuring the pulsewidths. All parameters are kept the same in the calculations, including the cavity length and coupling coefficient, only the modulation frequency is changed. The numerical simulation shows that the gain saturation has a significant effect on the pulsewidth. By choosing the gain saturation coefficient of 1×10^{-17} cm^3, a good agreement between theory and experiment has been achieved for nearly all frequency detuning as shown in figure 4.9. It can be seen that the short pulse may be obtained over a range of larger than 60 MHz frequency detuning in the actively mode-locked MGC laser.

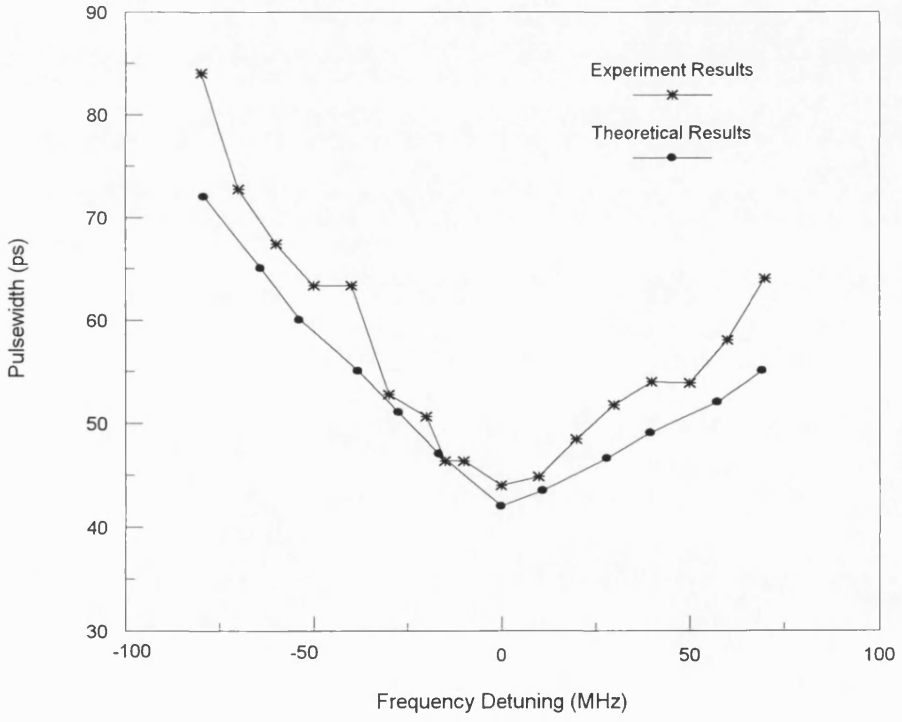

Figure 4.9. Pulsewidth as a function of frequency detuning in single channel operation of the actively mode-locked MGC laser.

4.5 Conclusion

The MGC laser is found to be suitable for narrow linewidth picoseond optical pulse generation using active mode-locking of the laser. With a 1200 lines/mm diffraction grating, picosecond pulses with a spectral linewidth as low as 0.088 nm have been achieved in a single channel. The dependence of pulsewidth and spectral linewidth of the short optical pulses on the MGC laser structure, especially on the bandwidth of the diffraction grating used, are experimentally examined. Compared with a single external cavity laser, the MGC laser has better optical spectral characteristic and generates narrower optical spectra. This characteristic is attractive for potential applications in the soliton based transmission wavelength switched systems. The wavelength switching of short optical pulses has also been demonstrated with this laser.

A theoretical model involving a set of coupled-cavity rate equations has been performed to simulate the mode-locking process of the MGC laser. The pulse shapes are calculated and compared with the experimental results. The theoretical simulations are in good agreement with experimental results. The minimum achievable pulsewidths generated by the actively mode-locked MGC laser are shown to be limited by the resolution bandwidth of the diffraction grating used. The dependence of the pulsewidth on RF drive frequency detuning has been theoretically and experimentally investigated and the results show that short pulses can be obtained over a wide range of detuning in the MGC laser.

References

[1] B. Zhu and I. H. White, "Multiwavelength short optical pulse generation using an actively mode-locked multichannel grating cavity laser," *IEEE J. Lightwave Technol.*, vol. LT-13, pp.2327-2335, 1995.

[2] R. S. Tucker, G. Eisenstein and S. K. Korotky, "Optical time-division multiplexing for very high bit-rate transmission," *IEEE J. Lightwave Technol.*, vol. LT-6, pp. 1737-1749, 1988.

[3] J. A. Valdmanis, G. A. Mourou, and C. W. Gabel, "Picosecond electro-optic sampling system, "*Appl. Phys. Lett.* vol. 41, pp.211, 1982.

[4] J. C. Diels, J. J. Fontaine, I. C. Mcmichael, and F. Simoni, "Control and measurement of ultrashort pulse shapes (in amplitude and phase) with femtosecond accuracy", *Applied Optics,* vol 24, pp.1270-1282, 1985.

[5] H. F. Liu, M. Furazawa, Y. Kawai, and T. Kamiya, "Gain-switched picosecond pulse (<10ps) generation from 1.3um InGaAsP laser diodes," *IEEE J. Quantum Electron.*, vol. QE-25, pp.1417-1424, 1989.

[6] J. T. Ong, R. Takahashi, M. Tsuchiya, S. H. Wong, R. T. Sahara. Y. Ogawa, and T. Kamiya, "Subpicosecond soliton compression of gain switched diode laser pulses using an Erbium-doped fiber amplifier," *IEEE J. Quantum Electron.*, vol. QE-29, pp.1701-1707,1993.

[7] J. E. Bowers, P. A. Morton, A. Mar, and S. W. Corzine, " Actively mode-locked semiconductor lasers," *IEEE J. Quantum Electron.*, vol. QE-25, pp. 1426-1439,1989.

[8] D. J. Derickson, R. J. Helkey, A. Mar, J. R. Karin, J. G. Wasserbauer, J. E. Bowers, "Short pulse generation using multisegment mode-locked semiconductor lasers," *IEEE J. Quantum Electron.*, vol. QE-28, pp. 2186-2201, 1992.

[9] I. Kim and K. Y. Lau, "Frequency and timing stability of mode-locked semiconductor lasers-passive and active mode-locking up to millimeter wave frequencies," *IEEE J. Quantum Electron.*, vol. QE-29, pp. 1081-1090,1993.

[10] K. Y. Lau, "Short pulse and high-frequency signal generation in semiconductor lasers," *IEEE J. Lightwave Technol.*, vol. LT-7, pp. 400-418, 1989.

[11] P. P. Vasil'ev, " Ultrashort pulse generation in diode lasers," *Optical and Quantum Electronics*, vol.24, pp.801-824, 1992.

[12] A. E. Siegman, Lasers, chapter 27, University Science books, Mill Valley, 1986.

[13] R. S. Tucker, U. Koren, G. Raybon, C. A. Burrus, B. I. Miller, T. L. Koch, and G. Eisenstein, "40 GHz active mode-locking in a 1.5 mm monolithic external cavity laser", *Electron. Lett.*, vol. 25, pp. 621-622, 1989

[14] M. Schell, A. G. Weber, E. H. Boettcher, E. Scholl and D. Bimberg, "Theory of subpicosecond pulse generation by active mode-locking of a semiconductor laser amplifier in an external cavity : Limits for the pulsewidth," *IEEE J. Quantum Electron.*, vol. QE-27,

pp.402-408, 1991.

[15] N. Stelmakh, J. M. Lourtioz, "230 fs, 25 W pulses from conventional mode-locked laser diodes with saturable absorber created by Ion implantation", *Electron. Lett.*, vol. 29, pp. 160-162, 1993.

[16] A. G. Weber, M. Schell, G. Fischbeck, and D. Bimberg, "Generation of single femtosecond pulses by hybrid mode locking of a semiconductor laser," *J. Quantum Electron.*, vol. QE-28, pp.2220-2229,1992.

[17] P. T. Ho, L. A. Glasser, E. P. Ippen, and H. A. Haus, "Picosecond pulse generation with a cw GaAlAs laser diode," *Appl. Phys. Lett.* vol. 33, pp.241-242, 1978.

[18] K. Lau, "Narrow-band modulation of semiconductor lasers at millimeter wave frequencies (<100 GHz) by mode-locking ," *J. Quantum Electron.*, vol. QE-26, pp.250-261,1990.

[19] E. P. Ippen, D. J. Eilenberger, and R. W. Dixon, "Picosecond pulse generation by passive mode-locking of diode lasers", *Appl. Phys. Lett.* vol. 37, pp.267-269, 1980.

[20]. S. Sanders, L. Eng, J. Paslaski, and A. Yariv, "108 GHz passive mode-locking of a multiple quantum well semiconductor laser with as intracavity absorber," *Appl. Phys. Lett.* vol. 56, pp.310-312, 1990.

[21] P. A. Morton, J. E. Bowers, L. A. Koszi, M. Soler, J. Lopata, and D. P. Wilt, "Monolithic hybrid mode-locked 1.3 μm semiconductor lasers," *Appl. Phys. Lett.* vol. 56, pp.111-113, 1990.

[22] Y. Chen, M. Wu, T. Tanbun-Ek, R. Logan, and M. Chin, "Subpicosecond monolithic colliding-pulse mode-locked multiple quantum well lasers", *Appl. Phys. Lett.* vol. 58, pp.1253-1255, 1991.

[23] Y. K. Chen, and M. C. Wu, "Monolithic colliding-pulse mode-locked quantum well lasers," *J. Quantum Electron.*, vol. QE-28, pp.2176-2185, 1992.

[24] W. B. Jiang, R. Mirin, and J. E. Bowers, "Mode-locked GaAs vertical cavity surface emitting lasers," *Appl. Phys. Lett.* vol. 60, pp.1677-679,1992.

[25]. S.W. Corzine, J. E. Bowers, G. Przbylek, U. Koren, B. I. Moller, and C. E. Soccolich, " Actively mode-locked GaInAsP laser with subpicosecond output," *Appl. Phys. Lett.* vol. 52, pp.348-350, 1988.

[26] J. P. Van der Ziel and R. A. Logan, "Dispersion of the group velocity refractive index in GaAs double heterostructure laser," *IEEE J. Quantum Electron.*, vol. QE-19, pp.164-169, 1983.

[27] P. A. Morton, R. J. Helkey and J. E. Bowers, "Dynamic detuning in actively mode-locked semiconductor lasers," *IEEE J. Quantum Electron.*, vol.QE-25, pp.2621-2633, 1989.

[28]. M. Schell, A. G. Weber, E. Scholl and D. Bimberg, "Fundamental limits on sub-ps pulse generation by active mode-locking of semiconductor lasers: the spectral gain width and the facet reflectivities", *IEEE J. Quantum Electron.*, vol.QE-27, pp.1661-1668, 1991.

[29] P. J. Delfyett, L. T. Florez, N. Stoffel, T. Gmitter, N. C. Andreadakis, Y. Silberberg, J. P.

Heritage and G. A. Alphonse, "High power ultrafast laser diodes," *IEEE J. Quantum Electron.*, vol.QE-28, pp.2203-2219, 1992

[30] J. Palaski, and K. Y. Lau, "Parameter ranges for ultrahigh frequency mode locking of semiconductor lasers", *Appl. Phys. Lett.* vol. 59, pp.7-9, 1991.

[31] G. P. Agrawal and N. K. Dutta, Long-Wavelength Semiconductor Lasers. New York: Van Nostrand Reinhold, 1986.

[32] E. H. Bottcher, and D. Bimberg, "Detection of pulse to pulse timing jitter in periodically gain switched semiconductor lasers," *Appl. Phys. Lett.* vol. 54, pp.1971-1973, 1991.

[33] M. Kuznetsov, J. M. Weisenfield, and L. R. Radzihovsky, "Compression of picosecond pulses from diode lasers using a modified grating pair compressor," *Opt. Lett.*, vol. 15, pp. 180-182, 1990.

[34] J. W. Hedrick, "Predicting post-detection pulse characteristics using the FFT," Microwave Journal, vol. 36, pp.93-102, 1993.

[35] H. A. Haus, "Theory of mode-locking of a laser diode in an external resonator," J. Appl. Phys., Vol. 51, pp.4042-4049,1980.

[36] G. J. Aspin and J. E. Carrol, "Simplified theory for mode-locking in injection lasers," Proc. IEE, part I, vol. 3, pp.220-, 1979.

[37] J. A. Yueng, "Theory of mode-locking of a laser diode semiconductor laser in an external cavity," *IEEE J. Quantum Electron.*, vol. QE-17, pp.398-, 1980.

[38] A. J. Lowery, N. Onodera, and R. S. Tucker,"Stability and spectral behavior of the grating-controlled actively mode-locked laser," *IEEE J. Quantum Electron.*, vol. QE-27, pp.2422-2430, 1991.

[39] M. S. Demokan,"A model of a diode laser actively mode-locked by gain modulation ," *Int. J. Electron.* , vol.60, pp. 67-85, 1986.

[40] L. Zhai, A. J. Lowery, Z. Ahmed,N. Onodera, and R. S. Tucker, "Locking bandwidth of mode-locked semiconductor lasers" , Electron Lett., 28, (6), pp.545-546, 1992.

[41] P. W. Smith, Y. Silberberg, and D. A. B. Miller, "Mode locking of semiconductor diode lasers using saturable excitonic nonlinearities", J. Opt. Soc. Am. B/vol. 2, pp. 1228-1235, 1985.

Chapter 5

MULTIWAVELENGTH SHORT PULSE GENERATION USING ACTIVELY MODE LOCKED MGC LASER

5.1 Introduction

Chapter one has introduced the wavelength division multiplexing (WDM) [1] and optical time division multiplexing (TDM) technologies [2] for increasing transmission capacity in the future communication network. The successful operation of WDM and TDM techniques requires the development of multiwavelength or tunable laser sources, which can produce multi-WDM channels simultaneously, each channel being capable of generating high speed picosecond pulses. Gain switching [3] and mode-locking [4] are two commonly used methods for the generation of short optical pulses from semiconductor lasers. These lasers typically generate pulses at only a single wavelength, however, so that more than two sources are necessary for the above applications. Moreover, it is difficult to adjust the wavelength separations and pulse timings of separate lasers. So far multiwavelength picosecond pulse generation has been demonstrated using a range of techniques including utilising supercontinuum in optical fibres [5]. In addition, a novel double external cavity laser has also been reported [6], using two external cavity gratings to achieve dual wavelength short pulse generation. However, it is difficult in these methods to control the operation of each wavelength individually.

As described in last two chapters, the MGC laser has been developed for application in high speed wavelength switched WDM systems, and narrow linewidth picosecond short pulses are also generated with this laser. It is shown that the laser can readily be used as a multi-WDM channel ultrashort pulse generator [7-10] to allow both WDM and TDM

techniques to be combined for application in communication systems [11]. One of the great advantages of the proposed actively mode-locked MGC laser is that it provides a number of WDM channel picosecond optical pulses which can easily be synchronised, or controlled with a programmable relative delay between the channels, or switched from one channel to another. Such flexibility makes the laser very attractive for future ultrafast all-optical switching and WDM-TDM networks. Another advantage is that the multiwavelength picosecond pulses are generated with very narrow spectral width (less than 0.1 nm), which is very attractive for potential applications in soliton transmission systems.

In this chapter, we describe multi-wavelength picosecond optical pulse generation using active mode-locking techniques with this laser. Section 5.2 presents the experimental demonstration of simultaneous generation of dual wavelength picosecond optical pulses using the actively mode-locked MGC laser. Section 5.3 demonstrates dual wavelength short optical pulse generation incorporating relative timing control. Theoretical modelling of two wavelength short pulse generation and crosstalk between two channels under picosecond pulse operation are discussed in the section 5.4. Conclusions are finally presented in section 5.5.

5.2 Simultaneous Generation of Dual Wavelength Short Optical Pulses

A. Operation Principle

The MGC laser has been used to simultaneously generate dual wavelength picosecond optical pulses. The physical construction of the MGC laser is schematically depicted in figure 5.1. A MGC laser with the same structure as reported in the last chapter, but with a different pumping configuration, is used for achieving simultaneous generation of dual wavelength short optical pulses. Here, the output amplifier laser stripe 3, is biased with continuous current, so that when the reflector stripe 1 is also dc biased, a

lasing mode propagates between the uncoated facets of the two stripes via the lens and grating, at wavelength λ_1. Applying a second dc bias to the reflector stripe 2 allows a second lasing mode to be generated at a different wavelength λ_2, as determined by the cavity structure. If now an RF signal of a frequency corresponding to the cavity resonance frequency is applied to the output amplifier laser stripe 3, dual wavelength picosecond pulses with repetition rates corresponding to the cavity round-trip time are simultaneously generated, with one of the cavities operating at a slight frequency detuning [7].

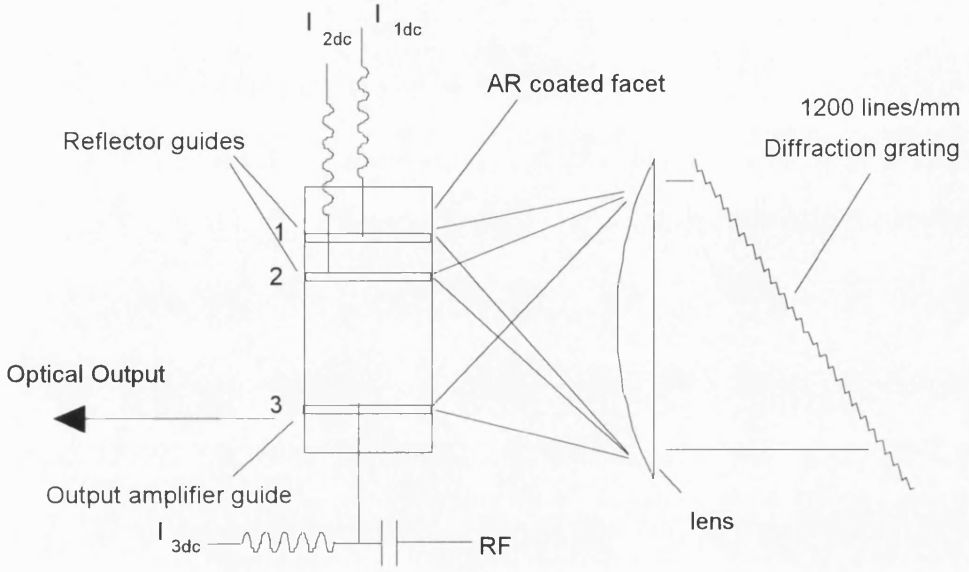

Figure 5.1 A schematic diagram of the actively mode-locked MGC laser for simultaneous generation of dual wavelength picosecond optical pulses

This cavity configuration has an advantage, in that it uses a single RF-frequency to generate two wavelength picosecond pulses. Also, the two current inputs required to generate a single channel can be varied to obtain optimum narrow picosecond pulse generation. It is anticipated that this laser can produce a range of wavelengths under short pulse generation similar to that achieved for long pulse or CW operation. As the cavity length is twice as long as that of a comparable single laser cavity, low modulation RF frequencies can be used. If required, the RF frequency can also be applied to the reflector stripes to achieve multiwavelength picosecond pulse generation without detuning in either

stripe.

B. Experimental demonstration

In order to demonstrate simultaneous generation of dual wavelength picosecond pulses, a laser array consisting of InGaAsP/InP ridge laser stripes was used. The structure of the laser array was the same as described in chapter 3. A high quality anti-reflection (AR) coating was applied to one facet of the laser bar, allowing the coated facet to have a residual reflectivity of less than 1%. In the experiment, the laser bar was bonded p-side up on a temperature controlled mount and set in the external cavity system. In operation, the coupling between the MGC laser bar and the grating was optimised by adjusting the grating angle and collimating lens positions. The 1200 lines/mm diffraction grating worked nearly in the Littrow configuration with a diffraction angle of 69° at 1.52 μm. A collimating lens was used with a focal length 6.5 mm, numerical aperture 0.62 and spot size of 0.8 μm. Before mode-locking , the laser operated mainly in single mode, with a side mode suppression ratio (SMSR) of greater than 20 dB. The wavelength separation between the two channels was 2.2 nm and was determined by the cavity configuration as described in chapter 3, the two channels emitting at wavelength of 1519.8 nm and 1522.0 nm, respectively.

The reflector stripes 1 and 2 and the output amplifier stripe 3 were dc biased at I_1=70 mA, I_2=71 mA and I_3=75 mA respectively. A sinusoidal RF signal at 1.6 GHz, corresponding to the cavity round-trip time, was generated by a microwave sweeper (HP8350B) and amplified by ZHL-42 Mini-circuit amplifier to provide 30 dBm RF power required for the active mode-locking. The RF signal was superimposed on the dc bias via a bias-tee and applied to the output laser amplifier. The pulse shapes were monitored using a fast InGaAs photodiode (< 18ps risetime) and sampling scope. The detected electrical signal was also coupled to a spectrum analyser (HP 8593A) with 26.5 GHz bandwidth, which provided the electrical spectrum of the generated optical pulses. The optical spectra

of the output pulses were characterised by using a scanning Fabry-Perot interferometer with a finesse of approximately 50 combined with a 1200 lines/mm grating to select a single channel and yet allow the locked modes to be well resolved.

C. Results

The MGC laser system was adjusted to produce the shortest pulses (estimated using a sampling scope) by adjusting the frequency and power of the RF drive and varying the dc bias levels of the output amplifier stripe and two reflector stripes. The pulsewidth was measured by monitoring the outputs from the reflector lasers. Figure 5.2 (a) and (b) shows the pulse trains measured from the sampling scope. An inverse fast Fourier transform (IFFT) was performed on the electrical spectrum data to provide further information on the pulsewidth of the generated optical pulses [12]. The measured full width at half maximum (FWHM) of the pulse profile of about 60 ps was measured using both methods.

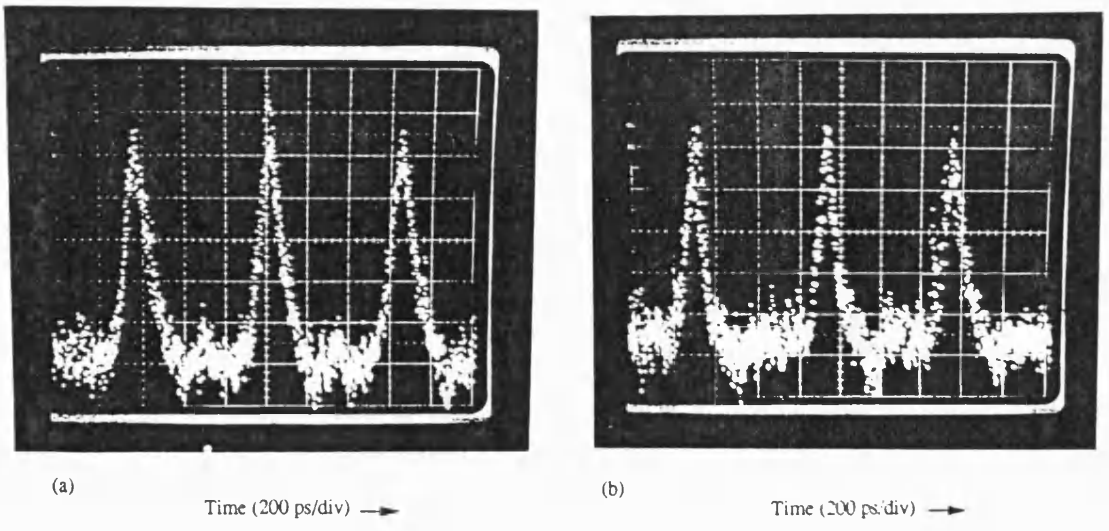

Figure 5.2. Dual wavelength short pulse trains from the actively mode-locked MGC laser as measured by the sampling scope, (a) and (b) for wavelength λ_1 =1519.8 nm and λ_2 = 1522.0 nm respectively.

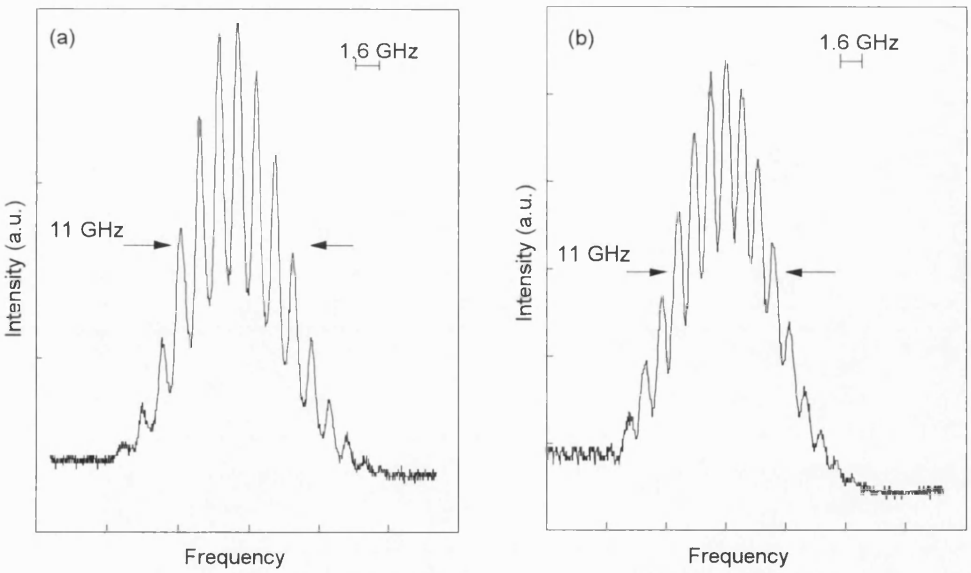

Figure 5.3. Measured optical spectra of the dual wavelength picosecond pulses generated from the actively mode-locked MGC laser, (a) and (b) for wavelength λ_1 and λ_2 respectively.

The spectral measurement of the generated pulses was carried out by monitoring the optical output from the output amplifier stripe. By rotating the measurement grating, the spectral output from each channel could be viewed. A typical spectral output is shown in figure 5.3 (a) and (b) with each being associated with one temporal short pulse. The FWHM of optical spectra of 11 GHz was measured for each channel, and so that the time-bandwidth product was 0.66. The pulsewidths are limited by the spectral dispersion of the grating used, but the optical spectra are quite narrow when compared with a single external cavity laser because of the CW driven reflector stripes locking the frequency chirp.

5.3 Variable Delay Dual-Wavelength Picosecond Optical Pulse Generation

A. Operation principle

The MGC laser has been employed to produce two wavelength picosecond optical pulse trains with a variable delay between them, which is important particularly for pump-probe applications. Figure 5.4 shows a schematic diagram of the MGC laser for dual wavelength short pulse generation with a relative time delay. In order to achieve mode-locking at the two wavelengths with a controlled delay, the output amplifier laser stripe 3 is continuously driven and two RF signals with a controlled relative delay are superimposed on the d.c. drive mode-locking of currents applied to the two reflector stripes 1 and 2 [8].

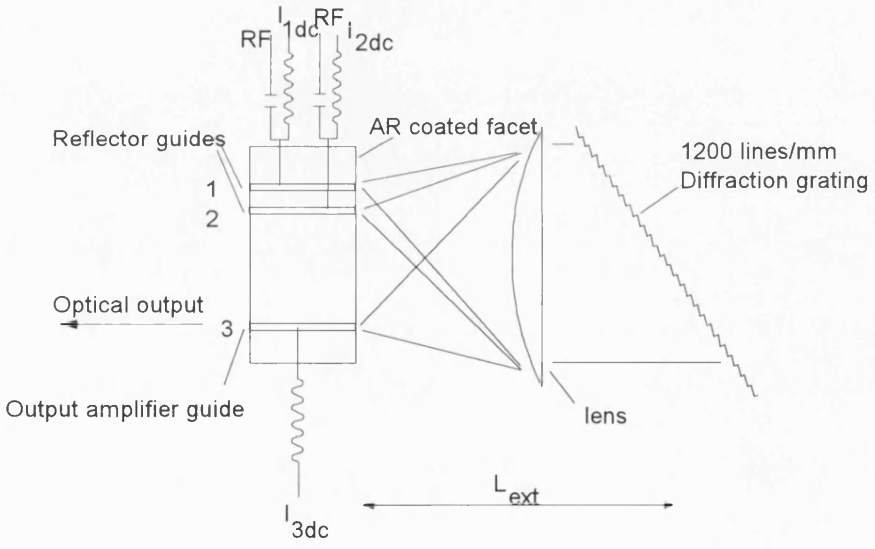

Figure 5.4. A schematic diagram of the actively mode-locked MGC laser fro the twin wavelength short pulse generation with a time delay.

This configuration has the advantage that it can be used to adjust the wavelength separations and the timings of the two pulse trains. Also, the two current inputs required to generate a single channel can be varied to obtain optimum narrow picosecond pulse

generation in a more robust manner than for the case of mode-locking a single stripe device.

B. Experimental arrangement

For experimental demonstration, a laser array consisting of InGaAsP/InP ridge laser stripes and with the same structure as described in last section was used. The external cavity was formed by a 1200 lines/mm diffraction grating and a collimating lens. The spectral channel spacing of 2.2 nm is determined by the cavity configuration, the two channels being at wavelengths of 1519.8 nm and 1522.0 nm respectively. In the experiment, a sinusoidal RF signal at around 1.78 GHz, corresponding to the cavity round-trip time, was generated by a microwave sweeper (HP 8350B) and divided into two by a microwave power splitter. Two identical ZHL-42 Mini-circuits amplifiers were used to amplify the RF signals, in order to provide the 30 dBm RF power required for active mode-locking. A coaxial phase shifter with a bandwidth of 12 GHz was placed in one arm and used to control the delay time between the two RF signals. The RF signals were superimposed on the d.c. bias via a bias-tee and applied to the reflector laser stripes. The light output was monitored mainly from stripe 3 and split in order for the pulsewidth and spectra of generated pulses to be simultaneously measured. The pulse width and optical spectra of the output pulses were characterised by using the same methods as shown in figure 4.1.

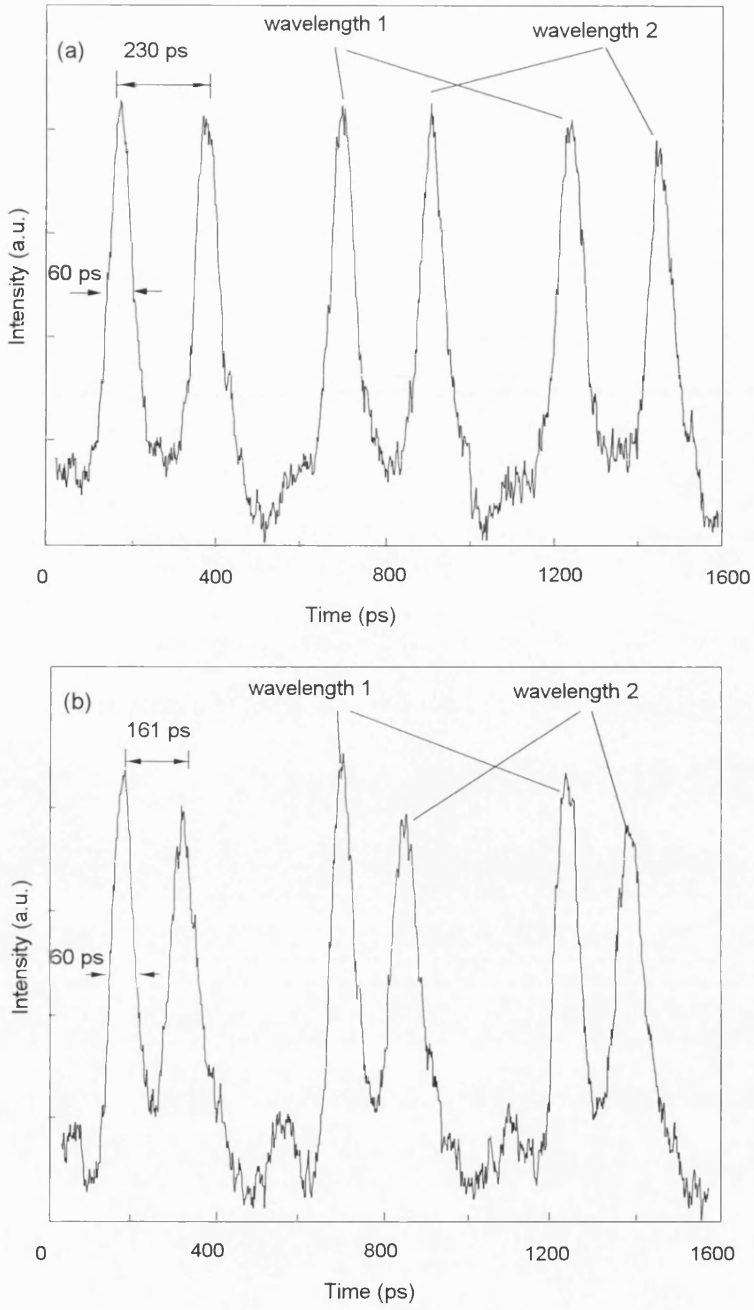

Figure 5.5. Dual wavelength short pulse trains with channel spacing of 2.2 nm generated from the actively mode-locked MGC laser at repetition rate of 1.78 GHz, (a) delay time 230 ps, (b) delay time 161 ps.

C. Results

Figure 5.5 (a) shows dual wavelength short pulse trains observed using the

sampling scope, with the master stripe 3 and reflector stripes 1 and 2 simultaneously d.c. biased at I_3=70 mA, I_1=61 mA and I_2=60 mA respectively. Here also two 1.78 GHz RF signals with a relative delay time of 230 ps were applied to the reflector stripes 1 and 2. The FWHM of the pulse profile was measured to be approximately 60 ps, and the peak power of the pulses was estimated to be around 40 mW. When the delay time between the two RF signals was changed using the coaxial phase shifter, a variable delay of dual wavelength short pulse trains from 0 to 561 ps, the periodic time, was achieved in this configuration. For example, figure 5.5 (b) shows the two wavelength optical pulse trains with a delay time of 161 ps.

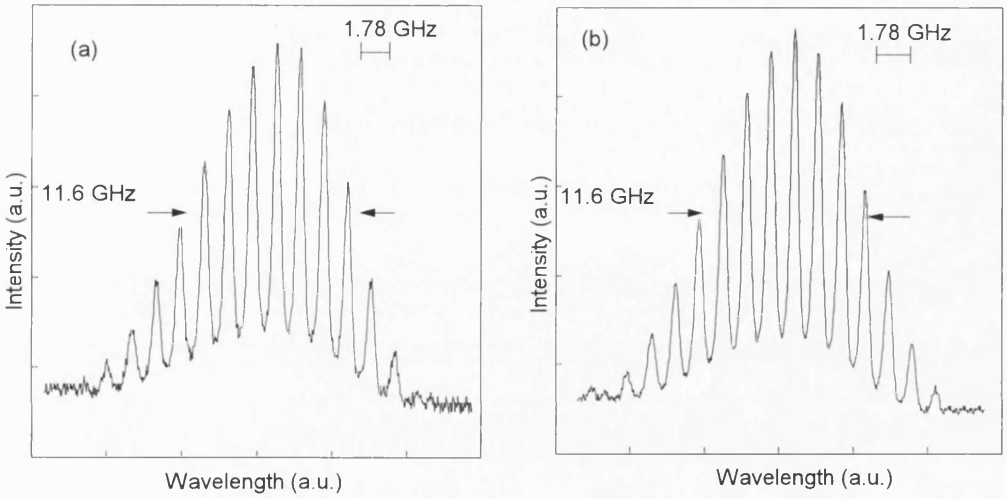

Figure 5.6. Measured optical spectra of dual wavelength short pulses trains with delay time of 230 ps from the active mode-locked MGC laser, (a) λ_1=1519.8, (b) λ_2=1522.0 nm.

The corresponding optical spectra, measured by using the scanning Fabry-Perot interferometer combined with a 1200 lines/mm grating, are shown in figure 5.6 (a) and (b), each being associated with one temporal short pulse. The measured bandwidth is 11.6 GHz for each channel, and the time-bandwidth product is approximately 0.7. The pulse width is limited by the spectral dispersion of the grating used, however, the optical spectrum are narrower than those observed for an identical single stripe external cavity actively mode-locked laser because of its special grating-loaded external cavity structure. The optical pulses still exhibit excess optical bandwidth beyond the Fourier transform limit

although a 1200 lines/mm diffraction grating is used as a bandwidth limiting filter element within the cavity. One of the possible causes of the excess bandwidth is self-phase modulation of the optical pulses induced by gain saturation [13]

For a relatively wide range of d.c. bias conditions, it was found that the pulse width and power did not change significantly with variable delay. The emission wavelengths were stable when the relative pulse delay was varied. The delay between the optical pulses corresponded exactly with that between the RF signals as it varied over a whole cycle. It should be pointed out that, as the optical path lengths of the two cavities are slightly different, one of the channels at above case operates at a slight frequency detuning (less than 10 KHz). However, the effect on the temporal and spectral behaviour of the mode-locking pulses is negligible because the MGC laser has a wide locking bandwidth (larger than 60 MHz) as reported in the last chapter.

5.4 Theoretical Modelling

In this section, theoretical modelling has been carried out to simulate the multiwavelength mode-locking process of the MGC laser. The model, developed in chapter 3, uses a set of coupled-cavity rate equations, which incorporates the effects of the external passive resonator formed by the lens and diffraction grating. The gain saturation due to effects such as dynamic carrier heating and spectral hole burning have also been included in the theoretical model using a gain saturation factor of $\frac{1}{1+\varepsilon\sum_{m} P_{jm}(t)}$. This is important, particularly concerning the investigation of pulse generation with a variable delay between the pulses, where crosstalk between two wavelengths due to gain saturation can be appreciated. In two channel operation, three stripes are pumped simultaneously and coupled together, therefore, a set of seven equations is used in the simulation. The numerical method is the same as that described in the last chapter, but the parameters are

modified for two channel short pulse operation.

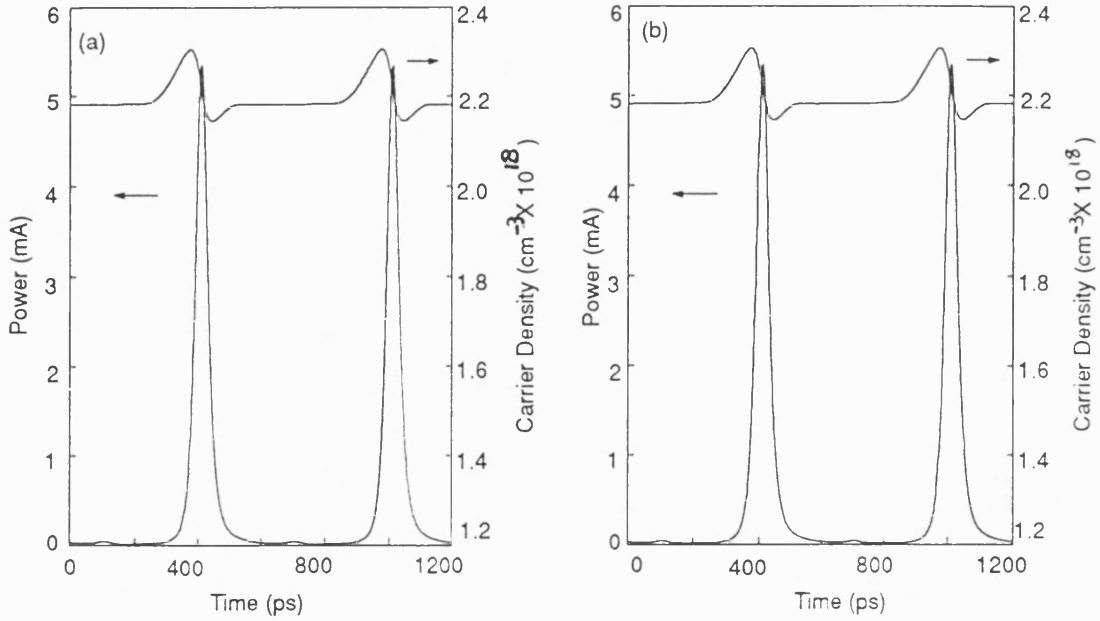

Figure 5.7. Theoretical results of dual wavelength short pulse simultaneously generated from an actively mode-locked MGC laser, (a) and (b) for the wavelength λ_1 and λ_2 respectively.

For the simulation of simultaneous generation of two wavelength short pulses, dc bias currents with 2 mA above threshold are applied to two reflector stripes. The injection current of the output amplifier stripe is written as a bias current and a sinusoidal modulation current with a frequency of the MGC laser cavity round trip time. A dc current of 5 mA above the threshold and 90 mA peak-peak RF current at 1.66 GHz were used in the output amplifier stripe. The pulsewidths for the two wavelengths are numerically calculated and found to be the same. The theoretical results of dual wavelength short pulse simultaneously generated from the actively mode-locked MGC laser at the above pumping conditions are shown in figure 1.7 (a) and (b). The shortest calculated pulse width is 54 ps for each channel, this being slightly narrower than the experimental results, but wider than that of the single channel.

For dual wavelength pulse generation with a controlled relative delay, the output amplifier stripe is driven continually and the reflector laser stripes are modulated with

sinusoidal pulses at periods equal to the MGC laser round-trip time. A delay time between two RF signals is set in order to study the effect of delay on the performance of dual wavelength pulse generation. Figure 5.8 shows the dual wavelength picosecond pulse waveforms with a delay time of 250 ps. The significant depletion in the carrier density that occurs with each optical pulse emission is also shown in figure 5.8. The calculated shortest pulsewidth is 53 ps for each wavelength, being slightly wider than that of a single channel under active mode-locking operation.

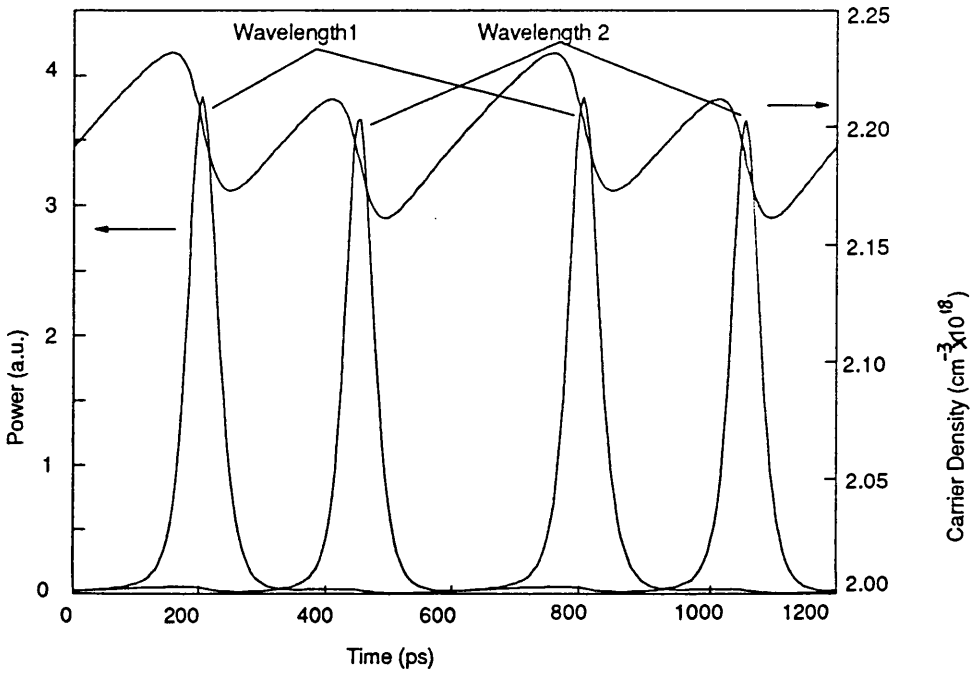

Figure 5.8. Theoretical results of variable delay dual wavelength short pulse generation by an actively mode-locked MGC laser.

Cross-talk and interchannel interference are important issues in practical WDM systems. These can originate from gain saturation in the output amplifier stripe 3 of the MGC laser. The gain saturation mechanism has previously been studied for multichannel amplification by travelling-wave amplifiers [14-15], where the level of gain suppression was found to depend upon the total intensity within the active stripe rather than upon the intensity at any single channel. As the two channels share the same gain medium in output amplifier stripe 3 of the MGC laser, the gain of either signal in the output amplifier stripe

is dependent on the power of the other. Hence depletion of carriers and gain saturation arises, resulting in the reduction of pulse power and broadening of pulse width. The crosstalk between two wavelengths under ultrashort pulse operation has been examined. It has experimentally been found that the output power of the pulses at one wavelength was decreased with increasing the pulse power at second wavelength. This behaviour was consistent with that under CW operation, which was previously found in the MGC laser [16] and multistripe array grating integrated cavity laser [17]. The pulse width at one wavelength was broadened about 25% with increasing the pulse power at second wavelength. By superimposing a component of the injection dc current into the output amplifier stripe 3, the power of two channels were brought up to the same level. In this case, the pulse widths of two channels were found to be approximately the same. Under the fixed current pumped condition, the pulse width as a function of the delay time between two channels was also experimentally and theoretically examined and the results are shown in figure 5.9. The experimental results were obtained by changing the delay time between the two RF signals using the coaxial phase shifter and repeating the measurements of the pulse width. All parameters were kept the same in the numerical simulation, only the delay time between two RF signals was changed. It can be seen from the experimental results that the pulse widths are stable to within about 6% for a whole delay cycle. The disagreement between the experimental and theoretical results was probably due to imperfect measurements of the pulse width.

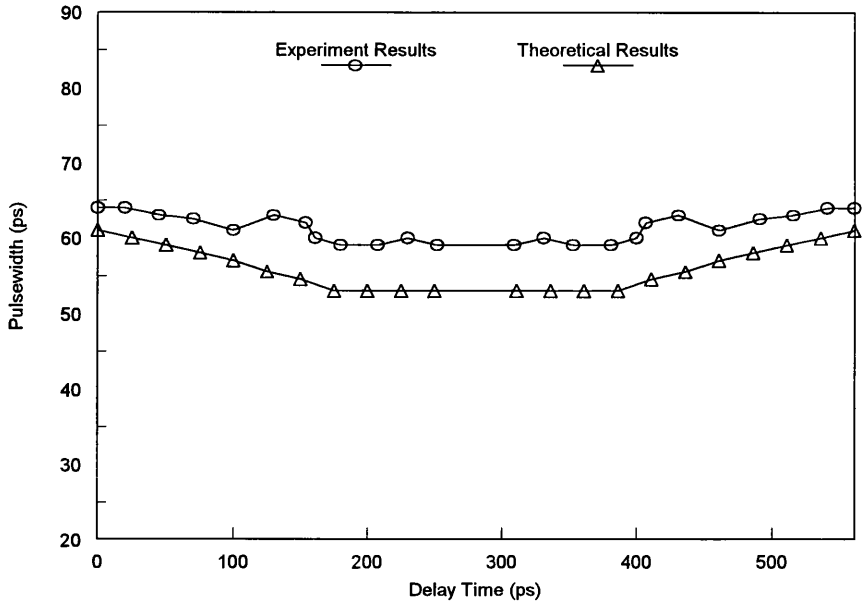

Figure 5.9. Pulsewidth as a function of delay time in dual wavelength short pulse operation.

5.5 Conclusion

The generation of multiwavelength short optical pulses by using active mode-locking of the MGC laser has been described in this chapter. Simultaneous generation of dual wavelength short optical pulses has been successfully demonstrated with good spectral quality for the first time. The pulses spectrally separated by 2.2 nm and each with a spectral width of 11 GHz and pulsewidth of approximately 60 ps have been achieved. Two optical pulse trains were also successfully generated at different wavelengths with a programmable delay between them making them for ideal pump-probe applications. Experiments showed that the pulsewidth was stable to within about 6% for a complete delay cycle. A numerical simulation of the multiwavelength mode-locking process of the MGC laser has been performed using a set of coupled-cavity rate equations. The pulse shapes were calculated and compared with the experimental results for various mode-locking configurations and a good agreement between theory and experiment was obtained. The interchannel cross-talk originating from gain saturation and carrier depletion was also discussed in this chapter

References

[1] C. A. Brackett, "Dense wavelength division multiplexing networks: Principles and applications," *IEEE J. Select. Areas Commun.*, vol. 8, pp. 948-964,1990.

[2] R. S. Tucker, G. Eisenstein and S. K. Korotky, "Optical time-division multiplexing for very high bit-rate transmission," *J. Lightwave Technol.*, vol. LT-6, pp. 1737-1749, 1988.

[3] H.F. Liu, M. Furazawa, Y. Kawai, and T.kamiya, "Gain-switched picosecond pulse (<10ps) generation from 1.3 um InGaAsP laser diodes", IEEE. J.Quantum Electron., QE-25, pp.1417-1424, 1989.

[4] D.J. Derickson, R.J.Helkey, A.Mar, J.R. Karin, J.G. Wasserbaner, J.E. Bowers, "Short pulse generation using multisegenent mode-locked semiconductor lasers", IEEE. J.Quantum Electron., QE-28, pp. 2186-2201, 1992.

[5] T. Morioka, K. Mori, S. Kawanishi, and M. Saruwatari, "Multi-WDM-channel, Gbit/s pulse generation from a single laser source utilizing LD-pumped supercontinuum in optical fibres," *IEEE Photon. Technol. Lett.* vol. 6, pp.365-368, 1994.

[6] D. Burns, G. Hay and W. Sibbett, "Dual-wavelength external cavity semiconductor lasers," Proceedings of the Conference on the Lasers and Electro-Optics (CLEO'93), vol. 11, pp. 444-447, 1993.

[7] B. Zhu, K. O. Nyariro, and I. H. White, " Dual-wavelength picosecond optical pulse generation using an active mode-locked multichannel grating cavity laser," *IEEE Photon. Technol. Lett.* vol. 6, pp.348-351, 1994.

[8] B. Zhu and I. H. White, "Dual-wavelength pulse generation incorporating relative timing control using an active mode-locked multichannel grating cavity laser," Proceedings on the Conference of the Lasers and Electro-Optics (CLEO'94), CWN3, pp. 254-255, 1994

[9] B. Zhu and I. H. White, "Variable delay dual wavelength picoseocond optical pulse generation using an actively mode-locked multichannel grating cavity laser," Appl. Phys. Lett., vol.65. pp. 2928-2930, 1994.

[10] B. Zhu and I. H. White, "Multiwavelength picoscond optical pulse generation using an actively mode-locked multichannel grating cavity laser," *J. Lightwave Technol.*, vol. LT-13, pp. 2327-2335, 1995.

[11] L. J. ST. Ville, C. L. Nuttall, P. W. Walland, J. C. Newell, A. Oliphant, G. J. Cannell, C. Bunney, J. P. Laude, P. Leroux, and M. J. Anson, "Developments in WTDM technology for high-capacity optical studio networks," *Optical and Quantum Electron.*, vol. 26, pp. s483-s496, 1994

[12] J. W., Hedrick, "Predicting post detection pulse characteristics using the FFT", Microwave Journal ,36(2), pp.337-342. 1993.

[13] L. Zheng, C. R. Menyuk and G. M. Carter, "A realistic model for actively modelocked

semiconductor lasers," *IEEE Photon. Technol. Lett.* vol. 6, pp.167-169, 1994.

[14] M. Tohyama, R. Takahashi, and T. Kamiya, "A scheme of picosecond pulse shaping using gain saturation characteristics of semiconductor laser amplifiers" *IEEE J. Quantum Electron.,* vol. QE-27, pp.2201-2210, 1991.

[15] T. Mukai, K. Inoue, and T. Saitoh, "Signal gain saturation in two-channel common amplification using a 1.5 mm InGsAsP travelling wave laser amplifier," *Electron. Lett.*, vol. 23, pp. 396-397, 1987.

[16] K. O. Nyairo, I. H. White, C. J. Armistead and P. A. Kirkby, "Multiple channel signal generation using multichannel grating cavity laser with crosstalk compensation," *Electron. Lett.*, vol. 28, pp. 261-268, 1992.

[17] K. R. Poguntke, J. B. D. Soole, A. Scherer, H. P. LeBlanc, C. Caneau, R. Bhat, and M. A. Koza, "Simultaneous multiple wavelength operation of a multistripe array grating integrated cavity laser," *Appl. Phys. Lett.* vol. 62, pp.2024-2026, 1993.

Chapter 6

MONOLITHIC INTEGRATED MULTICHANNEL GRATING CAVITY LASER

6.1 Introduction

Multiwavelength optical sources, which can generate multiple spectral channels with well defined channel spacing and good stability, are desirable for WDM systems employing direct detection techniques [1]. A range of laser structures has been developed for such requirements, including a bulk multichannel grating cavity (MGC) laser able to generate several wavelengths under CW and ultrashort pulse operation [2-3]. As discussed in chapter 3, 4 and 5, this device allows excellent wavelength registration. However, integration of a semiconductor laser on a single chip with an intracavity optical wavelength multiplexer potentially offers great advantages through reduced component count and packaging cost, as well as through improved reliability. Interest has therefore concentrated on developing monolithically integrated devices. Soole et al. first achieved such a laser employing amplifier sections together with a focusing reflective mirror grating [4-5]. Recently, Zirngibl et al. also demonstrated such a laser based on the integration of a waveguide grating multiplexer and an optical amplifier [6-7]. However, such sources have shown two major drawbacks, which are low generated output power and low modulation speed. The former is due to the high loss of the reflection grating, coupler and waveguide grating structures used, the latter is due to the large cavity size involved.

This chapter describes an integrated MGC laser that uses a transmission grating [8] as an intracavity wavelength selective element. The transmission grating is formed in a

double heterostructure InGaAsP/InP slab waveguide with a line of triangular-shaped recesses and has been shown to exhibit very low throughput loss and good spectral characteristics when compared with the other integrated wavelength selective elements [4-7]. Hence this laser has the potential for efficient operation. Additionally the transmission grating allows very compact device design with a particularly short total cavity length, thus benefiting device yield and high speed operation.

The basic concept of the monolithically integrated MGC laser, followed by a description of the device structure and fabrication, is described in section 6.2. The device operating characteristics including L-I curve, spectrum stability and dual wavelength operation are discussed in section 6.3. Section 6.4 looks at the modulation speed of the integrated MGC laser, which shows that the integrated MGC laser allows modulation rates in excess of 1 Gbit/s. Section 6.5 discusses the theory. The coupled-cavity rate equation model is modified for the integrated MGC laser, and the dynamic and modulation characteristics of the integrated MGC laser are investigated using this new modified model and compared with the experimental results. A conclusion is finally given in section 6.6.

6.2 Device Structure and Operation

Although earlier bulk MGC laser prototypes have been constructed using discrete components, it is becoming clear that an integrated device is much more attractive than discrete components in terms of cost and reliability. In order to obtain a broad wavelength tuning range and a high modulation speed, the integrated MGC laser is designed in a very compact form. A schematic diagram showing the integrated MGC laser design is depicted in figure 6.1. The device consists of an array of reflector waveguides, an output amplifier waveguide, a transmission grating and a pair of focusing mirrors, all integrated in the plane of the substrate to form a coupled cavity system.

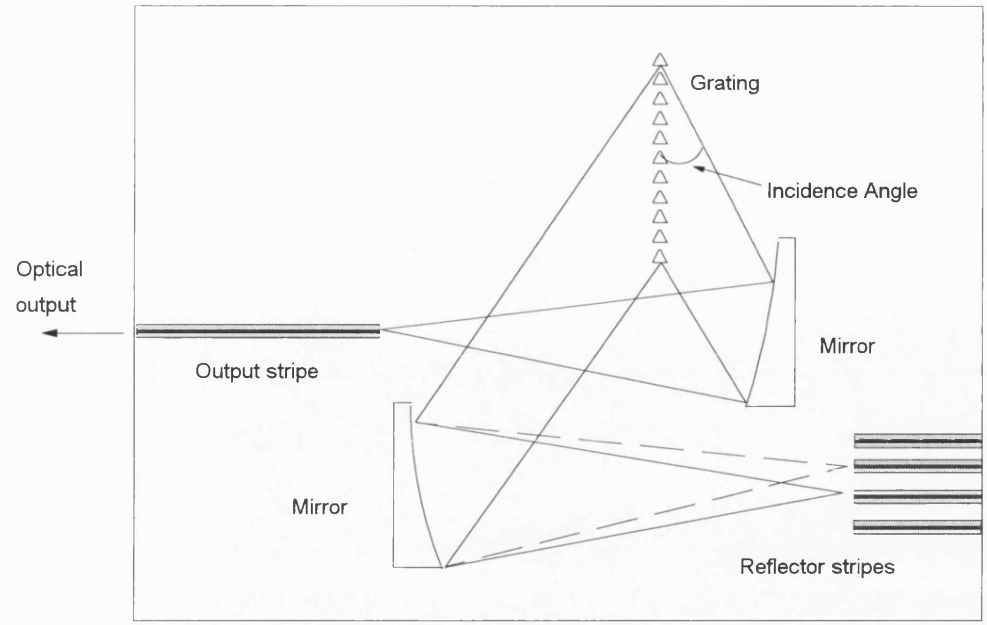

Figure 6.1. Schematic diagram of integrated MGC laser.

The operation of the device resembles that of the bulk MGC laser [9]. Light generated within each active reflector waveguide propagates in the plane of the slab and illuminates a collimating mirror, which directs the beam onto the transmission grating. The grating disperses the different wavelengths within the output spectrum, diffracting each through a slightly different angle. The dispersed optical modes from the grating fall on an output focusing mirror which directs the beams to the output amplifier waveguide. In this arrangement, the output amplifier waveguide and one of the reflector waveguides together can form a resonant cavity, via the transmission grating and focusing mirror pairs. Reflections at the cleaved end facets of both waveguides provide optical feedback and cause lasing to occur at one wavelength. The lasing wavelengths and the channel separation are determined by the geometry of the device, such as the grating pitch constant, focal lengths of the mirrors and the physical distances between reflector stripe etc. The grating structure consists of a set of triangular-shaped recesses designed so that they do not intercept the beams from adjacent elements. Wavelength switching is readily achieved by redirecting the current drive from one reflector waveguide to another. By

driving two reflector waveguides, as well as the output amplifier waveguide simultaneously, two wavelengths (or more if more reflector waveguides are driven) can be generated.

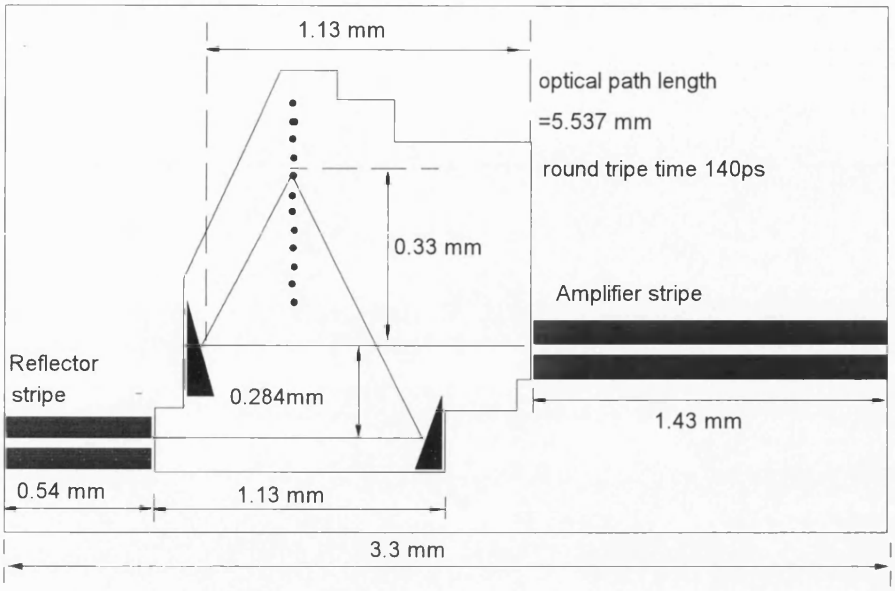

Figure 6.2 Layout of the prototype integrated MGC laser.

A prototype integrated MGC laser (with one output and two reflector waveguides) was fabricated to operate in the 1.5 μm wavelength range using 5 quantum well InGaAsP/InP material. Although the optimised design laser structure employed active/passive interfaces, and the grating region was passive, this prototype device used an all active cavity. This means that the grating section is also active and requires pumping to achieve transparency. The device layout is shown in figure 6.2. The output amplifier waveguide had a length of 1.43 mm. Each reflector waveguide was 540 μm long. The mirrors had focal lengths of 1.13 mm, and the grating structure had a periodicity of 26 μm and operated in the 89th diffraction order. All elements were fabricated using active material and the total length of the chip was 3.3 mm.

6.3 Laser Performance

A. Experimental Set-up:

For demonstration of a prototype integrated MGC laser, an experimental set-up was arranged as shown in figure 6.3. The device was mounted p-side up and operated without temperature stabilisation. The amplifier and reflector stripes were separately driven by an HP214B pulse generator, each capable of delivering up to 2A of current into a 50Ω via 50Ω matched lines. The grating section was expected to require significant pumping to reach transparency owing to its large area. It was, therefore, driven by an Avtech AVP-AV-C pulse generator unit which could deliver up to 8A through a 5Ω matched line into a 5Ω load. The pulses from all the generators were synchronised. The emitted light from the output amplifier stripe was collected by an antireflection coated micro-lens and illuminated a diffraction grating. For single channel operation, a 1200 lines/mm grating was used and was blazed for 1.5 μm wavelength for an incident angle of 56° (for two channel assessment, 600 lines/mm grating was used). The diffracted beam was detected via a high sensitivity detector or avalanche photo detector. A very narrow slit of about 100 μm wide was placed in front of the detectors. By scanning the angle of the grating, the optical spectrum of the generated light from the integrated MGC laser could be obtained. The resolution of this arrangement was estimated to be about 0.1 nm. The measurement of the output power was made by a HP optical power meter, which could be placed in front of the output amplifier stripe to detect the optical beam when it was needed.

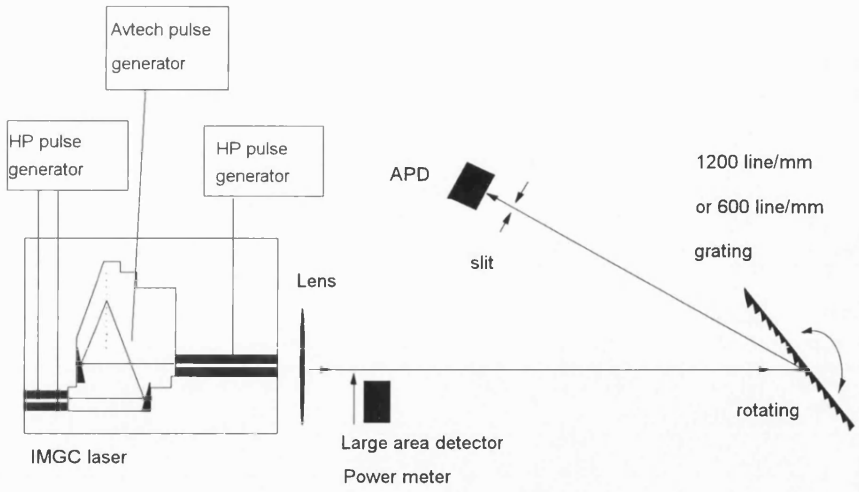

Figure 6.3. Experiment set-up used for demonstration of integrated MGC laser.

B. Single Channel Operation:

The integrated MGC laser was examined under pulsed operation (pulse width=50 ns, pulse rate=20 kHz). Each active waveguide and grating section were pumped separately. The time-averaged powers were first measured using an optical power meter and the results were then scaled appropriately. Figure 6.4 shows a typical light current characteristic for the emission from a single channel. The laser reaches threshold at 310 mA total current when the grating section is injected with a pulse current of 200 mA. This high threshold current may be accounted for by the large size of the grating section active region and by the large losses of the grating section which are estimated to be 10 dB. The poor electrical isolation between current pads may also be one of the reasons for the high threshold current (as discussed below). Using a passive grating section is expected to lead to significantly reduced threshold current. Above threshold, the L-I curve remains linear up to an output power in excess of 4.3 mW. This is believed to be the highest power yet reported from a monolithically integrated multiwavelength laser source. The differential quantum efficiency [(useful photon emission rate)/(photon generation rate)] is approximately 1%.

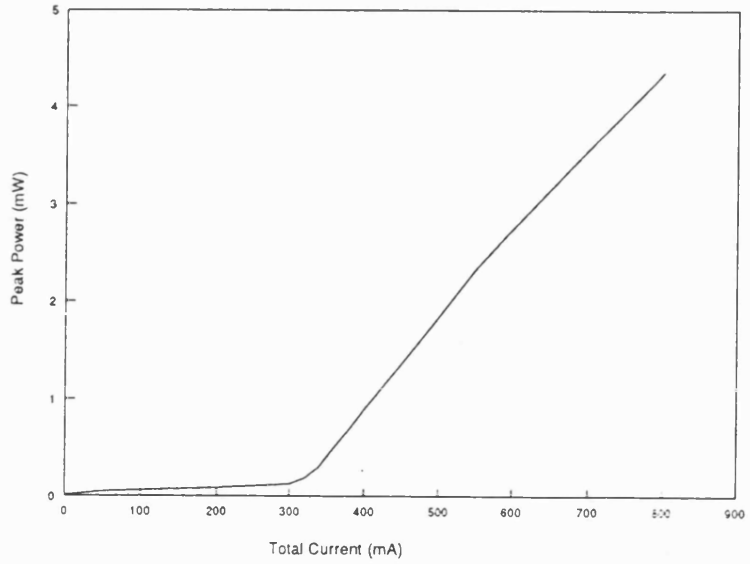

Figure 6.4. Light-current characteristic of integrated MGC laser.

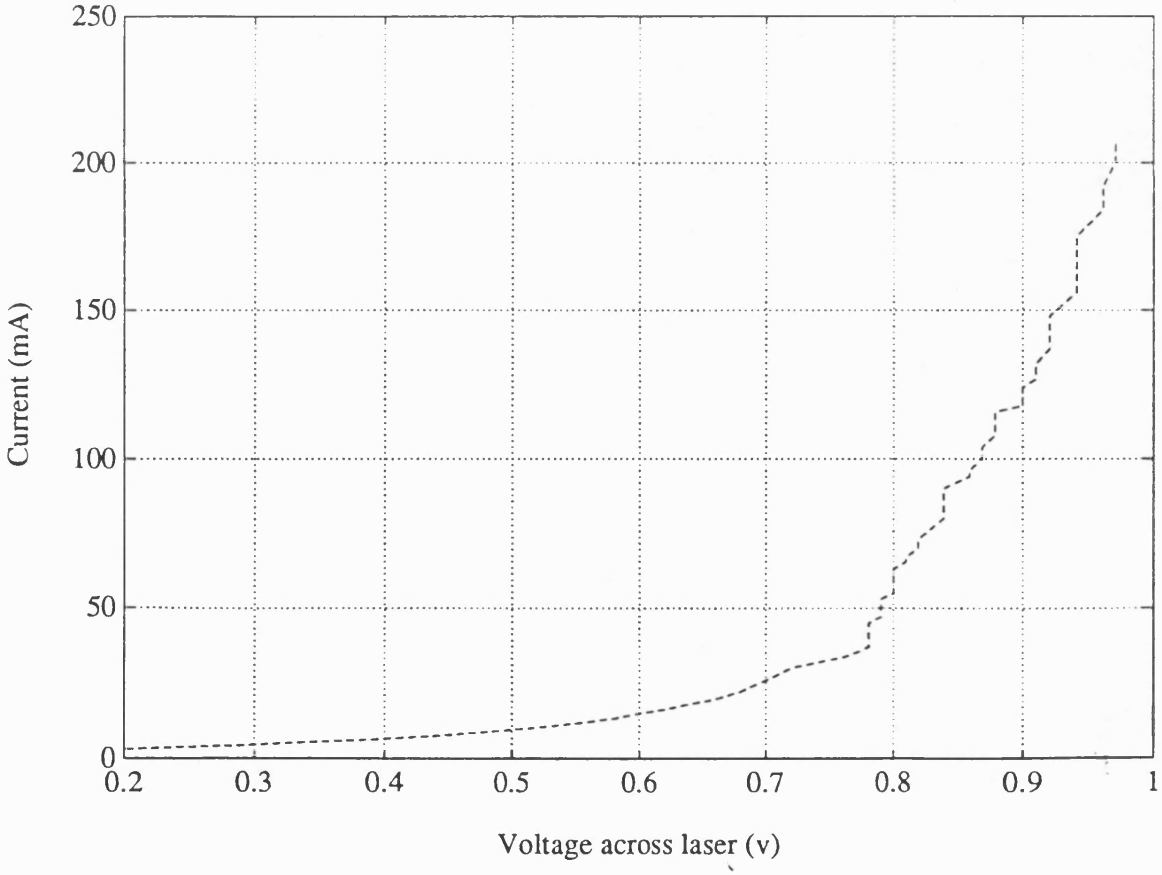

Figure 6.5. A typical I-V characteristic of the integrated MGC laser.

Electrical characterisation of this device indicated a series resistance under forward bias of ~1.5Ω, and a typical I-V characteristic for the laser is shown in figure 6.5. The resistance under reverse bias was in the 100 MΩ range, indicating good active region isolation. However, the resistances between output amplifier stripe, reflector stripe and the grating section active region were in the range of several hundred ohms. This indicated that the isolation between stripes and grating section was not perfect, and that significant current leakage could be taken place between stripes, grating and unpumped areas. The poor isolation of the active sections resulted in significant current wastage, thus resulting in high threshold current.

Varying the current applied to the grating section caused no significant change to the lasing characteristic of the device. In fact both the threshold current and output power of the device hardly changed. One possibility for this unexpected behaviour may be poor isolation between grating section and stripes, which lead to the drive current to the grating section being not large enough to cause transparency. Alternatively, the grating section may be transparency, however, the lasing wavelength of the grating section may not be within the gain bandwidth of the output and reflector stripes, therefore the grating section has little effect on the performance of the integrated MGC laser.

The near -field pattern of the laser's emission was examined by using an objective lens to image the cleaved output facet onto an infra-red video camera (an IR vidicon). The profile of the near-field pattern suggested that a single lateral mode operation was obtained in the MGC laser.

The spectral output of the integrated MGC laser was very stable and well defined. An optical spectrum separately taken at a drive current of 350 mA is shown in figure 6.6. The measured width of the spectrum was 0.1 nm, which was limited by the detection system used. The mode spacing of the whole cavity is 0.06 nm. It is therefore that the laser is highly likely operating a single mode. The spectrum was remarkably stable, the operating wavelength varying by less than 0.06 nm over a current range of 170 mA.

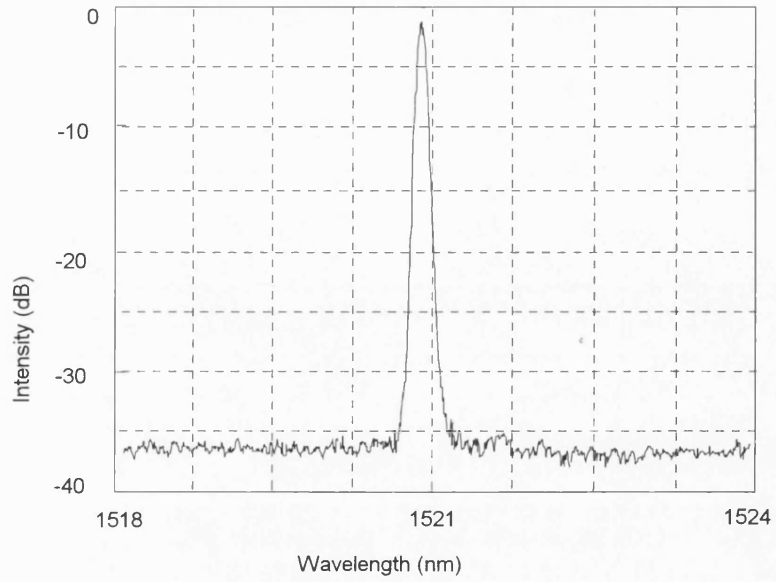

Figure 6.6. Optical emission spectrum taken at a total current drive of 350 mA.

C. Dual Channel Operation:

Simultaneous emission at two wavelengths has been achieved, as shown in figure 6.7, by driving the two reflector waveguides and the output amplifier waveguide simultaneously. In this case, the output amplifier waveguide was pumped at a higher current of about 650 mA, as it provided gain for both wavelengths. The two spectral peaks were separated by 21 nm. The imbalance in the power content of the two modes might readily be accounted for by noting that the channel separation in this case was substantial compared with the material gain bandwidth (approximate 30 nm).

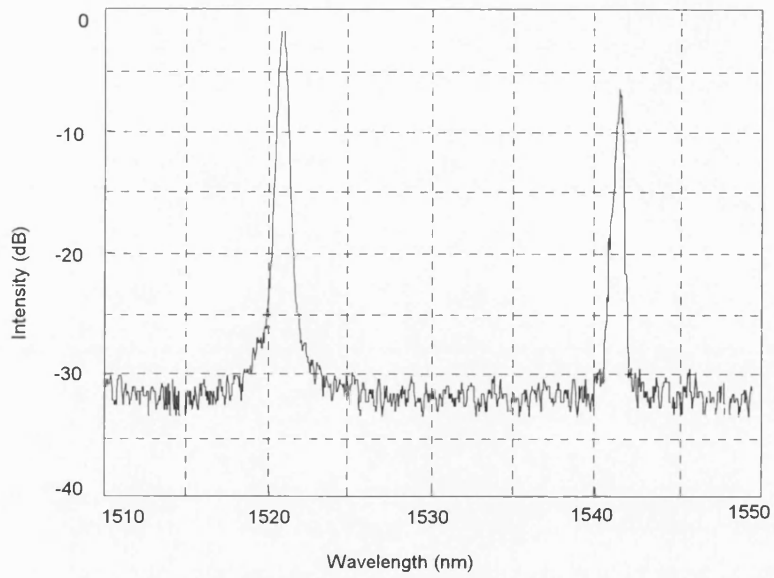

Figure 6.7. Two wavelength emission of integrated MGC laser with channel separation of 21 nm.

6.4 High Speed Modulation of Integrated MGC Laser

As we mentioned in chapter one, high speed modulation for the multiwavelength lasers is required for fibre optic WDM communication systems, particularly for long-distance high capacity links. The keys to achieving large modulation bandwidth of the laser are enhancement of the resonance frequency and reduction of the parasitic capacitance. The resonance frequency of a laser can be expressed as follows [10].

$$f_r = \frac{1}{2\pi}\left(\frac{g' P}{\tau_p}\right)^{1/2} \qquad (6.1)$$

where P is the optical power, g' is the differential gain, and τ_p is photon lifetime. It is obvious that an improvement in the laser output power and an enhancement of the differential gain will increase the resonance frequency. However, an additional method to increase the modulation bandwidth is to decrease the photon lifetime, τ_p, by making short-cavity lasers. In contrast to other integrated multiwavelength laser sources as described in chapter one [4-7], the integrated MGC laser is designed to have very compact device structure with a short total cavity length by using the transmission

grating, thus the modulation speed of the device is expected to be higher than other monolithic integrated multiwavelength laser sources. Therefore, in this section, we discuss the modulation characteristics of the integrated MGC laser.

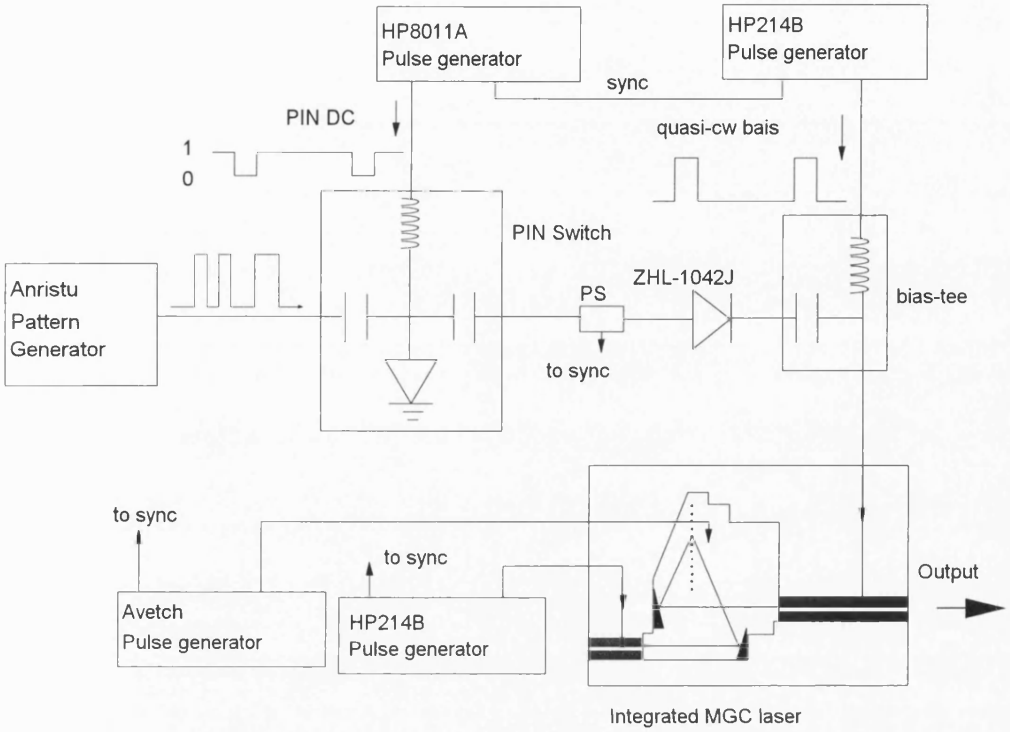

Figure 6.8. An experimental set-up for high speed modulation of the integrated MGC laser.

Because of the all-active design of the laser, most experiments were carried out under pulse conditions. As a result a special pumping technique was used to investigate the modulation characteristics of the laser. The output amplifier stripe was subjected to high speed NRZ digital modulation. A electrical pulse with a width of 600 ns was applied to the output amplifier stripe to bias the laser at threshold. An NRZ digital modulation signal with 2^{15}-1 bit pseudo-random sequence, generated from an Anritsu pattern generator, was PIN-switched, at a low frequency with a low duty cycle of 0.6 %. This NRZ digital signal was amplified using a ZHL-42 Mini-Circuits amplifier and superimposed on the quasi-cw bias current to modulate the laser in a controlled manner. The current to the reflector stripe and grating section were set to bias the laser at

threshold. The optical output was monitored using a fast Germanium avalanche photodiode and sampling oscilloscope. The experimental set-up is shown in figure 6.8.

Direct modulation at a rate of greater than 1 Gbit/s was demonstrated in the integrated MGC laser [11]. A typical temporal response of this device at a NRZ digital modulation rate of 1 Gbit/s is illustrated in figure 6.9, showing a good extinction ratio and well defined pulse generation without strong patterning. The integrated MGC laser shows typical rise and fall times of the pulses in the order of 250 ps and 550 ps respectively depending on the bias to the lasing stripes. In addition, optical pulses as short as 500 ps were generated in this laser with rise and fall times in the order of 200 ps and 500 ps respectively. The optical spectrum at this modulation rate is shown in figure 6.10. It is important to note however that even under high speed operation, the full width at half maximum (FWHM) of the laser spectrum remains less than 0.33 nm, which is limited by the resolution of the measurement system.

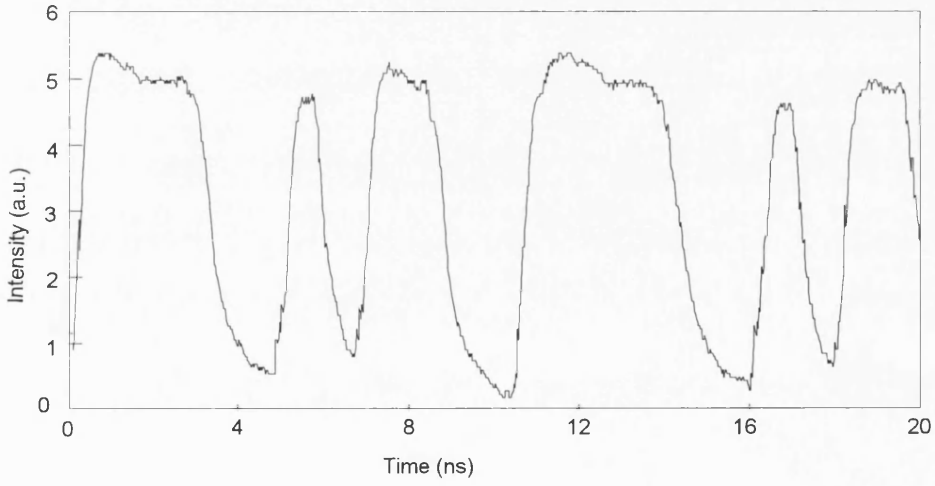

Figure 6.9. Modulated output of the integrated MGC laser with a 1 Gbit/s NRZ bit pattern.

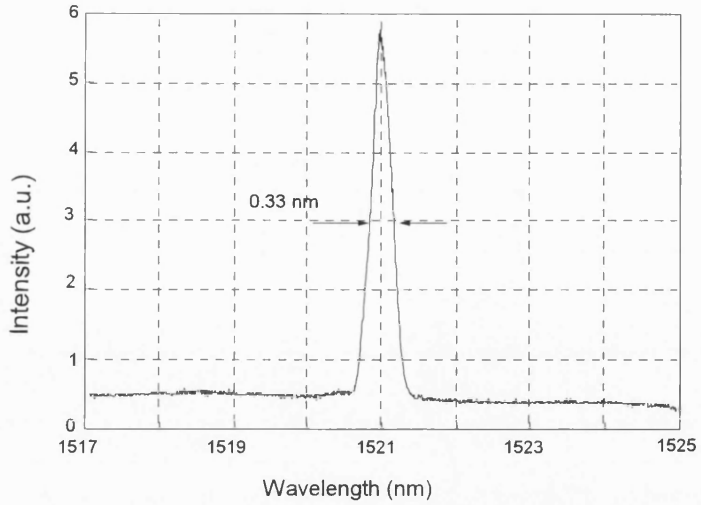

Figure 6.10. Optical spectrum of integrated MGC laser modulated at 1 Gbit/s with NRZ bit pattern.

Although it is possible to modulate several wavelengths simultaneously by injecting modulation current into the reflector stripes, the crosstalk due to gain saturation is likely to be important in the present configuration, as all spectral channels pass through the same output amplifier ridge. However, it is anticipated that on implementation of active/passive integration techniques, the output active amplifier stripe can be replaced by a passive waveguide, thus removing the dominant cause of signal crosstalk.

6.5. Modelling and Optimisation of the Device

A. Modelling:

To assess the potential performance of the integrated MGC laser and optimise the device designs, theoretical modelling has been carried to simulate the dynamic modulation characteristics of the integrated device, particularly concerning the effect of the optical cavity length on the modulation speed. The model used for numerical simulations on a computer is adapted from the coupled-cavity rate equation model for the bulk optic MGC laser, which was introduced in the chapter 3. The model uses a set of different rate equations for output amplifier and reflector stripes, respectively, and

considers the coupling between output amplifier stripe and reflector stripe via the transmission grating and mirror pair. The model includes the delayed optical feedback from each stripe, gain saturation effect, and linear gain. The model assumes that laser operates in a single mode.

The non-linear coupled equations are solved numerically using a fourth-order Runge-Kutta algorithm. Some of numerical values for the integrated MGC laser parameters used in the model are given in the table 6.1, and others are the same as shown in table 3.1. The values are based on the measured values of the device and the driving conditions used in the experiment. It should be pointed out that the value of the thickness of the active region, which was used in the model, is larger than the realistic one (0.05 μm), however this mistake does not significantly affect the dynamic response of the laser.

Table 6.1

Parameters	Symbol	Values
Output amplifier stripe length	L_o	1.45mm
Reflector stripe length	L_r	0.54mm
Width of the active region	w	4 μm
Thickness of active region	d	0.2 μm
Total passive loss	H	10~12 dB
Power reflectivity in output stripe facet	R_o	0.32
Power reflectivity in reflector stripe facet	R_r	0.32
Active-passive interface reflectivity	R_{AR}	0.001
Active region group refractive index	μ	3.7
Confinement factor	Γ	0.013/well
Internal loss	α	25 cm^{-1}

In the simulation, the reflector and output amplifier stripes were biased at the threshold current. An additional NRZ format pulse current of amplitude 0.25 I_{th} was

added to the bias on the amplifier stripe. A simulated temporal response of the device with the cavity length of 3.3 mm modulated at 1 Gbit/s is depicted in figure 6.11, which shows good extinction ratio and well defined pulse generation and is in good agreement with the experimental results for the rise and fall times of the pulses at this modulation speed.

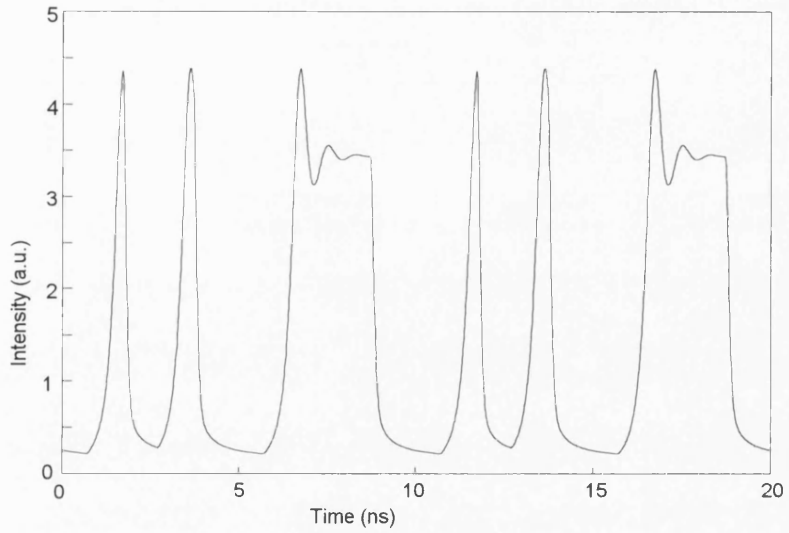

Figure 6.11. Theoretical results of the temporal response for the integrated MGC laser for 1 Gbit/s NGZ modulation.

The maximum modulation speed is limited by the cavity round-trip frequency of 7.7 GHz, corresponding to the cavity length of 3.3 mm. However, further device design optimisation should reduce the cavity length to 2 mm. The rate equation model has been used to simulate the modulation speed of such an optimised device and figure 6.12 shows the temporal pulse shape generated at a modulation speed of 5 Gbit/s. This indicates that a potential modulation rate of up to 5 Gbit/s per channel can be anticipated, allowing the laser device to be suitable for a wide range of WDM applications.

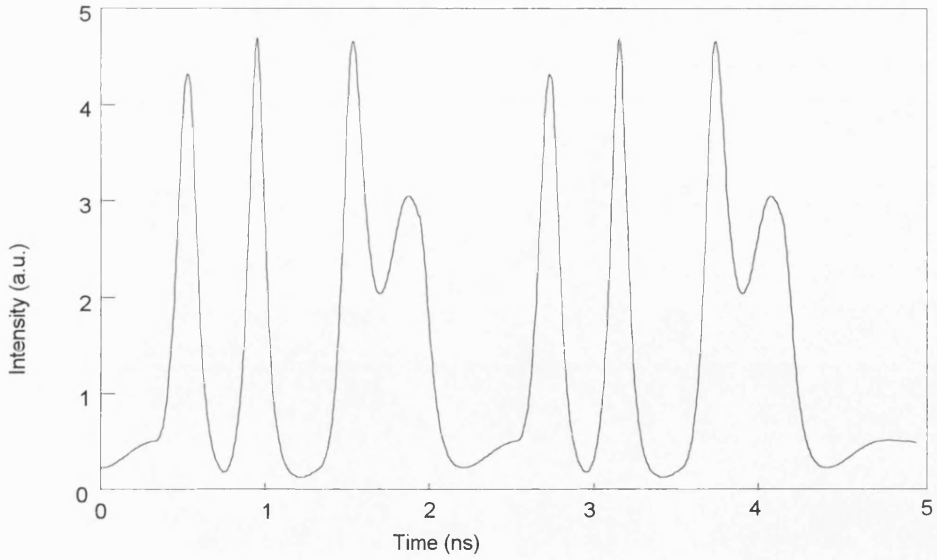

Figure 6.12. Theoretical results of the temporal response for the optimised device at 5 Gbit/s NRZ modulation.

B. Future Improvements:

The device tested here was a prototype fabricated by BT, and potential for considerable optimisation exists. Losses of the grating structure in this devices are particularly high. This could be due to roughness on mirror surfaces caused by poor fabrication processes. However, devices fabricated with losses as low as 7.2 dB had already been reported [12]. Reduction of loss of the grating is possible and should allow for substantial improvements to the threshold current and output power levels. Electrical isolation between the different pads is poor, which results in significant current spreading. Better isolation in the optimised device would significantly improve the device performance such as threshold current, output power and optical spectra.

The use of active/passive interfaces to define the active waveguide and grating regions will allow substantial reductions in drive currents and ensure good optical coupling between output amplifier and reflector stripes. It is anticipated that the size of the device can be further reduced, allowing potential modulation rates of up to 5 Gbit/s. It is also anticipated that the output active amplifier waveguide will be replaced by a passive waveguide, thus reducing the potential signal crosstalk and interchannel mixing

due to gain saturation effects in the active amplifier ridge. Longer reflector stripes can be employed to compensate for the reduction of total device gain.

6.6 Conclusion

An integrated MGC laser has been illustrated in this chapter with its elegant compact structure and successful operation of a prototype device. The device is essentially a two-dimensional implementation of the bulk MGC laser. The output amplifier stripe and an array of reflector stripes are monolithically integrated with a transmission grating, which acts as an intracavity wavelength selective filter. The prototype device fabricated by BT exhibits a threshold current of 310 mA and is able to generated 4.3 mW of output power. The optical spectrum of the device is remarkably stable and well defined, with a width of 0.1 nm limited by the detection system used. Dual channel operation is also demonstrated with a channel separation of 21 nm.

An investigation of the dynamic performance of an integrated MGC laser shows that direct modulation rates of in excess of 1 Gbit/s have been achieved by the 3.3 mm long device. Even under these high speed conditions, the spectral linewidths are narrower than 0.33 nm, the resolution of the measurement system. Theoretical modelling has confirmed the experimental observations and predicts that optimised devices should allow modulation rates as high as 5 Gbit/s per channel. Future optimised improvements on the device have been considered, and lower passive losses for the grating and mirror structures along with good electrical isolation between different sections should allow significantly lower threshold currents and higher output powers.

References

[1]. C. A. Brackett, " Dense wavelength division multiplexing networks: Principles and Applications", *IEEE J. Select. Areas Commun.*, vol.8, pp.948-964. 1990,

[2]. B. Zhu and I. H. White,"Multiwavelength picosecond optical pulse generation using an actively mode-locked multichannel grating cavity laser", *J. Lightwave Technol.*, vol.13, pp. 2327-2335, 1995.

[3]. B. Zhu, K. O. Nyairo, and I. H. White, "Dual-wavelength picosecond optical pulse generation using an actively mode-locked multichannel grating cavity laser", IEEE Photon. Technol. Lett., vol.6, pp.348-351, 1994.

[4]. J. B. D. Soole, K. R. Poguntke, A. Scherer, H. P. LeBlanc, C. Chang-Hasnain, J. R. Hayes, C. Caneau, R. Bhat, and M. A. Koza, "Wavelength-selectable laser emission from a multistripe array grating integrated cavity laser", *Appl. Phys. Lett.*, vol. 61, pp.2750-2752, 1992.

[5]. K. R. Poguntke, J. B. D. Soole, A. Scherer, H. P. LeBlanc, and M. A. Koza, "Simulataneous multiple wavelength operation of a multistripe array grating integrated cavity laser", *Appl. Phys. Lett.*, vol. 62, pp.2034-2036, 1993.

[6]. M. Zirngibl, B. Grance, L. W. Stulz, C. H. Joyne r, G. Raybon, and I. P. Kaminow, "Characterization of a multiwavelength waveguide grating router laser", *IEEE Photon. Technol. Lett.*, 6, pp.1082-1084. 1994.

[7]. M. Zirngibl, C. H. Joyner, and L. W. Stulz, "Demonstration of 9X200 Mbit/s wavelength division multiplexed transmitter," *Electron .Lett.*, vol. 30, pp.1484-1485, 1994.

[8]. M. Asghari, B. Zhu, I. H. White, C. P. Seltzer, C. Nice, I. D. Henning, A. L. Burness, and G. H. B. Thompson, "Demonstration of an integrated multichannel grating cavity laser for WDM applications",*Electron .Lett.*, vol. 30, pp.1674-1675,1994.

[9]. I. H. White, "A multichannel grating cavity laser for wavelength division multiplexing applications", *J. Lightwave Technol.*, LT-9, pp.893-899, 1991.

[10]. K. Y. Lau, N. Bar-Chaim, I. Ury, and A. Yariv, "11 GHz direct modulation bandwidth of GaAlAs window laser on semi-insulating subatrate operating at room temperature," *Appl. Phys. Lett.*, vol. 45, pp.316-318, 1984.

[11]. M. Asghari, B. Zhu, I. H. White, C. P. Seltzer, C. Nice, I. D. Henning, A. L. Burness, and G. H. B. Thompson, "High-speed integrated multiwavelength laser source for WDM optical-fibre communication systems ", in Optical Fibre communications Conference. vol. 8, 1995 OSA. Technical Digest Series (Optical Society of America, Washington, D. C. , 1995), pp. 307-308.

[12]. S. M. Ojha, G. H. B. Thompson, C. G. Cureton, C.B. Rogers, S. J. Clements, M. Asghari, I. H. White, "Demonstration of low loss integrated InGaAs/PInP demultiplexer device with low polarisation sensitivity," *Electron .Lett.*, vol. 29, pp.805-806,1993.

Chapter 7

HIGH POWER PICOSECOND OPTICAL PULSE GENERATION USING BROAD AREA TAPERED LASER AND AMPLIFIERS

7.1 Introduction

In the last four chapters it has been seen that both bulk optic and monolithically integrated MGC lasers exhibit several distinct advantages, including stable multiwavelength emission, narrow spectral linewidth, and multiwavelength ultrashort pulse generation. However, the available output powers of the MGC laser for both CW and ultrashort pulse operation are relatively low [1], which limits a wider application of these compact and robust sources. If the laser chip has a good AR coating and efficient feedback from the grating, the output powers are mainly limited by the gain saturation in the narrow output amplifier stripe, especially for multiwavelength operation. It is hoped that this can be overcome by using a broad area tapered output amplifier waveguide in the MGC laser. A schematic diagram of the proposed tapered waveguide MGC laser is shown in figure 7.1. In this device, the reflector stripes, which are used to control and register the different wavelengths using the diffraction grating, have the same structures as those described in chapter 3. The output stripe, however, consists of a broad area waveguide which is tapered from a narrow width input to a larger area for increased output power. The narrow width input is used to provide both spatial and spectral mode selectivity via the grating loaded external cavity. The tapering to a large output width permits the power that is generated to be spread out, thus reducing the intensity at the output facet to avoid catastrophic facet damage. Gain saturation effects should also be reduced as the optical cross-sectional area increases towards the output facet. This device has not been fabricated yet. An alternative

demonstration of high power generation, however, has been carried out using various broad area tapered devices. In this chapter, we describe a high power ultrashort pulse generation from semiconductor lasers using Q-switching and amplification techniques.

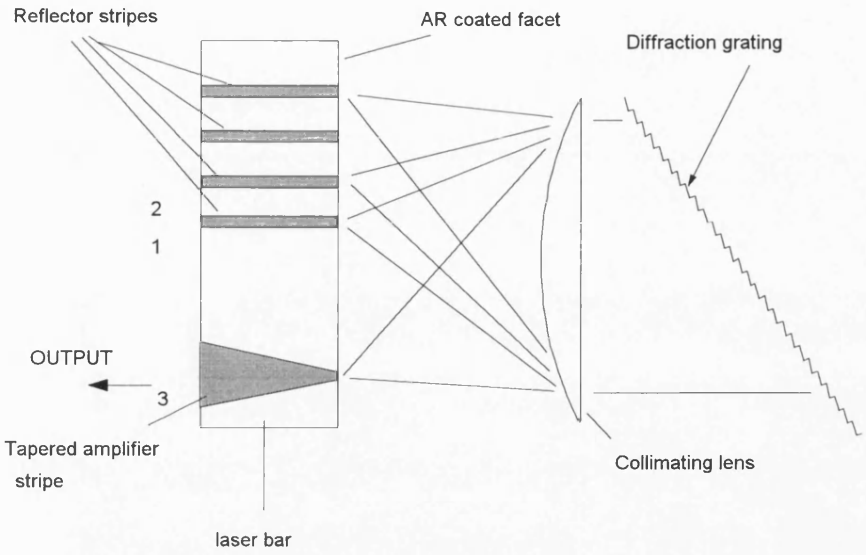

Figure 7.1. A schematic diagram of a tapered waveguide MGC laser

For many industrial and scientific applications, such as free space communications and optical sensing, high peak power ultrashort optical pulses with good spatial mode quality are increasingly required. Recently, a range of semiconductor laser structures and techniques have been developed for such requirements, including Q-switching of a broad area laser [2-3], post amplification [4], and mode-locking of narrow stripe lasers with a tapered semiconductor amplifier [5-6]. Q-switching of multicontact diode lasers is one of the simplest methods for generating high energy ultrashort optical pulses on demand. Post amplification has been successful in generating pulses of very high peak power and pulse energy [4]. The tapered amplifier has been demonstrated to be capable of multi-watt CW powers by using Ti:Sapphire injection [7] and by external diode injection [8]. The tapered gain region leads to increased pulse energies, because the saturation energy is relatively large at the flared output end of the amplifier. With post-amplification, the Q-switched multicontact laser generates much higher peak power and pulse energy than previously reported for Q-switched semiconductor lasers.

The structure of this chapter is as follows: Section 7.2 briefly reviews the techniques for Q-switching of semiconductor lasers. Section 7.3 describes the Q-switched three-contact bow-tie laser, and presents experimental results of short pulse generation with this laser. Section 7.4 discusses the amplification characteristic of the tapered amplifier for both quasi-cw and Q-switched short pulse operation, including signal gain, peak power, pulse energy, and near and far field patterns. Section 7.5 finally ends with conclusions.

7.2 Q-Switching Techniques

Q-switching is one of the simplest methods for generating ultrashort optical pulses, and gives compact, flexible, and easily fabricated sources for high energy short pulse generation [9]. The principle of the Q-switching technique for short pulse generation is as follows: the cavity loss is raised to a high level by an intracavity element (i.e., ensuring a low Q state), so that the laser can be pumped to a very high gain level without lasing. The Q is then abruptly raised and the laser suddenly finds itself with a huge amount of excess gain, and responds by emitting a short intense pulse that dissipates all of the excess gain. If the switching is caused by an external influence, this technique is called active Q-switching. However, there also exists passive Q-switching (or self -Q-switching), where the switching is caused by a saturable absorber in the cavity of the laser.

When an optical pulse is passed through a saturable absorber, the initial amplitude fluctuations of the beam are found to be distorted, the peak-to-peak ratio of the fluctuations being increased and their time duration being decreased as a result of the non-linear transmission characteristics of the absorber [9]. This process is repeated over and over again by reflecting the light back and forth between the laser facets, leading to ultrashort optical pulse generation. A feature of semiconductor diode lasers is their ability to allow ready incorporation of saturable absorbers of the same material as the active medium of the laser. In contrast with other types of lasers, the diode laser does not need to have any external saturable absorber, but it is necessary to divide the diode into several segments and apply different currents to them. The parts of the diode with high current injection (high

carrier density) act as gain sections, while the unpumped segments, reverse-biased segments or segments with low current injection act as saturable absorbers.

A typical actively Q-switched diode laser is a multiple-contact laser, and it often consists of two or three sections (gain section, a modulator section, and a passive waveguide section in between) [10-11]. The intracavity loss is modulated electrically or optically in a laser under active Q-switching. Since the modulator section and gain section are fabricated monolithically and have exactly the same material composition, the band gap in the gain section must be shifted to lower energies to prevent direct band-to-band absorption. This can be done using heavy doping by Zn diffusion in a conventional diode laser [10] or using the carrier-induced band shrinkage effect in QW lasers[11]. The structure of a passively Q-switched laser is similar to that of an actively Q-switched diode laser, and it often consists of a multicontact diode laser (for example, one saturable absorber section, and one or two amplifier gain sections). In passively Q-switched lasers, a saturable absorber located in the laser cavity is responsible for the generation of short optical pulses. The difference between the two techniques is that, in contrast to active Q-switching, no external electrical or optical modulation is required to produce ultrashort pulses. For passive Q-switching, the pulse repetition frequency is governed by the laser parameters and pumping conditions, whereas in the case of active Q-switching the frequency is determined by an external RF or optical signal.

One of the requirements for generating self-sustained Q-switched pulses [12] is that the differential loss *da/dn* of the absorber should be larger than the differential gain *dg/dn* of the amplifier section. Owing to the specific dependence of the gain/absorption on the carrier concentration in the diode lasers [9], the values of *dg/dn* and *da/dn* can be readily controlled by using different currents in different sections of the laser. As a result, the pulsewidth, the peak power, and the repetition rate are dependent on the driving currents. Another requirement for producing Q-switched pulses is that the recovery time of the saturable absorber should be faster than the recovery time of the gain. This is conveniently achieved in diode lasers using proton bombardment of the facets [13], or with a segmented electrode multicontact structure [2-3,14-16]. A three contact diode laser, which consists of two

amplifier sections with a saturable absorber located between them, is recommended to decrease the recovery time of the absorber [14]. Optical loss in the cavity can be changed by a reverse dc bias applied to the central absorber section. Rectangular current pulses (1ns to 100 ns in duration at a rate of 0 to 100 MHz) are applied to the end sections of the laser. By reverse dc biasing the absorber, electron-hole pairs in the absorber can be rapidly removed from the active layer by the electric field, thus leading to a significant decrease in the absorber recovery time, so that the improvement of the pulse parameters has been achieved in three-section lasers. Optical pulses as short as 1.6 ps with a peak power in excess of 10 W were measured [14].

7.3 Q-Switched Multicontact Bow Tie Laser

This section describes a new multicontact Q-switched laser [3], which is designed for generating high peak power picosecond optical pulses in a single transverse mode. The laser, called the tapered bow-tie laser, incorporates a narrow central waveguide for spatial mode control and two large area tapered waveguide sections for increased optical power. In this section, the device structure, the experimental arrangement, and the characteristics of its Q-switching operation, are discussed.

A. Device Description

A schematic diagram of the three contact bow-tie laser for high power Q-switching operation is shown in figure 7.2. It contains a central narrow non-tapered waveguide and two large area tapered waveguide end sections. The central waveguide region acts both as a transverse mode filter and saturable absorber under Q-switched operation. Based on the use of the tapered devices for high power cw and short pulse operation [5-6, 17], two tapered end sections allow the generated high optical powers to be expanded, thus reducing the optical intensities to avoid catastrophic facet damage, and reducing the effects of non-linear gain suppression. The advantages of the device are that it combines the enhanced optical power of a broad area laser with spatial mode control in the narrow ridge waveguide.

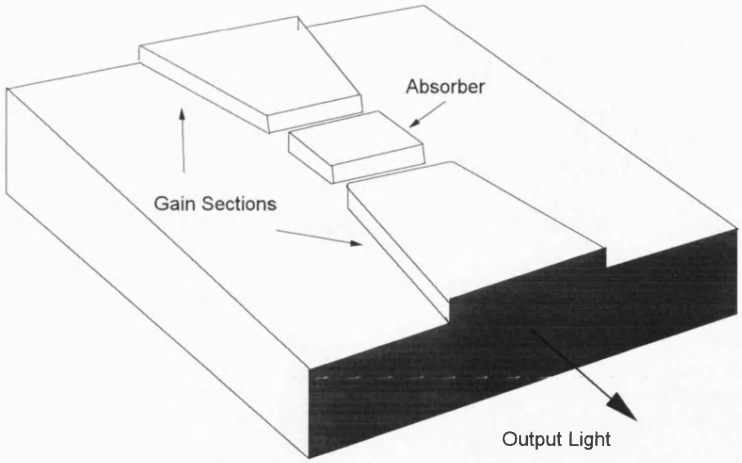

Figure 7.2. A schematic diagram of bow-tie three section laser

The device structure was grown on n-doped GaAs substrates using atmospheric pressure MOVPE [3]. The layer configuration used in experiment was 1 μm p-type Zn: GaAs capping layer, 1.6μm p-type C: $Al_{0.36}Ga_{0.64}As$, 0.3μm undoped GaAs, 2.0μm n-type Si: $Al_{0.36}Ga_{0.64}As$, and 0.5μm n-type Si: GaAs. The central non-tapered ridge waveguide was 5 μm wide and 125 μm long, and two 130 μm long gain guided end sections were tapered out from the central ridge waveguide at an half angle of 4^{o}. Electrical isolation of about 1 kΩ between the absorber and gain sections was achieved using 10 μm wide etched grooves, giving a total device length of 405 μm and output apertures 25 μm wide. The output facets were formed by cleaving and were left uncoated. Chips were bonded p-side up on a copper heatsink that permitted separate contacting of the central and end segments. Bonded devices were attached to a thermoelectrically cooled fixture with a temperature control system. For the quasi-cw operation characteristic investigations, all three sections were forward-biased in parallel. The threshold current was 140 mA, measured when all three contacts are joined together.

B. Experiment Set-up

In order to achieve high peak power short pulse operation, a modification of the Q-switched technique, which was followed by Peter Vasil'ev[14], was employed. Here, the three section bow-tie laser were separately driven, with different pumping currents I_g and I_a into the end tapered regions and centre region, respectively. The central segment which

provided the spatial mode control was used as a saturable absorber under Q-switched operation. This central region was reverse biased to decrease the saturable absorption recovery time, allowing improved pulse control. The two end tapered segments were joined together off-chip and were driven with rectangular current pulses to provide the necessary gain.

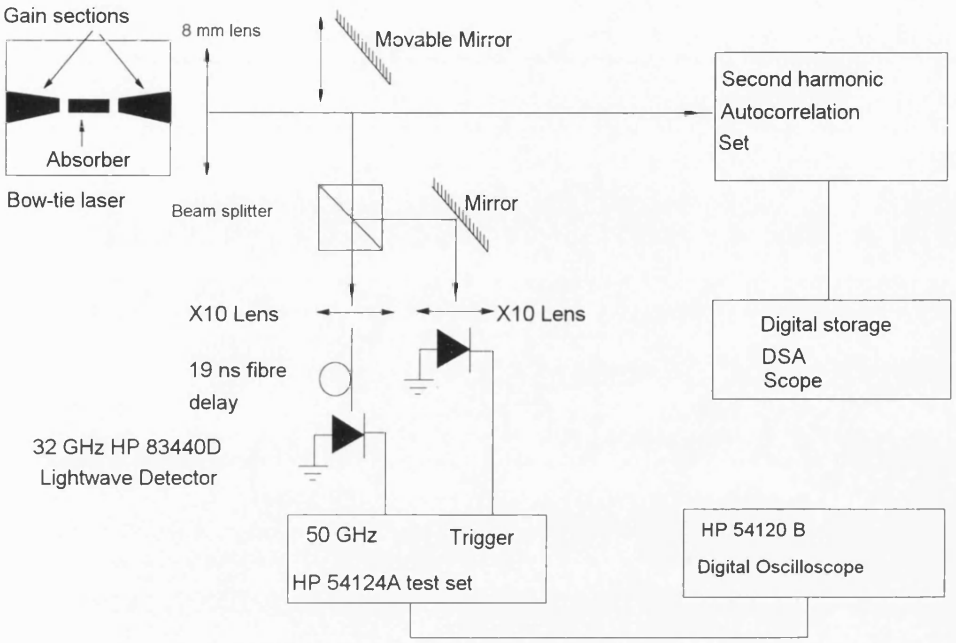

Figure 7.3. An experiment set-up for Q-switched operation of the bow-tie laser.

An experimental set-up for Q-switched operation of the bow-tie laser is shown in figure 7.3. The two end tapered sections were pumped initially with electrical pulses of 50 ns width and 50 V amplitude at 100 KHz from an HP214B generator. A pulse shapper (step recovery diodes with biasing circuits) was later employed to improve the high power operation of the Q-switched bow-tie laser. The central section was unpumped or reverse biased with a stabilised DC power supply. The output power was measured using either a calibrated Silicon photodiode or HP8153A optical power meter. The optical pulses were detected with a 32 GHz HP83440D lightwave detector and 50 GHz bandwidth test set HP54120 digital storage oscilloscope. Precise measurement of the pulsewidth was carried out using second harmonic autocorrelation.

C. Q-switched Operation

High power Q-switched operation was achieved by applying 1A peak and about 20 ns electrical pulses to the end sections of the bow-tie laser while the central absorber section was reverse biased at 3.0V. For this input drive pulse widths, multiple pulsing was observed after the high energy front pulse. Shortening the electrical pulse to about 5ns allowed the generation of pulses without subsequent pulsing. Using average power measurements, the energy and peak power of the pulses were measured to be 60 pJ and 3 W. The repetition rate was 100 kHz. The pulsewidth measurement was made by second harmonic autocorrelation and an autocorrelation trace of these Q-switched pulses is shown in figure 7.4. The pulses have an autocorrelation FWHM of 18 ps, corresponding to a pulsewidth of 13 ps, assuming a Gaussian pulse shape. The pulse profile recorded by using 32 GHz photodiode and 50 GHz oscilloscope is also shown in figure 7.5. This suggested an approximately Gaussian intensity profile with a FWHM of about 18 ps.

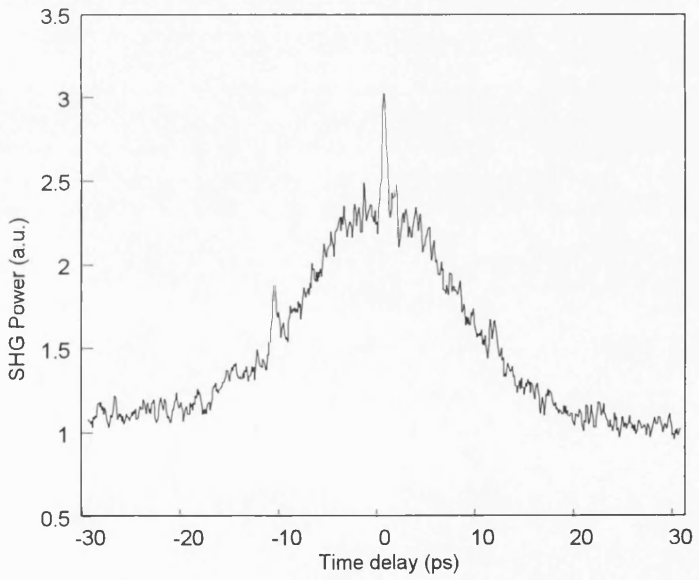

Figure 7.4 . Second harmonic autocorrelation of optical pulses, indicating 13 ps duration Q-switched pulses.

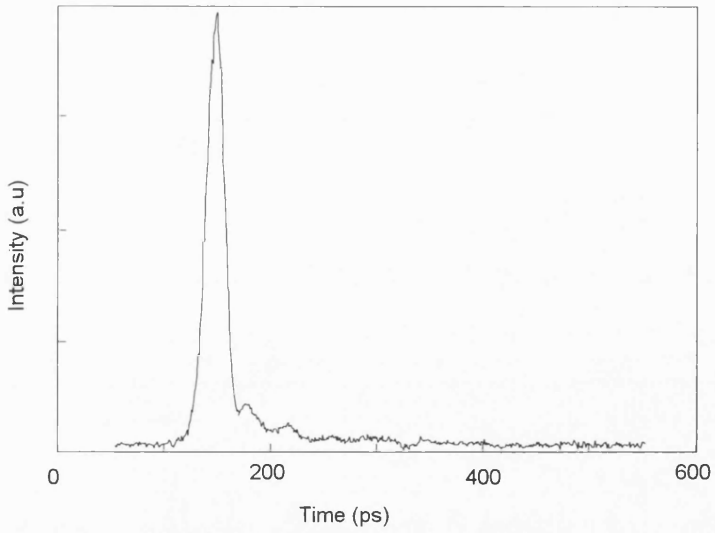

Figure 7.5. Pulse profile recorded using a 32 GHz detector with a 50 GHz sampling oscilloscope.

As mentioned in section 7.2, the reverse bias applied to the central section formed a saturable absorber and resulted in a decreasing absorber recovery time in the Q-switched laser [14-15]. This reverse-biased central section of the laser behaved as a waveguide photodetector, and the incoming optical pulse saturated the band-to-band absorption and bleached the central section. After the passage of the optical pulse through the absorber section, the electric field in the photodetector swept the carriers out of the active region and returned the section to the high attenuation state. An examination of the effects of the reverse-bias voltage on the Q-switched pulsewidth of the bow-tie laser has been made and the pulsewidth as a function of reverse dc voltage is shown in figure 7.6. In this figure, the pulse width of the gain section bias was optimised for each bias condition to enable a high power tail free pulse. As the reverse bias was increased, the optical losses were increased, the carrier concentration prior to pulse turn on was enhanced, leading in turn to a faster depletion and shorter duration pulses. The shortest pulsewidth of 13 ps was achieved for a reverse bias of 3.1 V. A rebroadening was then noted as the optical losses became too high.

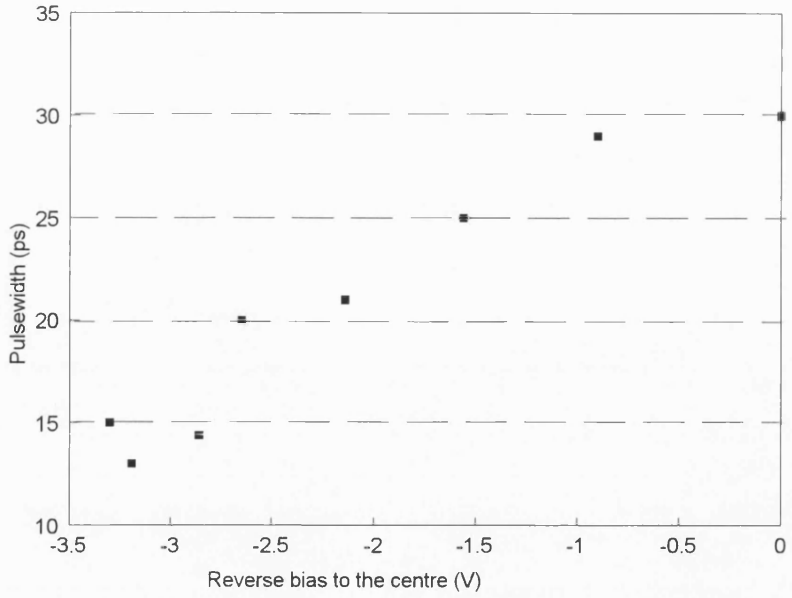

Figure 7.6. Q-switched pulsewidth as a function of reverse dc voltage.

D. Discussion

The energy of the Q-switched pulses is proportional to the difference between the total number of carriers accumulated in the active medium just before pulse emission and the number of carriers after pulse emission. This difference can be enhanced in two ways: first, by increasing the prepulse inversion density (carrier density) via an increase in the "hold-off" capacity of the saturable absorber, and secondly, by increasing the total number of carriers. The first approach requires an increase in the saturation intensity of the absorber, which can be accomplished by reducing the recovery time via a low reverse bias voltage applied to the absorber section. However, the maximum reverse voltage is limited to less than about 10V by avalanche breakdown at the doping levels used in the laser diodes. Although the total number of carriers can be increased by enlarging the geometrical dimensions of the active region, it is limited by the onset of higher-order transverse modes. In addition, experimental studies have found that the peak powers of Q-switched pulses could not be increased but the pulsewidth became wider by enlarging the geometrical dimension of the active region[18]. It was also shown that the Q-switched pulsewidth was widened with multipeaked fine structure, but the peak power of the pulses remained

unchanged when the device dimensions were enlarged from 600×100 μm^2 to 800×300 μm^2 for broad area (rectangular shaped active region) lasers [19]. Therefore alternative techniques have to be found to achieve much higher output power ultrashort optical pulses.

7.4 High Peak Power Picosecond Optical Pulse Generation Using Post Amplification

The results presented in the preceding section characterising the Q-switched bow-tie laser indicate that the use of a bow-tie structure allows an increase of output peak power in the Q-switching picosecond pulse operation. Pulse energies of tens of pJ can be readily obtained in this device, however a further increase of the output power becomes difficult, as discussed in the previous section. This section describes amplification of the Q-switched short pulses to increase further the output peak power while maintaining good spatial mode quality.

A. Broad Area Tapered Travelling Wave Amplifier

Recently, the use of large-active-area semiconductor amplifiers [17] has been demonstrated to be an attractive approach for achieving high-power emission in a semiconductor device while maintaining diffraction-limited output beam characteristics. Using single-pass broad-area (rectangular-shaped active region) travelling wave amplifiers, record near-diffraction-limited output powers have been demonstrated, with 21 W generated [20] under pulsed (300ns) conditions and 3.3 W in CW operation [21]. Such high power levels, generated with high electrical to optical conversion efficiency in a compact source, are required in a wide applications, including optical printers, satellite optical communication, and remote sensing. When compared with other solid-state lasers, large-area semiconductor amplifiers offer the advantages of high speed modulation, a wide variety of operating wavelengths, tunability, simple fabrication, and the potential for compactness and low cost.

Although high output power has been achieved in broad-area (rectangular-shaped active region) travelling wave amplifiers [20-21], there are two significant drawbacks of the broad-area amplifier structures. The first is the relatively large input power required to achieve saturation and , in the single pass structure, a decrease in conversion efficiency due to an unsaturated region near the input side. The second drawback, particularly in the double pass structure [22], is the degradation of the far field pattern at high powers caused by filamentation. These deficiencies can been partially overcome by amplifying a diverging beam in a tapered stripe travelling wave amplifier [7-8]. The tapered shape of the pumped region functions to maintain a relatively constant power density and gain saturation level along the amplifier stripe. A diverging wavefront of the amplified beam can also be expected to result in a greater resistance to filament formation [23]. Because the amplifier width is narrow at the input end, the input power required to saturate the output power is decreased in comparison with non-tapered amplifiers having the same output aperture width. In addition, since the amplified beam is diverging, the extent of the spatial overlap of the reflected reverse-travelling wave and forward input wave is reduced relative to non-tapered structures. By using the tapered-stripe amplifier, cw output powers of 2.0 W in a near diffraction limited beam lobe have been demonstrated when injected with only 25 mW of single mode laser diode emission [8], and cw output powers have recently been increased to 4.5 W using a larger area tapered-stripe device [24]. Narrow straight waveguide distributed Bragg reflector lasers have been monolithically integrated with a tapered amplifier, leading to output powers of 1.3 W cw with a single diffraction-limited lobe and sidemode suppression in excess of 20 dB from a monolithically integrated master oscillator flared amplifier device [25]. A diffraction grating -loaded external cavity tapered laser [26] was also demonstrated as a high power (1 W cw), diffraction-limited source with a 35 nm wavelength tunability and sidemode suppression of greater than 20 dB.

Since the semiconductor laser amplifier has an exceptionally large bandwidth (~ 5THz), it can amplify optical pulses as short as subpicosecond. The peak power of picosecond optical pulses can therefore be increased by using post amplification [27-28]. The broad area tapered stripe amplifier also benefits from the increasing of pulse energies,

because the saturation energy is relatively large at the flared output end of the amplifier. By expanding the gain cross-section area along the length of the amplifier, as the amplified power grows, a more uniform power density and degree of gain saturation is maintained throughout the amplifier. Therefore, the temporal and spectral distortion effects of gain saturation are also less deleterious in the tapered post-amplifiers [4,27-28]. Recently, high power pulsed operation of the tapered waveguide amplifier and laser system has been focused on mode-locked operation. 12 ps duration pulses with a peak power of 16 W and pulse energies of 0.5 nJ were demonstrated by actively mode-locking of a narrow stripe laser with a tapered amplifier [5]. Passively mode-locked 4.2 ps duration pulses with peak powers as high as 28.1 W were also demonstrated using a tapered-waveguide post-amplifier [6].

B. Experiment Arrangement

An experimental set-up for high power generation and amplification of ultrashort optical pulses from a Q-switched bow-tie laser and a tapered travelling wave amplifier is shown in figure 7.7 . It was formed by a three-contact bow-tie diode laser, a tapered travelling wave amplifier and coupling lenses. The three section bow-tie laser had the same device structure as described in the previous section. The 1.5 mm long tapered amplifier had a 30 μm wide input waveguide which expanded within the device to 250 μm width at the output end, and both the input and output facets of the amplifier were AR coated. The amplifier was mounted p-side up on a thermo-electric cooler and a copper heatsink with a temperature control system. The gain peaks of both the bow-tie laser and amplifier were at about 882 nm. Two AR-coated coupling lenses were used to image the output of the bow-tie laser onto the input aperture of the tapered amplifier, and an optical isolator was inserted between the lenses to prevent back-emitted amplified spontaneous emission from the amplifier from being injected into the bow-tie laser. The isolator included a half-wave plate at the laser output for polarisation matching to the amplifier. A microscope objective was used to collimate the output of the amplifier. The pulses were characterised both by using a high speed photodiode and sampling oscilloscope, and by second harmonic autocorrelation.

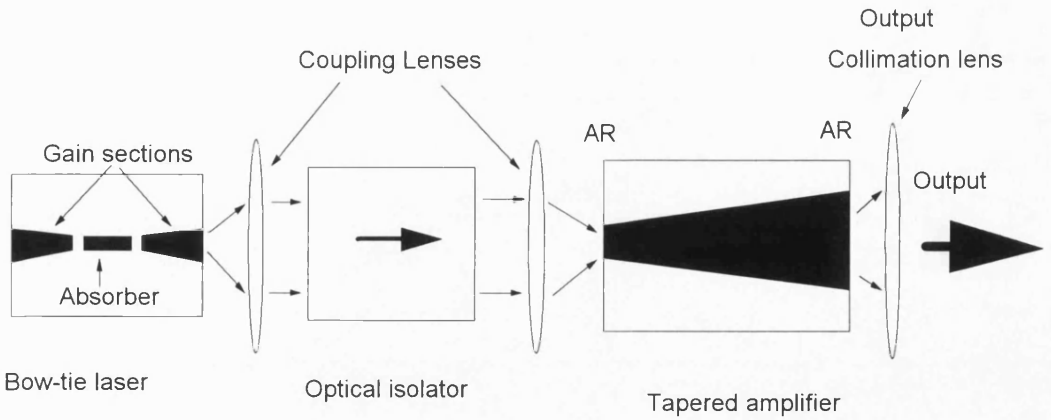

Figure 7.7. An experimental set-up for high power generated from a Q-switched bow-tie laser and tapered amplifier.

C. Results

The light- current curve of the amplifier recorded with incident power of 15 mW from the bow-tie laser is plotted in figure 7.8, and was measured under quasi-CW pulsed conditions (75 ns electrical pulses at a repetition rate of 100 kHz). The output power under injection increased linearly with an external slope efficiency of 0.3 W/A. By properly subtracting ASE from the total output power, the signal gain of the amplifier under quasi-cw operation was calculated to be 8.9 dB. Here a total peak power of 0.3 W was obtained at the a current of 2.0 A. However, at elevated power levels the slope efficiency was decreased. The relatively small slope efficiency was probably attributed to the relatively high reflectivity of the AR coated facets of the amplifier, which results in rather high ASE levels.

The pulse characteristics after post-amplification were measured under various levels. The tapered amplifier was pumped at quasi-cw condition and the input Q-switched pulses had pulse energies of 60 pJ and 13 ps duration. It was found that the use of the isolator between the bow-tie laser and amplifier is necessary in achieving both pulse amplification and Q-switching operation of the bow-tie laser. The isolator prevented ASE from the amplifier from being injected back into the bow-tie laser, and was also necessary to prevent the formation of an external lasing cavity. The output power was estimated using a large area calibrated photodetector. The output from the amplifier was composed of the short pulse output and ASE, which can be thought of as unwanted noise. ASE values were

measured by blocking the input Q-switched pulse beam. The short pulse output power was therefore determined by subtracting the ASE values from the total amplifier output power values, so that the pulse power was not over-estimated. With this method, the pulse energy gain under Q-switched short pulse operation was estimated to be 9.8 dB at a amplifier bias current of 2.0 A without including coupling losses. Peak powers as high as 44.7W were achieved and the highest pulse energy measured was 580 pJ. The average power was 58 μW due to the low duty cycle, which was limited by the repetition rates of the pulse generator used. No temporal broadening or distortion of the pulse shape after amplification was observed [29].

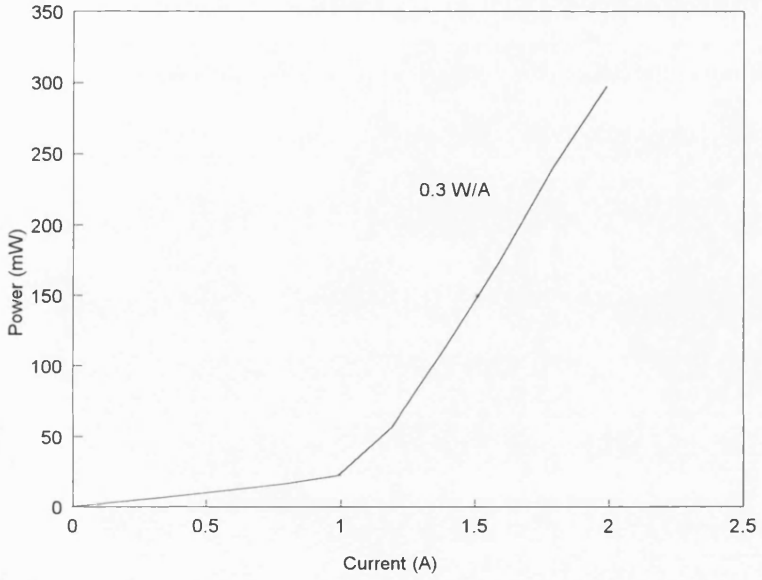

Figure 7.8. Light-current curve of tapered amplifier measured under quasi-cw condition (75ns, 100kHz) with incident power of 15 mW on the input coupling lens.

D. Near and Far Field Patterns

The near field distributions of the amplifier were observed by imaging the intensity profile at the output facet on a linearised infrared camera with a microscope objective. The pattern was recorded with a digital storage oscilloscope, and the near field width was readily measured by illuminating the waveguide and using the ridge waveguide width at the facet for calibration. Figure 7.9 plots the measured near field pattern of output light from the amplifier under different operating conditions. With the bow-tie laser injection blocked,

the amplifier emission consisted only of amplified spontaneous emission. In contrast, with a Q-switched pulse incident on the amplifier, the near field intensity profile was nearly flat and showed a low-intensity ripple near the device centre. The relative intensity for the quasi-cw operation was higher than that for Q-switched short pulse operation. The high degree of uniformity exhibited in the near field results in most of total power being radiated into the central lobe of the far field.

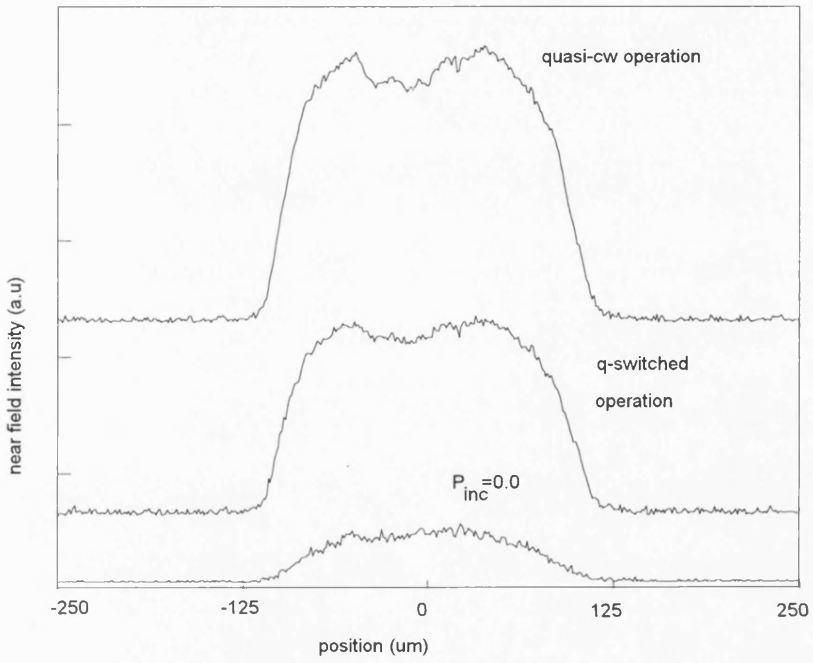

Figure 7.9. Measured near field pattern of the tapered amplifier under quasi-cw injection and Q-switched short pulse injection.

The direct far field pattern parallel to the pn junction plane was a broadly diverging beam similar to other tapered gain region devices [7-8], and was taken through a 8 mm focal lengths lens positioned behind the output facet. The measured far field patterns under quasi-CW and Q-switched operation are presented in figure 7.10, along with the far field pattern obtained by blocking the bow-tie laser input. The far field exhibited a single lobe with a FWHM of 0.3^{o}, which is about 1.5 times the diffraction limit for a uniformly illuminated 250 μm aperture. There was no measurable change of the lobe width and position for all measured currents and the short pulse and quasi-cw far field patterns are

nearly identical. However, for quasi-cw operation, an increase in the power contained within the pedestal portion of the far-field pattern is observed.

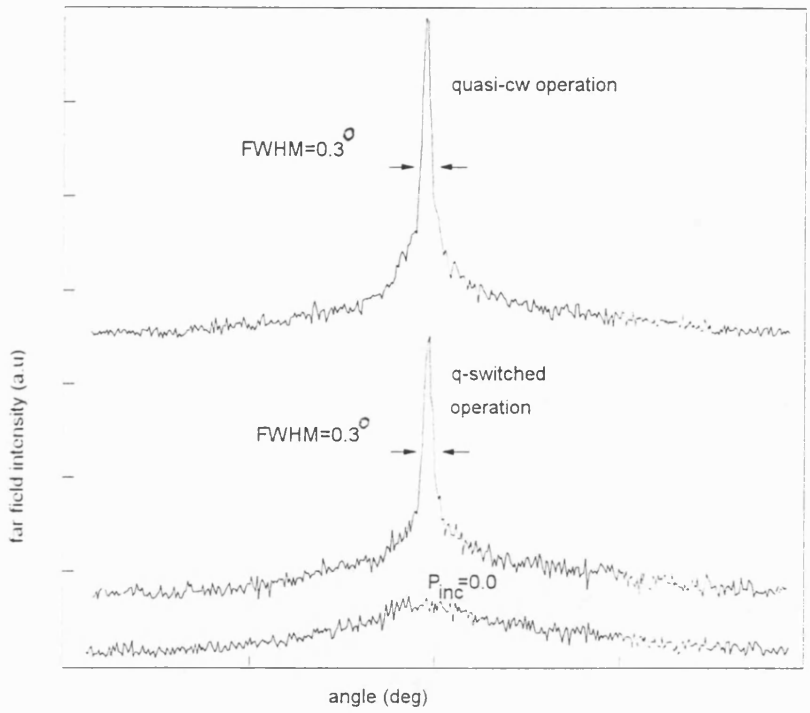

Figure 7.10. Measured far field pattern of the tapered amplifier under quasi-cw injection and Q-switched short pulse injection

7.6 Conclusion

An attempt to increase the optical powers of the MGC laser has stimulated interest in the use of broad area tapered devices. The generation of high powers using various broad area tapered lasers and amplifiers has been demonstrated. This chapter has described the generation of high peak power short optical pulses using a Q-switched tapered bow-tie laser and a tapered travelling wave post-amplifier.

Through a brief introduction of Q-switching techniques, a tapered bow-tie laser is described as a high power Q-switched laser source for generating picosecond optical pulse. Optical pulses with duration of 13 ps and pulse energy of 60 pJ have been obtained in a

single transverse mode. The practical implementation, characteristics and limitations of high power Q-switched short pulse generation in this device are discussed.

The research field in the broad area tapered lasers and travelling wave tapered optical amplifiers is reviewed. Tapered waveguides allow the optical mode to be expanded during propagation along the cavity length. The reduced optical intensity therefore experiences a reduced non-linear gain suppression. The tapered gain region also leads to an increase in pulse energy in amplifiers, because the saturation energy is relatively large at the flared output end. Using post amplification by a tapered travelling wave amplifier, picosecond optical pulses with peak powers of 44.7 W, and pulse energies as high as 0.58 nJ have been obtained. The near and far field distributions of the tapered amplifier have been measured and it has exhibited a single lobed, near-diffraction-limited radiation pattern.

The output powers of the MGC laser are therefore expected to be dramatically increased by using a broad area tapered waveguide MGC laser.

References

[1]. B. Zhu, and I. H. White; "Multiwavelength picosecond optical pulse generation using an actively mode-locked multichannel grating cavity laser," *J. lightwave Technol.* Vol.13, pp.2327-2335, 1995.

[2]. P. Gavrilovic, N. Stelmakh, J. H. Arrabi, and D. M. Beyea,"High energy CW Q-switched operation of multicontact semiconductor laser," *Electron. Lett.*, vol. 31, pp.1154-1155, 1995.

[3]. K. A. Williams, J. Sarma, I. H. White, R. V. Penty, I. Middlemast, F. R. Laughton, and J. S. Roberts, "Q-switched bow-tie lasers for high energy picosecond pulse generation", *Electron. Lett.*, vol. 30, pp. 320-321, 1994.

[4]. P. J. Delfyett, L. T. Florez, N. Stoffel, T. Gimitter, N. C. Andreadakis, Y. Silberberg, J. P. Heritage, G. A. Alphonse:"High-power ultrafast laser diodes", *IEEE Quantum Electron.*, vol.28, pp.2203-2219, 1992.

[5].L. Goldberg, D. Mehuys, and D. Welch, "High power mode-locked compound laser using a tapered semiconductor amplifier", *IEEE Photonics Technol. Lett.*, vol.6, pp. 1070-1072, 1994.

[6]. A. Mar, R. Helkey, J. Bowers, D. Mehuys, and D. Welch, "Mode-locked operation of a master oscillator power amplifier", *IEEE Photonics Technol. Lett.*, vol.6, pp. 1067-1069, 1994.

[7]. E. S. Kintzer, J. N. Walpole, S. R. Chinn, C. A. Wang, and L. J. Missagia, " High-power, strained-layer amplifiers and lasers with tapered gain regions," *IEEE Photonics Technol. Lett.*, vol. 5, pp. 605-608, 1993

[8]. D. Mehuys, D. Welch, and L. Goldberg, "2.0 W CW diffraction limited tapered amplifier with diode injection," *Electron. Lett.*, vol. 28, pp. 1944-1946, 1992,

[9]. P. P. Vasil'ev,"Ultrashort pulse generation in diode lasers",*Optical. and Quantum Electron.* vol. 24, pp.801-824,1992

[10]. D. Z. Tsang, J. N. Walpole, S. H. Groves, J. J. Hsieh, and J. P. Donnelly, "Intracavity loss modulation of GaAsInP Diode lasers," *Appl.. Phys. Lett.*, vol. 38, pp.120-122, 1981

[11]. Y. A. Arakawa, A. Larsson, J. Paslaski, and A. Yariv, "Active Q-switching in a GaAs/GaAlAs multiquantum well laser with an intracavity loss modulator," *Appl Phys. Lett.*, vol. 48, pp. 561-563,1986.

[12]. M. Ueno, and R. Lang, "Conditions for self-sustained pulsation and bistability in semiconductor laser," *J. Appl. Phys.* vol.58, pp.1689-1692, 1985.

[13] J. P. Van der Ziel, W. T. Tsang, R. A. Logan, and W. M. Augustyniak, " Pulsating output of separate confinement buried optical guide lasers due to the deliberate introduction of saturable loss," *Appl. phys. Lett.*,39,pp.376-378, 1981.

[14]. P. P. Vasil'ev, "Picosecond injection laser: A new technique for ultrafast Q-switching," *IEEE Quantum Electron.*, vol.24, pp.2386-2391, 1988..

[15]. P. P. Vasil'ev, "High-power high-frequency picosecond pulse generation by passively Q-switched 1.55 μm diode lasers", *IEEE Quantum Electron.*, vol.29, pp.1687-1691, 1993.

[16]. P. P. Vasil'ev, I. H. White, M. J. Fice, "Narrow line high power picosecond pulse generation in a multicontact DFB laser using modified q-switching, " *Electron. Lett.*, vol. 29, pp. 561-563.

[17]. L. Goldberg, D. Mehuys, M. R. Surette, and D. C. Hall, "High-power, near-diffraction limited large-area travelling wave semiconductor amplifiers", *IEEE Quantum Electron.*, vol.29, pp.2028-2043, 1993.

[18]. K. A. Willams, "Q-switched diode lasers" Bath University PhD thesis, 1995.

[19]. B. J. Thedrez, S. E. Saddow, Y. Q. Liu, C. Wood, R. Wilson, and C. H. Lee, "Experimental and theoretical investigation of large output power Q-switched AlGaAs Semiconductor lasers", *IEEE Photonics Technol. Lett.*, vol.5, pp. 19-22, 1993.

[20]. L. Goldberg, D. Mehuys,"21 W broad area near-diffraction limited semiconductor amplifier," *Appl. Phys. Lett.*,vol. 61, pp.633-635,1992

[21]. L. Goldberg, D. Mehuys, and D. C. Hall, "3.3 W CW broad diffraction limited broad area semiconductor amplifier," *Electron. Lett.*, vol. 28, pp. 1944-1946, 1992,

[22]. M. Tamburrini, L. Glodberg, and D. Mehuys, "Periodic filaments in reflective broad area diode laser amplifier," *Appl. Phys. Lett.*,vol. 60, pp. 1292-1294,1992.

[23]. M. L. Tilton, G. C. Dente, A. H. Paxton, J. Cser, R. K. Defreez, C. E. Moeller, and D. Depatie, "High power, nearly diffraction-limited output from a semiconductor laser with an unstable resonator," *IEEE Quantum Electron.*, vol.27, pp.2098-2108,1991.

[24]. L. Goldberg, D. Mehuys, R. Waarts and D. F. Welch, "4.5 W cw, near-diffraction-limited tapered-stripe semiconductor optical amplifier," *Electron. Lett.*, vol. 29, pp. 219-221, 1993.

[25]. S. O'Brien, D. Mehuys, J. Major, R. Lang, R. Parke, D. F. Welch, and D. Scifres, "1.3 W cw, diffraction-limited monolithically integrated master oscillator flared amplifier at 863 nm," *Electron. Lett.*, vol. 29, pp. 2109-2110, 1993.

[26]. D. Mehuys, D. Welch, and D. Scrifres, "1W cw, diffraction-limited, tunable external cavity semiconductore laser," *Electron. Lett.*, vol. 29, pp. 1254-1255, 1993.

[27]. G. P. Agrawal and N. A. Olsson, "Self-phase modulation and spectral broadening of optical pulses in semiconductor laser amplifiers," *IEEE Quantum Electron.*, vol.25, pp.2297-2306, 1989.

[28]. M. Y. Hong, Y. H. Chang, A. Dienes, J. P. Heritage, and P. J. Delfyett,"Subpicosecond pulse amplification in semiconductor laser amplifier:Theory and Experiment," *IEEE Quantum Electron.*, vol.30, pp.1122-1131, 1994.

[29.] B. Zhu, I. H. White, K. A. Williams, F. R. Laughton and R. V. Penty, "High peak power picosecond optical pulse generation from Q-switched bow-tie laser with a tapered travelling wave amplifier," *IEEE Photonics Technol. Lett.*,Vol.8, pp. 503-505, 1996.

Chapter 8

CONCLUSION

8.1 Summary

This thesis presented the design and characteristics of a type of multiwavelength semiconductor laser source for applications in the WDM and optical TDM communication systems. The laser, called an MGC laser, had both bulk optic and monolithic integrated versions. The laser gave emission at a number of discrete wavelengths from a single output port, each wavelength could be independently selected and modulated by direct current injection into an appropriate stripe of the device, so that the device functioned as both a discretely tunable and a multiwavelength laser source. In addition, the laser was able to generate a number of WDM channel picosecond optical pulses which could easily be synchronised, or controlled with a programmable relative delay between the channels, or switched from one channel to another.

Chapter one reviewed the status and trends of optical fibre communication systems. In particular, it identified the optical multiplexing technologies, which were basically classified as WDM and optical TDM systems. The WDM systems promise not only to increase transmission capacity but also to provide new flexible network-oriented functions such as wavelength switching and signal routing. This technology requires that different spectral channels are well allocated to different services, where tunable or multiwavelength laser sources are particularly required. The optical TDM technology requires that different services can be transmitted during different time slots, where optical short pulse generation and modulation, optical multi/demultiplexing are essential photonic techniques. The practical deployment of WDM and optical TDM systems presents major challenges to

optical laser source technology. Depending on the application, optical terminals may be expected to provide rapid wavelength tuning or selection, or to independently offer extraordinary wavelength precision and stability, or simultaneously provide multi-wavelength high speed modulation or ultrashort pulse operation.

Chapter two surveyed a variety of semiconductor lasers that appear to be the most promising candidates for use in the WDM systems. These lasers were broadly grouped into wavelength tunable lasers, multiwavelength laser arrays and monolithic integrated multiwavelength lasers. The challenges for wavelength tunable lasers has currently been to develop a device whose lasing wavelength can be rapidly tuned over a broad spectral range, while the development in the multiwavelength laser arrays have mainly consisted of increases in the level of integration of their components and improvement of their performance. Monolithic integrated multiwavelength lasers, such as the MAGIC laser and WGR laser, exhibit many advantages in term of high performance, cost and versatility. These lasers are able to produce a comb of exactly spaced frequencies from a single output port, hence they do not need an extra optical multiplexer to combine the different wavelengths. The direction of future multiwavelength laser sources will be focused on the development of the monolithic integrated device

Chapter three described the basic characteristics of the bulk optical MGC laser, including the device structure, operating principles, steady-state and dynamic performance. The laser was demonstrated to allow the generation of two stable spectral channels simultaneously, and wavelength switching at the channel spacing of 2.2 nm. A theoretical dynamic model involving a set of coupled cavity rate equations was developed for the MGC laser. The model included the non-linear gain saturation effects, the optical bandwidth of the diffraction grating used and the delayed optical feedback. The transient response and digital modulation characteristics in a single channel operation were investigated and it was found that the direct modulation rate for each channel was limited by the round trip time of the long external cavity at 500 Mbit/s. The carrier depletion effects in dual channel operation were also discussed using the coupled cavity rate

equation. The simulated results agreed closely with those of experiments, indicating that the theoretical model gave a useful understanding of the dynamics of the MGC laser

Chapter four and five discussed the issues that related to the generation of multiwavelength picosecond optical pulses using active mode-locking techniques with the bulk optic MGC laser, particularly for WTDM network applications. With a 1200 lines/mm diffraction grating, picosecond optical pulses with a spectral linewidth as low as 0.088 nm were achieved in single channel. Compared with a single stripe external cavity laser, the MGC laser had better optical spectral characteristics and generated narrower optical spectra. These characteristics are very attractive for potential applications in soliton-based transmission systems. For the first time, simultaneous generation of dual-wavelength picosecond optical pulses was successfully demonstrated. Two optical pulse trains were also produced at different wavelengths with a controlable relative time delay. Pulses were generated with a spectral separation of 2.2 nm, pulsewidths of 60 ps and spectral widths of 11 GHz. Experiments showed that the pulsewidth was stable to within about 6%, irrespective of variable delay for a wide range of bias conditions. Extensive theoretical modelling of the multiwavelength mode-locking process of the MGC laser was carried out by using the coupled-cavity rate equation model, and a good agreement between theory and experiment was obtained. The minimum achievable pulsewidth generated from the actively mode-locked MGC laser was shown to be limited by the resolution bandwidth of the diffraction grating used. The effect of the RF drive frequency detuning on the pulsewidth was theoretically and experimentally investigated and it was found that the mode-locking short pulses could be obtained over a wide range of frequency detuning in the MGC laser. The interchannel cross-talk originating from the gain saturation and carrier depletion was also discussed in chapter five.

Chapter six illustrated a monolithic integrated MGC laser, which was essentially a two-dimensional implementation of the bulk optic device. The prototype device fabricated by BT exhibited successful operation with a threshold current of 310 mA and total output power of 4.3 mW. Dual channel emission with wavelength separation of 21 nm was also

demonstrated. Owing to its elegant compact structure, the integrated MGC laser showed the direct modulation rates of in excess of 1 Gbit/s, and the optimised device should allow the modulation speed as high as 5 Gbit/s per channel.

A high power MGC laser using a broad area tapered waveguide was introduced in *Chapter seven*. High peak power generation and amplification of short optical pulses were experimentally demonstrated by using tapered bow-tie laser and tapered travelling wave amplifier. Optical pulses with duration of 13 ps and peak powers of 44.7 W were achieved with a single -lobe, near diffraction-limited beam mode. Record pulse energies of 580 pJ were observed.

8.2 Direction of Future Work

Research into the multiwavelength laser sources will continue to prove fruitful from both the fundamental physics and also the device application viewpoint. In chapter seven, it was demonstrated that the use of broad area tapered laser and amplifier could provide high power operation with a good spatial mode qualities. The problem of relative low power operation in the MGC laser is expected to be overcome by using tapered waveguide device as proposed in chapter seven. Investigation of this device could be very interesting, particularly on high output power, the controlling of spatial and spectral mode in the grating-load external cavity both on cw and short pulse operation.

The preliminary integrated MGC laser, described in chapter six, exhibited a number of characteristics that require further improvement. These include high threshold current, poor electrical isolation, unreasonable channel separation design, and low differential quantum efficiencies. Better electrical isolation between stripes and grating section, low losses in the grating section can significantly improve the threshold current and output power levels. The laser's size can be further reduced, allowing a number of benefits, including higher maximum modulation rates, lower material costs and further reduction of the cavity round trip losses. A reasonable design of channel separation can be achieved by

properly reducing the spatial separation between the stripes in the reflection array. The channel separation for the preliminary device was 21 nm. Reduction to a value at about 2~3 nm might be expected to improve the mutlichannel performance and to enhance the total number of the spectral channels. However, greater attention must then be paid to avoid the electrical and thermal crosstalk between adjacent waveguides in reduction of the spatial separation of the reflector stripes. In addition, the use of the active/passive interfaces to define the active waveguide and grating region will allow a substantial reduction of the drive currents and a good optical coupling between output amplifier and reflector stripes. The low threshold optimised device with reasonable channel spacing is expected to provide both good cw operation and short pulse performance. Furthermore, high repetition rate, near transform-limited multi-WDM short optical pulses are expected to be generated from the optimised device by using mode-locking techniques, which are very attractive for the multiwavelength soliton transmission systems.

The survey of the multiwavelength laser sources, carried out in chapter two, indicated that VCSELs exhibit a number of advantages such as small size, high device yield, possibility of large 2-D arrays and narrow circular output beam. However, the accuracy of the wavelength in present multi-wavelength VCSEL arrays tends to be fairly low. Moreover, the technologies involved can become prohibitively expensive due to the complex manufacturing process. The VCSEL arrays with the *same structure* may be used to provide a lower cost multiwavelength laser sources by using a grating loaded external cavity system. However, particular attention must be paid to design the device and the external cavity system. Multiple quantum wells with increased compressive strain may be used in the active region of the VCSEL arrays to provide high optical gain. The rear mirror should have high reflectivity, but the front mirror may have a modest or low reflectivity in order to get high external cavity coupling. The external cavity can consist of an antireflection coated lens and high reflection diffraction grating. Developing and investigating this kind of device could be very interesting from both the physics and the device application viewpoint.

Appendix 1

OPTICAL CAVITY DESIGN OF BULK OPTIC MGC LASER

A.1 Channel Separation

In order to minimise the potential optical crosstalk between spectral channels, the optical cavity of the MGC laser is designed with its grating set for the highest resolution in a near autocollimation regime. In this situation, the spectral spacing may be simply determined using a geometrical optical approach.

Consider an MGC laser which is constructed with two reflector stripes in geometrical diagram as shown in the figure A.1. For a reflection grating, the following equation must hold,

$$a_g(\sin(\theta_i)+\sin(\theta_r)) = m_d\lambda \qquad \text{(A.1)}$$

where θ_i and θ_r are the angles of incidence and diffraction respectively measured from the grating normal. a_g is the grating constant, m_d is diffraction order, and λ is the wavelength. In autocollimation regime (i.e., a ray in the optical axis could follow the same path after reflection from the grating) we can define the angle between the optical axis and the normal to the grating, θ_a, which from (A.1) is given by ;

$$\theta_a = \sin^{-1}\left(\frac{m_d\lambda}{2a_g}\right) \qquad \text{(A.2)}$$

Assuming a paraxial ray system the angle of the incidence at the grating is given by

$$\theta_i = \theta_a - \tan^{-1}\left(\frac{x_2}{f}\right) \qquad \text{(A.3)}$$

Hence from the grating equation (A.1) and (A.3), the angle of diffraction beam to the grating normal, θ_r, can be calculated from;

$$\theta_r = \sin^{-1}\left(\frac{m_d\lambda}{a_g} - \sin\left(\theta_a - \tan^{-1}\left(\frac{x_2}{f}\right)\right)\right) \qquad \text{(A.4)}$$

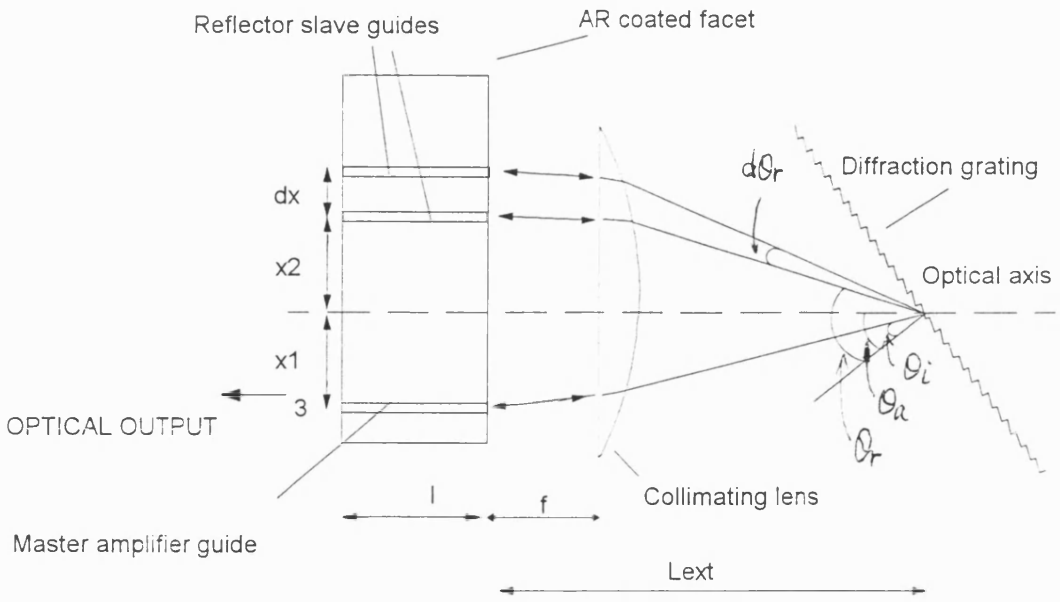

Figure A.1 A schematic diagram of the bulk optic MGC laser used for geometrical analysis

Based on equation (A.1), the spectral dispersion of the grating in this near autocollimation regime is given by;

$$\delta\lambda_c = \frac{a_g}{m_d}\cos(\theta_r)\delta\theta_r \qquad (A.5)$$

where $\delta\theta_r$ is the difference in the angles of reflection of the rays to reflector stripes 1 and 2 and can be approximated by ;

$$\delta\theta_r = \tan^{-1}\left(\frac{x_2 + dx}{f}\right) - \tan^{-1}\left(\frac{x_1}{f}\right) \qquad (A.6)$$

For very small dx compared to focal length f this further reduces to

$$\delta\theta_r = \tan^{-1}\left(\frac{dx}{f}\right) \cong \frac{dx}{f} \qquad (A.7)$$

The channel spacing can therefore be determined using specific cavity parameters and approximated using the following expression

$$\delta\lambda_c = \frac{a_g}{m_d}\cos(\theta_r)\frac{dx}{f} \qquad (A.8)$$

In addition, the half power resolution R of the grating in this situation can be shown to be given by

$$R = Na_g\left(\sin(\theta_r) - \sin(\theta_i)\right)/\lambda \qquad \text{(A.9)}$$

where N is the number of grooves covered by the incident beam on the grating.

A.2. Derivation of the MGC Laser Modal Spacing

The following derivation of the modal spacing of the MGC laser assumes a Fabry Perot cavity system. The cavity can consist of sections of different refractive index. The standing wave produced within such cavity must be an integral number of half-wavelengths over the total length of the cavity.

$$m = \frac{2}{\lambda}\sum_i n_i l_i \qquad \text{(A.10)}$$

where n_i represents the index of refraction of region i and λ represents the operating wavelength. Differentiating (A.10) with respect to λ gives,

$$\frac{\delta m}{\delta \lambda} = -\frac{2}{\lambda^2}\sum_i n_i l_i + \frac{2}{\lambda}\sum_i l_i \frac{\delta n_i}{\delta \lambda} \qquad \text{(A.11)}$$

the expression for mode spacing is therefore found by taking $\delta m=1$ in equation

$$\delta\lambda_m = \frac{\lambda^2}{2\sum_i n_i l_i - 2\lambda\sum_i l_i \frac{\delta n}{\delta \lambda}} \qquad \text{(A.12)}$$

The MGC laser system as shown in figure A.1 consists of three regions(laser material-air-laser material). The total cavity length is therefore internal cavity 2l and external cavity $2l_{ext}$. From equation (A.12), the mode spacing in the MGC laser systems is

$$\delta\lambda_m = \frac{\lambda^2}{4l_{ext} + 4l\left(n - \lambda\frac{\delta n}{\delta \lambda}\right)}$$

The factor $n-\lambda\delta n/\delta\lambda$ takes into account the dispersion of the refractive index and is called the effective group index μ_g of the laser material. The longitudinal mode spacing of MGC laser can be approximated by

$$\delta\lambda_m = \frac{\lambda^2}{4\left(\mu_g l + l_{ext}\right)} \qquad \text{(A.13)}$$

where μ_g is the effective refractive index of the laser diode and l and l_{ext} are the lengths of the diode laser and external cavity length, respectively.